MOLECULAR DESIGN AND ENGINEERING OF PHOTONIC CRYSTAL HYDROGELS FOR BIOSENSING APPLICATIONS

by

KELSEY IRENE MACCONAGHY

B.S., Oregon State University, 2011

A thesis submitted to the

Faculty of the Graduate School of the

University of Colorado at Boulder in partial fulfillment

Of the requirement for the degree of

Doctor of Philosophy

Department of Chemical and Biological Engineering

2016

This thesis entitled:
Molecular Design and Engineering of Photonic Crystal Hydrogels for Biosensing Applications
written by Kelsey Irene MacConaghy
has been approved for the Department of Chemical and Biological Engineering

_____
(Dr. Joel L. Kaar)

_____
(Dr. Mark P. Stoykovich)

Date _____

The final copy of this thesis has been examined by the signatories, and we
find that both the content and the form meet acceptable presentation standards
of scholarly work in the above mentioned discipline

MacConaghy, Kelsey Irene (Ph.D., Chemical and Biological Engineering)

Molecular Design and Engineering of Photonic Crystal Hydrogels for Biosensing Applications

Thesis directed by Dr. Joel L. Kaar and Dr. Mark P. Stoykovich

The rise of personalized medicine, increasing threat of bioterrorism, and growing concern of environmental pollutants necessitates the development of alternative biosensing techniques. Towards this end, we investigated the utility of using chemically and structurally modified photonic hydrogels for optical biosensing applications. Photonic crystal hydrogels are comprised of a crystalline colloidal array polymerized into a stimuli-responsive hydrogel. The crystalline colloidal array is comprised of highly charge nanoparticles that self-assemble into a photonic crystal that Bragg diffracts. The hydrogel is designed to undergo a volume transition in the presence of a target analyte. Altering the hydrogel volume in turn alters the lattice spacing of the photonic crystal, causing the diffraction peak to shift.

Initially, we explored the use of photonic hydrogels for the detection of enzymatic phosphorylation through the fabrication of kinase-responsive optically diffracting materials. The responsive nature of the hydrogel was confirmed via diffraction measurements and was seen to exhibit a time- and dose-dependent response. A theoretical model for swelling in ionic polymer networks was then utilized to elucidate the key parameters that modulate response sensitivity. The determined parameters were experimentally tuned and a detection limit of 0.1 U/μL was achieved in a 2 h reaction time.

We then developed a photonic hydrogel approach for DNA detection. Via hybridization events with a complementary probe strand, we were able to detect down to picomole amounts of a target p53 sequence. Moreover, we demonstrated that this approach could readily detect a

single base pair mutation in the target strand. We further showed that this approach is sensitive to epigenetic changes through the detection of a fully methylated form of the target sequence.

Lastly, we developed a high-throughput glucose- and ethanol-responsive photonic crystal hydrogel for monitoring microbial fermentation. A platform was developed for the fabrication of photonic hydrogels in 96-well plates to allow for rapid detection and the response sensitivity tuned through blending a thermally responsive polymer with hydrophilic and hydrophobic co-monomers. The 96-well platform was then used as a high-throughput method to monitor both glucose consumption and ethanol production during fermentation growth of *Saccharomyces cerevisiae.*

This work is dedicated to David J. MacConaghy, my husband and co-conspirator, without whose support, encouragement, and excellent machining skills this thesis would not have been possible.

ACKNOWLEDGEMENTS

Graduate school has been a journey that I could not have completed without the guidance, support, and encouragement of numerous people along the way. The greatest source of support and guidance for my thesis work was from my research advisers, Dr. Joel Kaar and Dr. Mark Stoykovich. Their difficult questions and high expectations drove me to constantly improve my skills as a scientific researcher and my ability to think critically. They constantly encouraged me to venture outside my comfort zone to try more challenging research, develop more creative solutions, and explore many different avenues in the completion of this thesis.

I would also like to thank my committee members: Dr. Ted Randolph, Dr. Chris Bowman, and Dr. Xuedong Liu. Their feedback on my thesis throughout my tenure at CU was instrumental to the development of this dissertation and my skills as a scientist. The students in their labs also provided a valuable resource for learning and using a large variety of instrumentation and for the development of various technical skills.

Past and present members of the both the Kaar and Stoykovich groups encouraged me, provided helpful discussions, and were always around to provide a laugh and for this I am very grateful. Of particular note, I would like to thank Dr. Erik Nordwald, Joseph Plaks, Ryan Mowbray, and Kate Morrissey for providing insightful, and usually sarcastic, comments and discussions on this thesis and for their friendship and encouragement over the years. I would also like to thank David Faulon for always being willing to discuss non-research topics when I needed break. I would also like to thank my undergraduate research assistants Christopher Geary, Duncan Chadly, and Graham Henry for their help in the development of many of the processes used in this work.

I am very grateful to the various funding sources that have supported my research throughout the years including a Dean's Fellowship from the University of Colorado, a grant from the Liquid Crystals Material Research Center, a Pharmaceutical Biotechnology Training Grant from the National Institute of Health. The training grant program provided a wonderful opportunity to meet researchers in other fields and learn about important work being done in the area of pharmaceutical biotechnology.

Last, but certainly not least, I would like to acknowledge and thank the many friends and family that provided emotional support and encouragement throughout my graduate career. They put up with me during both the highs and lows that inevitably arise during graduate school and were always there to share a drink or provide a much needed distraction. I am eternally grateful to my husband, David MacConaghy, for his love and support during this process. He was always ready to cheer me up when I had a bad day, listen to my rants (while trying to solve every problem I had – even when he should not have), and, when all else failed, provide chocolate.

TABLE OF CONTENTS

LIST OF TABLES

LIST OF FIGURES

NOMENCLATURE

2-Hydroxyethyl Acrylate	HEA
Acrylamide	AA
Adenosine Triphosphate	ATP
Allyl Glycidyl Ether	AGE
Crystalline Colloidal Array	CCA
Flory-Huggins Interaction Parameter	χ
Forskolin	FSK
Human Embryonic Kidney 293 Cells	HEK293
N-Hydroxyethyl Acrylamide	HEAA
N,N'-Methylenebisacrylamide	BA
N-Propargyl Acrylamide	PA
N-tert-Butylacrylamide	tBA
N-Isopropylacrylamide	NIPAM
Photonic Crystal	PC
Polymerized Crystalline Colloidal Array	PCCA
Polystyrene	PS
Protein Kinase A	PKA
Protein Kinase Inhibitor	PKI

CHAPTER 1 – INTRODUCTION

1.1 The Importance of Biological Sensing

Detection of chemical and biological agents plays a fundamental role in a multitude of analytical tasks ranging in application from medical diagnostics to environmental monitoring.[1-3] Biosensor-related research has experienced a high rate of growth over the last 30 (**Figure 1.1)** years from approximately 20 scientific publications in 1985 to nearly 9,000 in 2015.[4] Along with the increase in biosensor-related research, the commercial market for bioanalytics is also rapidly expanding. For example, the fields of biosensing and *in vitro* diagnostics are expected to reach market values of US$20.7 billion by 2020 and US$69.1 billion by 2017, respectively, which is a dramatic increase from their respective values of US$12.5 billion and US$53.3 billion in 2013.[4-6] Factors contributing to the great increase in bioanalytical-related research and commercial spending on assaying techniques include a shift towards more personalized medicine, increased awareness of bioterrorism, and increased demand from emerging markets for rapid diagnostics and treatment of infectious diseases.[7-8]

In general, the field of bioanalytics is comprised of two main categories of instrumentation: (1) equipment that is highly sophisticated and capable of high-throughput measurements that are sensitive and accurate and (2) easy-to-use, portable devices for use by non-specialists. Instrumentation that falls into category (1) tend to be expensive and require highly trained personal, whereas instrumentation in category (2) are mass produced and directed towards point-of-care and personalized medicine uses, such as handheld glucose monitoring.[4, 9] With the increased demand for bioassaying techniques, there is great interest in developing sensing platforms that span the divide between highly sophisticated, sensitive instrumentation and easy-to-use, rapid testing.[9-10] Such instrumentation would ideally allow for one-step, rapid

detection that is low-cost and capable of being used by semi-skilled operators.[11-13] Though there has been rapid increase in research directed towards new sensing platforms, few technologies have migrated from the research phase to achieve commercial viability due to the challenges of developing analytical techniques that are specific, sensitive, and do not require multiple steps and highly specialized equipment.[10, 14]

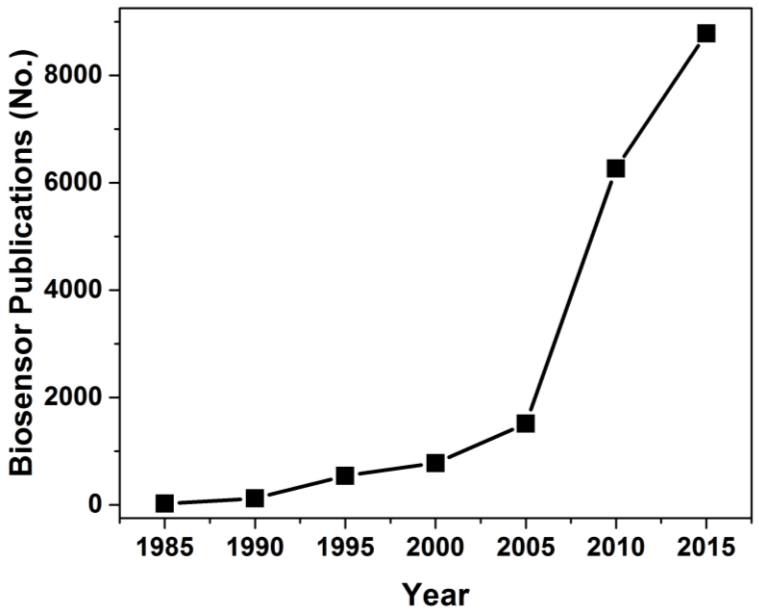

Figure 1.1 Number of articles found per year on Web of Knowledge for the period of 1985 to 2015 using the search term "biosensor."

1.2 Traditional Approaches to Biological Sensing

Biosensing platforms traditionally function through the coupling of a biologically derived sensing element to a transducer.[2, 10] The sensing, or recognition, element functions to provide selective and sensitive interaction with the target analyte. Common sensing elements include enzymes, nucleic acids, antibodies, and whole cells.[11] The transducer functions to translate the signal from the sensing element to a measurable output. Electrochemical,[15-18] piezoelectric,[19-22] and optical[23-27] techniques are commonly used transducers in biosensing applications. Though

these types of transducers have been heavily researched for the past 30 years and although demand for new bioanalytical techniques is increasing, few of these technologies have progressed past the infancy of development due to the increasing rigors required for new analysis techniques.[28]

With the increasing demand for new bioanalytical techniques, there is great interest in developing an idealized sensing platform that is capable of rapid, sensitive, and selective detection while still being easy-to-use and not require specialized equipment.[29] Though recent advances in analytical technologies are making vast strides towards the improvement of sensing technologies, no current technique fulfills the role of the idealized sensing platform. For instance, electrochemical sensors are highly attractive because of their low detection limits, low cost, and ease-of-use.[30] However, they may be prone to signal interference and low selectivity.[31] Piezoelectric sensors are capable of real-time, sensitive detection, but are also sensitive to temperature and non-specific biomolecule adsorption.[22] Optical based sensing approaches are particularly appealing because they are immune to electromagnetic interference, can provide multiplexed detection, and, in many cases, are capable of label-free sensing. Unfortunately, optical approaches may also suffer from signal interference and laborious labeling processes.[32-34] To achieve a more idealized sensing platform, significant improvements to current technologies is required. Response time, sensitivity, selectivity, and the signal-to-noise ratio is heavily dependent upon the functional components of the detection method and, therefore, the design of more effective sensing platforms depends on the development of novel materials to improve both recognition and signal transduction.[3]

1.3 Photonic Hydrogels as Optical Transducers

Photonic hydrogels are one such novel material and show great promise as a new biosensing platform. A photonic hydrogel is considered to be a structural color-based transducer due to the ability of the material to modulate light in the visible spectrum.[35] Structural color-based transducers are advantageous over traditional transducers in that they have tunable response ranges, are immune to interferences from biomolecule absorption (UV range), and enable label-free detection.[7] The benefits of label-free detection are two-fold. First, it allows for the detection of analytes in their natural form thus eliminating the need for time consuming labeling steps[36] and, second, the sensing element is immobilized directly to the transducer, enabling a faster, simpler, and more physiologically relevant detection scheme than a label-based counterpart.[37-38] It is also important to note that unlike traditional optical transducers where the signal strength decreases with the optical path length, photonic-based transducers provide local optical modes which enhance the light-matter interaction, enabling such sensing platforms to be used for a greater variety of applications.[39]

Photonic hydrogels are comprised of a photonic nanostructure embedded within a hydrogel material. The photonic nanostructure possesses spatial dielectric periodicity, enabling it to interact with incident light.[40] The photonic nanostructure may be fabricated through the self-assembly of colloidal particles, laser writing, and lithographical approaches.[41] The hydrogel material may exist either in a non-functionalized, non-analyte specific state or as a functionalized highly selective material. Upon interaction of the hydrogel material with a target analyte, the hydrogel undergoes a volumetric transition, thus altering the embedded photonic structure and modulating the optical properties of the material.[42] Modulation in the optical properties of the material is reported by changes in reflection, diffraction, refraction, surface plasmon resonance,

or emission.[43] The changes in optical properties may then be analyzed spectroscopically and correlated to analyte concentration. Additionally, photonic hydrogels can be tuned to report color changes which allows for rudimentary quantification to be performed visually, without the need for spectroscopic equipment. Unlike many traditional biosensing approaches, photonic hydrogels offer the potential for reversible, real-time analyte detection, they possess tunable detection ranges from UV to near-infrared, and they are compatible with standard photometric devices. Most importantly, photonic hydrogels are advantageous over standard assay formats in that they do not rely on labels or electrochemical reporting and so are immune to bleaching and electromagnetic and fluorescent interferences.[7] The successful development of photonic hydrogel sensing platforms would represent a significant improvement over many current sensing technologies and come a long way towards the development of an ideal sensing platform in that it would be rapid, selective, require little specialized training, and be compatible with mobile, low cost spectrophotometers.

1.4 References

(1) Ispas, C. R.; Crivat, G.; Andreescu, S., *Anal Lett* **2012,** *45* (2-3), 168-186.

(2) Sagadevan, S.; Periasamy, M., *Rev Adv Mater Sci* **2014,** *36* (1), 62-69.

(3) Saha, K.; Agasti, S. S.; Kim, C.; Li, X.; Rotello, V. M., *Chem Rev* **2012,** *112* (5), 2739-79.

(4) Turner, A. P. F., *Chem Soc Rev* **2013,** *42* (8), 3184-3196.

(5) Global Industry Analysts, I. *Biosensors - A Global Strategic Business Report*; San Jose, 2014; p 287.

(6) Markets&Markets *In Vitro Diagnostic (IVD) Market, Technique, & Applications - Forecast to 2017*; Pune, 2013.

(7) Yetisen, A. K.; Butt, H.; Volpatti, L. R.; Pavlichenko, I.; Humar, M.; Kwok, S. J. J.; Koo, H.; Kim, K. S.; Naydenova, I.; Khademhosseini, A.; Hahn, S. K.; Yun, S. H., *Biotechnology Advances* **2015**.

(8) Wang, J., *J Pharm Biomed Anal* **1999,** *19* (1-2), 47-53.

(9) Cai, Z. Y.; Smith, N. L.; Zhang, J. T.; Asher, S. A., *Anal Chem* **2015,** *87* (10), 5013-5025.

(10) Wang, J., *Biosens Bioelectron* **2006,** *21* (10), 1887-1892.

(11) Grieshaber, D.; MacKenzie, R.; Voros, J.; Reimhult, E., *Sensors (Basel)* **2008,** *8* (3), 1400-1458.

(12) Narsaiah, K.; Jha, S. N.; Bhardwaj, R.; Sharma, R.; Kumar, R., *J Food Sci Tech Mys* **2012,** *49* (4), 383-406.

(13) Marrazza, G., *Biosensors (Basel)* **2014,** *4* (3), 301-17.

(14) Prevel, C.; Pellerano, M.; Van, T. N.; Morris, M. C., *Biotechnol J* **2014,** *9* (2), 253-65.

(15) Soper, S. A.; Brown, K.; Ellington, A.; Frazier, B.; Garcia-Manero, G.; Gau, V.; Gutman, S. I.; Hayes, D. F.; Korte, B.; Landers, J. L.; Larson, D.; Ligler, F.; Majumdar, A.; Mascini, M.; Nolte, D.; Rosenzweig, Z.; Wang, J.; Wilson, D., *Biosens Bioelectron* **2006,** *21* (10), 1932-42.

(16) Kotanen, C. N.; Moussy, F. G.; Carrara, S.; Guiseppi-Elie, A., *Biosens Bioelectron* **2012,** *35* (1), 14-26.

(17) Karra, S.; Gorski, W., *Anal Chem* **2013,** *85* (21), 10573-10580.

(18) Zelada-Guillen, G. A.; Sebastian-Avila, J. L.; Blondeau, P.; Riu, J.; Rius, F. X., *Biosens Bioelectron* **2012,** *31* (1), 226-232.

(19) Ramadan, K. S.; Sameoto, D.; Evoy, S., *Smart Mater Struct* **2014,** *23* (3).

(20) Tzou, H. S.; Tseng, C. I., *J Sound Vib* **1990,** *138* (1), 17-34.

(21) Babacan, S.; Pivarnik, P.; Letcher, S.; Rand, A. G., *Biosens Bioelectron* **2000,** *15* (11-12), 615-21.

(22) Liu, Y.; Yu, X.; Zhao, R.; Shangguan, D. H.; Bo, Z. Y.; Liu, G. Q., *Biosens Bioelectron* **2003,** *19* (1), 9-19.

(23) Guo, X. W., *J Biophotonics* **2012,** *5* (7), 483-501.

(24) Li, Y. J.; Xie, W. H.; Fang, G. J., *Anal Bioanal Chem* **2008,** *390* (8), 2049-2057.

(25) Zhong, X.; Chai, Y. Q.; Yuan, R., *Talanta* **2014,** *128*, 9-14.

(26) Law, W. C.; Yong, K. T.; Baev, A.; Prasad, P. N., *Acs Nano* **2011,** *5* (6), 4858-4864.

(27) Cai, Z.; Smith, N. L.; Zhang, J. T.; Asher, S. A., *Anal Chem* **2015,** *87* (10), 5013-25.

(28) Ma, H. C.; Deacon, S.; Horiuchi, K., *Expert Opin Drug Dis* **2008,** *3* (6), 607-621.

(29) Turner, A. P., *Biosens Bioelectron* **2013,** *40* (1), 1-2.

(30) Stradiotto, N. R.; Yamanaka, H.; Zanoni, M. V. B., *J Brazil Chem Soc* **2003,** *14* (2), 159-173.

(31) Wang, J., *Biosens Bioelectron* **2006,** *21* (10), 1887-92.

(32) Moerner, W. E., *P Natl Acad Sci USA* **2007,** *104* (31), 12596-602.

(33) Sang, S.; Wang, Y.; Feng, Q.; Wei, Y.; Ji, J.; Zhang, W., *Crit Rev Biotechnol* **2015**, 1-17.

(34) Fan, X.; White, I. M.; Shopova, S. I.; Zhu, H.; Suter, J. D.; Sun, Y., *Anal Chim Acta* **2008,** *620* (1-2), 8-26.

(35) Zhang, Y. N.; Zhao, Y.; Lv, R. Q., *Sensor Actuat a-Phys* **2015,** *233*, 374-389.

(36) Cox, W. G.; Singer, V. L., *Biotechniques* **2004,** *36* (1), 114-+.

(37) Haake, H. M.; Schutz, A.; Gauglitz, G., *Fresenius J Anal Chem* **2000,** *366* (6-7), 576-85.

(38) Perkel, J. M., *Science* **2009,** *324* (5928), 815-817.

(39) Threm, D.; Nazirizadeh, Y.; Gerken, M., *J Biophotonics* **2012,** *5* (8-9), 601-616.

(40) Zhao, Y. J.; Zhao, X. W.; Gu, Z. Z., *Adv Funct Mater* **2010,** *20* (18), 2970-2988.

(41) Zhao, Y. X.; Wostyn, K.; de Schaetzen, G.; Clays, K.; Hellemans, L.; Persoons, A.; Szekeres, M.; Schoonheydt, R. A., *Appl Phys Lett* **2003,** *82* (21), 3764-3766.

(42) Holtz, J. H.; Asher, S. A., *Nature* **1997,** *389* (6653), 829-832.

(43) Gerlach, G.; Arndt, K. F., *Springer Ser Chem Se* **2009,** *6*.

CHAPTER 2 – PHOTONIC CRYSTALS AND PHOTONIC HYDROGEL SENSORS

2.1 Background of Photonic Crystals

2.1.1 History and Definition of a Photonic Crystal

Photonic crystals (PCs) are materials with a periodicity in dielectric constant that creates a range of forbidden frequencies called the photonic bandgap. Photons with energies within that photonic bandgap cannot propagate through the material, creating an optical phenomenon that can be utilized for a variety of purposes.[1-2] If the photonic bandgap is in the range of visible light (*i.e.* ~400-700 nm), it creates vibrantly colored material. The field of photonic crystal research was pioneered by the work of Yablonovitch[3] and John[4] in 1987. Since then, photonic crystal materials have been intensively studied and used in the areas of optical fibers, photovoltaic devices, displays, sensors, and more.[5-8] Though researchers have been studying and fabricating photonic crystals for a few decades, Nature has been creating and fabricating a wide variety of photonic materials for millions of years.[9] For example, photonic structures can be found on many insects, such as butterflies, worms, and beetles, and gems, such as opal.[10-13]

2.1.2 Structural Components of Photonic Crystals

PC materials can possess a periodic dielectric in 1 dimension (1D), 2 dimensions (2D), or 3 dimensions (3D) **(Figure 2.1)**. One-dimensional PCs are comprised of either a grating of two materials or a multilayer stack of materials of differing dielectrics. They are only capable of exhibiting a photonic bandgap in one direction, meaning that the bandgap is only present when incident light contacts at single orientation and that the bandgap energy is not angle dependent. The wavelength of that bandgap is controlled by the differences in the refractive indexes and the periodicity of the materials. Of the three types of PCs, 1D structures are the simplest to fabricate using traditional lithographic and chemical etching approaches.[14-15] In nature, these PC structures

are also the most commonly found and are seen in insects, bird feathers, fish, and plant leaves. The most well-known example of this type of PC is the brilliant blue color of the *Morpho* butterfly wing.[16]

Compared to 1D PC structures, 2D structures generally provide for richer color.[17] Two-dimensional PCs are generally comprised of cylinders or pillars of one material surrounded by a secondary material of differing refractive index (RI). As with 1D PCs, 2D PCs only exhibit a local photonic bandgap. However, due to the 2D periodicity of the material, the reflectance is angle-dependent and strong Bragg-scattering can only be seen in certain directions.[1] Fabrication of 2D PCs, is traditionally achieved through lithographical and self-assembly based approaches.[18] In nature, 2D PCs are less common than 1D and not commonly used for generating bright colors. Rather, 2D PCs are used for antireflection to increase the efficiency of an animal's vision.[19]

Of the three structures, 3D photonic crystals provide for the richest color. They were first studied in the 1960s when it was realized that close-packed silica spheres, a 3D photonic structure, were responsible for the iridescence of opal gems.[20] Three dimensional PCs are commonly fabricated through approaches that utilize self-assembly or deposition of nanoparticles.[21-23] Unlike with 1D and 2D PCs, 3D PCs are capable of producing partial photonic bandgaps, which diffract a variety of bright colors over broad angles.[24-26] The bandgap wavelength and, therefore, the diffraction wavelength for 3D PCs can be determined using Bragg's Law:[27]

$$m\lambda = 2ndsin\theta \quad (\mathbf{2.1})$$

where m is the order of diffraction, λ is the wavelength of diffracted light, n is the mean refractive index, d is the lattice spacing of the crystal, and θ is the angle between incident light and the diffraction plane.

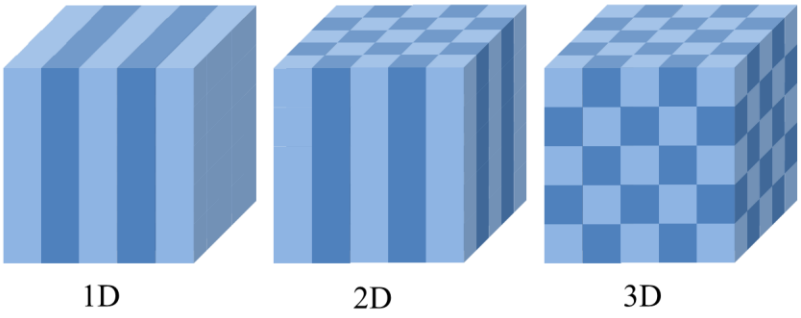

Figure 2.1 Depiction of 1D, 2D, and 3D photonic structures. Light and dark colored segments represent materials of differing dielectric constant.

2.2 Photonic Crystal Sensing Mechanism

Through the use of Bragg's law, the diffraction wavelength can be rationally tuned by altering the lattice spacing, ordered state, or the mean refractive index (RI) of the materials. Similarly, by coupling a stimuli-responsive mechanism to the same tuning properties (**Figure 2.2**), it is possible to create sensitive PC-based sensors for a variety of chemical, environmental, and biological analytes (**Table 2.1)**.[28] Commonly, PC-based sensing platforms rely on response mechanisms that alter either the mean RI of the material or the lattice spacing of the system. PC-based sensors with stimuli-responsive RI have been successfully shown to detect analyte binding events, such as the binding of proteins or wholes cells, and may be used in cell-based assays to detect cytotoxicity, apoptosis, protease excretion, and cell migration.[28-33] These types of sensors are commonly comprised on 1D and 2D photonic crystals that are functionalized with a ligand to facilitate analyte binding. Due to the difference in RI between water (n = 1.33) and most biomolecules (n ~ 1.4-1.5), surface adsorption alters the mean RI of the system, causing a diffraction shift. RI-based sensors are sensitive and possess a sharp diffraction signals due the ability to create highly uniform structures with lithographical approaches. Due to the simple fabrication techniques, these types of sensors are also easily implemented into multiwall formats

for high-throughput applications, unlike many other photonic crystal based approaches. However, they tend to have small diffraction shifts, on the order of hundreds of picometers, requiring sensitive equipment and precise temperature control to ensure accurate results.[29] In general, RI-based PC sensors are also fabricated using ridged materials, limiting the ability to tune the mechanical properties of the sensor.

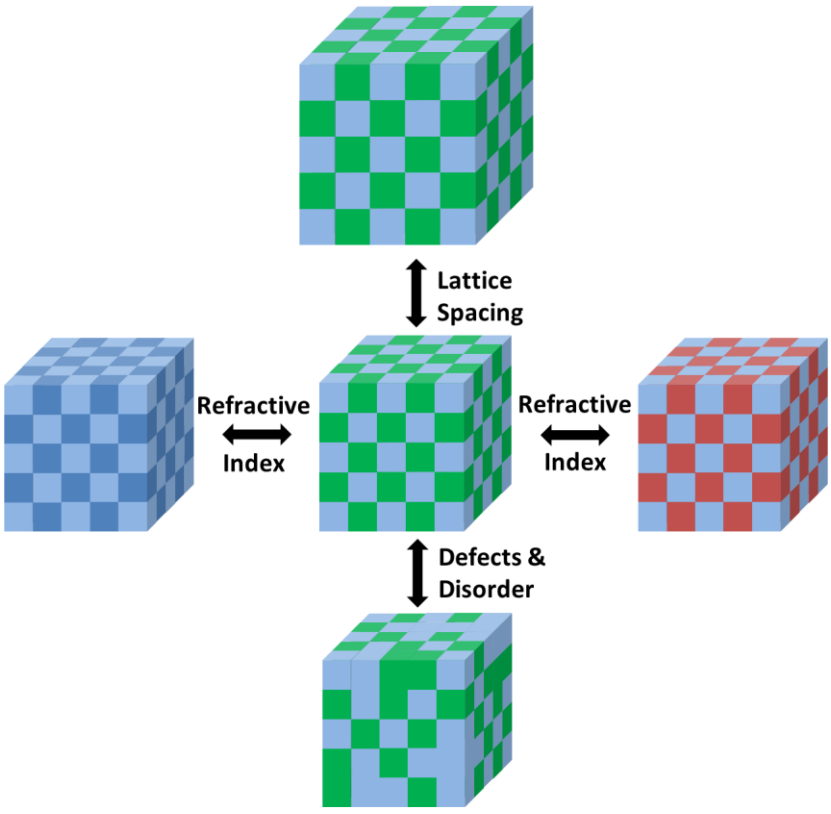

Figure 2.2 Schematic of parameters that may be tuned to create stimuli-responsive 3D photonic crystals.

An alternative to RI-based PC sensing techniques, is the use of composite materials with stimuli-responsive lattice spacing. These types of materials are generally formed by embedding a 3D photonic structure into a stimuli-responsive polymer matrix, such as a crystalline colloidal array (CCA) based[34-35] or inverse opal based sensors.[36-39] CCA based sensors utilize a 3D PC comprised of highly-charged nanoparticles that form a pseudo-crystalline dispersion in solution.[40-42] A hydrogel network is then polymerized around the 3D photonic structure, locking

it into place. Subsequently, the hydrogel network is functionalized with a molecular recognition motif that stimulates a volume transition in the presence of an analyte. Volume transitions may be triggered by altering the immobilized charge state of the hydrogel, creating or breaking cross-links, or by altering the polymer-solvent interactions.[43-45] Due to the encapsulation of the CCA in the polymer network, a volume transition in the hydrogel modifies the lattice spacing of the particles and shifts the diffraction wavelength. By tuning the diffraction wavelength to the visible range, it is possible to make bright devices that change color in the presence of an analyte, allowing for visual detection. Because of this, composite materials with stimuli-responsive lattice spacing have gained significant interest for use as chemical and biological sensors and have been fabricated for the detection of glucose,[46-47] ethanol,[48] metal ions,[49-53] creatinine,[54] organophosphorus compounds,[55-56] pH and ionic strength,[57-59] surfactants,[60] and carbohydrates.[61] Such sensors are advantageous because they provide for facile detection of a large variety of analytes with the added benefit of not requiring specialized equipment. Not only could such sensors be useful for rapid detection, providing a large advantage over many other sensing approaches, but the ability to precisely tune the mechanical and material properties of the sensor allows for use in a variety of different applications from real-time monitoring of cell culture to detection in non-aqueous environments. Due to the large potential of CCA-hydrogel based sensing platforms, the remainder of this work will focus on explaining and further developing this analytical technique.

Table 2.1 Selected photonic crystal sensors, analytes, and response mechanisms

Sensor Type	Target analyte	Recognition molecule/strategy	Mechanism of hydrogel response	Sensitivity	Dynamic range	Ref.
CCA	Hg^{2+}	Urease-Urea Reaction	Donnan Potential	1 ppb	< 20 ppb	49
	Pb^{2+} / Hg^{2+}	Aptamer	Cross-linking	1 nM	< 1 mM	53
	Creatinine	Creatinine deiminase/ 2-nitrophenol	Polymer-solvent interaction parameter, χ	10 µM	< 1 mM	54
	Ethanol	Polymer-solvent interaction	Polymer-solvent interaction parameter, χ	10%	< 100%	48
	Glucose	Phenylboronic acid	Donnan potential	50 µM	< 40 mM	61
	Parathion	Acetylcholinesterase	Donnan potential	4.2 fM	< 42 pM	56
	Candida albicans (bacteria)	Concanavalin A	Cross-linking	32 CFU/mL	< 6 x 10^7 CFU/mL	35
	Concanavalin A	Mannose	Crosslinking	0.02 mg/mL	< 2 mg/mL	34
Inverse Opal	Acetate	Thiourea	Donnan potential	1 mM	< 10 mM	36
	Cyanide	Trifluoroacetyl	Donnan potential (major) Polymer-solvent interaction parameter, χ (minor)	0.1 µM	< 1 mM	37
	Alcohols	Polymer-solvent interaction	Polymer-solvent interaction parameter, χ	10%	< 90%	38
	Glucose	Phenylboronic acid	Donnan Potential	0.1 mM	< 100 mM	39
RI	Warfarin	Human serum albumin	Mean RI change	0.12 µM	< 400 µM	29
	4-carboxybenzene sulfonamide	Carbonic anhydrase II	Mean RI change	2 µM	< 500 µM	29
	Pepsin	Protein zein	Mean RI change	240 ng	< 1 µg	32
	Human IgG	Protein A	Mean RI change	1 nM	< 2.5 µM	29
	Cell secreted MMP	Gelatin	Mean RI change	0.37 pM	< 0.37 µM	33

2.3 Crystalline Colloidal Array Synthesis and Self-Assembly

The highly-charged nanoparticles are typically synthesized through free-radical emulsion polymerization in the presence of a charged comonomer. This synthesis technique can be used to prepare monodispersed particles ranging in diameter from ~100 nm to 500 nm.[62] The reaction includes an emulsifier, low water-soluble monomers and cross-linkers, and an initiator. The

surface charge and size of the particles may be tuned by varying the charged monomer concentration, non-charged monomer concentration, and surfactant concentration.

Aqueous suspensions of the monodispersed, highly-charged particles self-assemble into ordered 3D arrays in low ionic strength environments. Self-assembly is driven through electrostatic repulsion of the thousands of charge groups present on the surface of the particles. The 3D arrays are non-close packed structures that minimize the system free energy by assembling into either face-centered cubic (FCC) or body-centered cubic (BCC) lattice structures. The self-assembled structure is dependent upon the size, surface charge, and volume fraction of the colloidal particles. BCC structures are typically found in low volume fractions (less than ~5%) and smaller particle sizes (< 100 nm), whereas FCC structures are typically found in higher volume fractions and larger particle sizes.[63-64] The lattice spacing is typically several times the diameter of the particle and assembled structures have been found to be stable with particle-particle distances up to 1 μm.[65] Lattice spacing can be rationally tuned by changing the particle size, surface charge, particle concentration, and ion concentration in the aqueous medium. By tuning the lattice spacing it is possible to achieve efficient diffraction in the near-UV, visible, and near-IR spectral regions.

2.4 Hydrogel-Encapsulated Crystalline Colloidal Arrays

The self-assembly and ordering of the CCA is dependent upon the electrostatic repulsion between particles and can easily be disordered by the presence of ions, impurities, or through vibration, giving rise to a highly dynamic system. Given that many analytes of interest are themselves ionic or occur in ionic solutions, it is necessary to stabilize the CCA. This is achieved by polymerizing the nanoparticles into a hydrogel network, thereby locking the structure in place and forming a polymerized crystalline colloidal array (PCCA) (**Figure 2.3**). Fabrication of

PCCAs is performed by solubilizing water soluble, nonionic monomers and cross-linkers in the aqueous CCA solution. Commonly used chemically cross-linked monomers include acrylamides and their derivatives,[60-61] (meth)acrylate and their derivatives,[66] and physically cross-linkable polymers, such as poly(vinyl alcohol).[67-68] To that solution a mixed bed ion exchange resin is added to remove any ionic impurities that may destabilize the pseudo-crystalline structure. The solution is injected into a mold and polymerization is performed by UV initiation of a free radical photoinitiator.

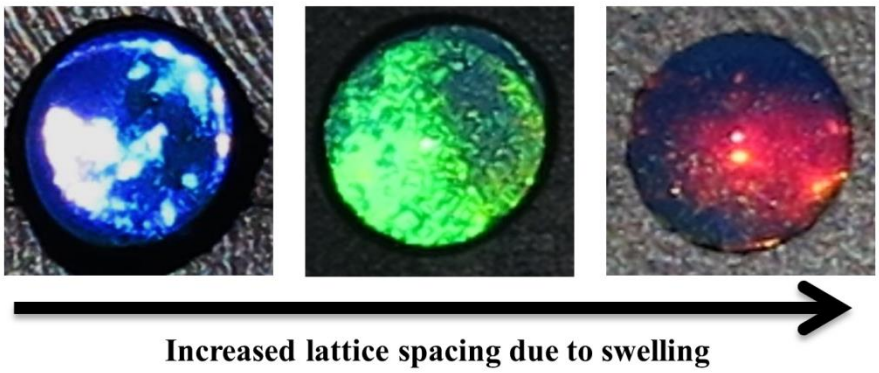

Figure 2.3 Optically diffracting hydrogels functionalized with negative charge groups. Swelling and diffraction shift is caused by equilibration in solutions of decreasing ionic strength.

2.5 Response Mechanism for Analyte Induced Hydrogel Volume Transitions

The individual components of the composite nanoparticle-hydrogel material have very specific functions. The CCA provides the optical, or measurable, response of the sensing platform via Bragg diffraction. The hydrogel matrix provides the stimuli-responsive aspect of the device through volumetric transitions in response to a specific analyte. By combining these two components it is possible to develop a stimuli-responsive material with an easily visualized, colorimetric output.

2.5.3 Smart Hydrogels

Hydrogels are cross-linked polymers capable of absorbing large volumes of water.[69] They possess a wide degree of mechanical flexibility due to their water content and can be tailored for specific functionalities. The network properties of hydrogels are influenced by the monomers and cross-linkers used and are highly tunable. Over the past several decades, researchers have developed a variety of stimuli-responsive hydrogels, termed smart hydrogels, which are capable of undergoing large property changes in response to a small environmental signal.[70-71]

Smart hydrogels can undergo changes in swelling state via a multitude of external stimuli such as pH and ionic strength,[72-74] temperature,[75-76] solvent conditions,[77-78] and enzyme activity.[79] Though there are a variety of polymer species available for fabricating smart polymers, the majority are synthesized from meth(acrylate) derivatives.[80] The hydrogel response type is dependent upon the functional group of the polymer, the basic polymer repeat unit, and the copolymer composition.[81] For example, hydrogels that are pH responsive contain either acid or base pendant groups on the polymer network that elicit a pH induced volume transition (See **Table 2.2** for further examples). The behavior of most stimuli-responsive hydrogels can be understood in terms of ionic interactions, hydrophobic interactions, hydrogen bonding, and van der Waals interactions.[82] Due to the immense tunability of smart hydrogels, they have found widespread applications in the biomedical research,[83-84] sensor development,[85] and drug delivery.[82]

Table 2.2 Select stimuli and functional group for smart hydrogel systems

Stimulus	Common Functional Groups	Example Monomers	Ref.
pH	Pendant acid or base groups	Acrylic Acid	42, 85
Temperature	Hydrophobic groups	N-isopropylacrylamide	60, 85
Ionic Strength	Ionic groups	Acrylic Acid	57, 58, 85
Glucose	Boronic-based groups	3-(acrylamido)phenylboronic acid	46,47, 85
Metal Ions	Crown ether	4-acrylamidobenzo-18-crown-6	49, 50, 51
Enzyme	Natural enzymatically degradable polymers or peptide cross-linkers	Hyaluronic Acid	33, 79, 82

2.5.4 Osmotic Pressures of the Hydrogel Systems

Volume transitions within the majority of smart hydrogel may be elicited via three distinct mechanisms, as presented by the Flory-Huggins theory.[86] Within the hydrogel, the total Gibbs free energy (ΔG_{tot}) is the sum of the elastic free energy (ΔG_{elas}), the free energy of mixing (ΔG_{mix}), and the ionic free energy (ΔG_{ion}):

$$\Delta G_{tot} = \Delta G_{elas} + \Delta G_{mix} + \Delta G_{ion} \qquad (\mathbf{2.2})$$

Similarly to the total free energy, the total osmotic pressure (Π_{tot}) of the system, derived by dividing the change in free energy by the change in hydrogel volume, is the sum of the component osmotic pressures:

$$\Pi_{tot} = \Pi_{elas} + \Pi_{mix} + \Pi_{ion} \qquad (\mathbf{2.3})$$

At equilibrium the total osmotic pressure of the system sums to zero. Thus, analyte derived changes to any of the three free energies results in a change in osmotic pressure and a volume transition within the hydrogel, resulting in a visible color change of the composite material that can be correlated to analyte concentration.

2.5.5 Elastic Free Energy

The osmotic pressure due to the elastic free energy of the system is dependent upon the cross-link density (v_e), system temperature (T), the unstrained volume of the hydrogel (V_m), and the equilibrated hydrogel volume (V):

$$\Pi_E = -\frac{1}{2} RT v_e \left(\frac{V_m}{V}\right)^{1/3} \qquad \textbf{(2.4)}$$

The main sources of change to the osmotic pressure of the elastic free energy are due to altering the cross-link density which may be achieved through making or breaking polymer or ionic bonds or through the formation of supramolecular complexes.[87-88] An increase in cross-link density increases the elastic restoring force of the system and, thus, acts to reduce the hydrogel volume. Conversely, decreasing the elastic restoring force reduces the energetic penalty for swelling, resulting in a larger hydrogel volume. Sensing mechanisms that rely on altering cross-link density are desirable because the response is less dependent upon solution conditions such as ionic strength and pH.

2.5.6 Free Energy of Mixing

As with the osmotic pressure due to the elastic free energy, the osmotic pressure due to the free energy of mixing is dependent upon the system temperature and the equilibrium polymer volume. Along with those parameters, the osmotic pressure due to the free energy of mixing is also dependent upon the molar solvent volume (V_s), the dry hydrogel volume (V_o), and the Flory-Huggins interaction parameter (χ):

$$\Pi_M = -\frac{RT}{V_s}\left[ln\left(1 - \frac{V_o}{V}\right) + \frac{V_o}{V} + \chi\left(\frac{V_o}{V}\right)^2\right] \qquad \textbf{(2.5)}$$

The predominant method for altering the osmotic pressure of the free energy of mixing is to alter the Flory-Huggins interaction parameter. The Flory-Huggins interaction parameter accounts for the thermodynamic preference of the polymer to interact with itself relative to interacting with

the solvent. Altering the Flory-Huggins interaction parameter may be achieved through changing the composition and structure of the polymer or by changing the solvent environment. For example, polymer-solvent systems with large interaction parameters indicate a greater dislike of the polymer for the solvent and a preference for the polymer network to exclude solvent and, thus, contract. The opposite is also true, polymer-solvent systems with smaller interaction parameters will tend to favor mixing and, therefore, an increased equilibrium volume. Although altering the interaction parameter can have a powerful effect on the equilibrium volume of the hydrogel and can be used to increase the sensitivity of the polymer system to a given analyte, it is also a potential source of interference due to solution conditions such as ionic strength, temperature, and system impurities potentially altering the value of the parameter.[89-90]

2.5.7 Ionic Free Energy

The osmotic pressure due to the ionic free energy is predominantly dependent upon the concentration gradient of mobile ion inside the hydrogel (c_x) to the surrounding environment (c_x^*):

$$\Pi_{ion} = RT \sum (c_x - c_x^*) \qquad (1)$$

The magnitude of the concentration gradient, and therefore the osmotic pressure due to the ionic free energy, is dependent upon the concentration of immobilized ions inside the hydrogel.[91] The presence of immobilized ions inside the hydrogel creates a local ion concentration which is greater than the ion concentration of the surrounding solution, thus creating an ion gradient and electrical potential called a Donnan potential.[86] This Donnan potential results in an osmotic pressure differential between the interior and exterior of the hydrogel and causes solvent and counterions to rush into the hydrogel, increasing the hydrogel volume and neutralizing the charges. The Donnan potential may be attenuated by altering the ionic strength of the solution.

For example, at high ionic strengths the magnitude of the concentration gradient is greatly reduced and the osmotic pressure due to the ionic free energy goes to zero. Thus, a hydrogel response that is dependent upon the Donnan potential is only feasible when the ionic strength of the solution is low and the ionic strength and pH are well controlled.

2.6 References

(1) Wang, H.; Zhang, K. Q., *Sensors (Basel)* **2013,** *13* (4), 4192-4213.

(2) Joannopoulos, J. D.; Villeneuve, P. R.; Fan, S. H., *Nature* **1997,** *386* (6621), 143-149.

(3) Yablonovitch, E., *Phys Rev Lett* **1987,** *58* (20), 2059-2062.

(4) John, S., *Phys Rev Lett* **1987,** *58* (23), 2486-2489.

(5) John, S., *Nat Mater* **2012,** *11* (12), 997-999.

(6) Paquet, C.; Kumacheva, E., *Mater Today* **2008,** *11* (4), 48-56.

(7) Yan, Q. F.; Wang, L. K.; Zhao, X. S., *Adv Funct Mater* **2007,** *17* (18), 3695-3706.

(8) Ma, X. Y.; Yan, Z. J., *Int J Mod Phys B* **2007,** *21* (16), 2761-2768.

(9) Zhao, Y. J.; Xie, Z. Y.; Gu, H. C.; Zhu, C.; Gu, Z. Z., *Chem Soc Rev* **2012,** *41* (8), 3297-3317.

(10) Whitney, H. M.; Kolle, M.; Andrew, P.; Chittka, L.; Steiner, U.; Glover, B. J., *Science* **2009,** *323* (5910), 130-133.

(11) Wang, J. Y.; Cao, Y.; Feng, Y.; Yin, F.; Gao, J. P., *Adv Mater* **2007,** *19* (22), 3865-+.

(12) Parker, A. R.; McPhedran, R. C.; McKenzie, D. R.; Botten, L. C.; Nicorovici, N. A. P., *Nature* **2001,** *409* (6816), 36-37.

(13) Vukusic, P., *Phys World* **2004,** *17* (2), 35-39.

(14) Choi, S. Y.; Mamak, M.; von Freymann, G.; Chopra, N.; Ozin, G. A., *Nano Lett* **2006,** *6* (11), 2456-2461.

(15) Colodrero, S.; Ocana, M.; Miguez, H., *Langmuir* **2008,** *24* (9), 4430-4434.

(16) Kinoshita, S.; Yoshioka, S., *Chemphyschem* **2005,** *6* (8), 1442-1459.

(17) Zi, J.; Yu, X. D.; Li, Y. Z.; Hu, X. H.; Xu, C.; Wang, X. J.; Liu, X. H.; Fu, R. T., *P Natl Acad Sci USA* **2003,** *100* (22), 12576-12578.

(18) Zhang, X. P.; Ma, X. M.; Dou, F.; Zhao, P. X.; Liu, H. M., *Adv Funct Mater* **2011,** *21* (22), 4219-4227.

(19) Vukusic, P.; Sambles, J. R., *Nature* **2003,** *424* (6950), 852-855.

(20) Darragh, P. J.; Gaskin, A. J.; Terrell, B. C.; Sanders, J. V., *Nature* **1966,** *209* (5018), 13-&.

(21) Carlson, R. J.; Asher, S. A., *Appl Spectrosc* **1984,** *38* (3), 297-304.

(22) Zhao, Y. J.; Zhao, X. W.; Hu, J.; Xu, M.; Zhao, W. J.; Sun, L. G.; Zhu, C.; Xu, H.; Gu, Z. Z., *Adv Mater* **2009,** *21* (5), 569-+.

(23) Blanco, A.; Chomski, E.; Grabtchak, S.; Ibisate, M.; John, S.; Leonard, S. W.; Lopez, C.; Meseguer, F.; Miguez, H.; Mondia, J. P.; Ozin, G. A.; Toader, O.; van Driel, H. M., *Nature* **2000,** *405* (6785), 437-440.

(24) Vukusic, P.; Sambles, J. R., *Nature* **2003,** *424* (6950), 852-5.

(25) Lou, S.; Guo, X. M.; Fan, T. X.; Zhang, D., *Energ Environ Sci* **2012,** *5* (11), 9195-9216.

(26) Ge, J. P.; Yin, Y. D., *Angew Chem Int Edit* **2011,** *50* (7), 1492-1522.

(27) Nair, R. V.; Vijaya, R., *Prog Quant Electron* **2010,** *34* (3), 89-134.

(28) Cunningham, B. T.; Laing, L., *Expert Rev Proteomic* **2006,** *3* (3), 271-281.

(29) Cunningham, B. T.; Li, P.; Schulz, S.; Lin, B.; Baird, C.; Gerstenmaier, J.; Genick, C.; Wang, F.; Fine, E.; Laing, L., *J Biomol Screen* **2004,** *9* (6), 481-490.

(30) Shamah, S. M.; Cunningham, B. T., *Analyst* **2011,** *136* (6), 1090-1102.

(31) Chan, L. L.; Gosangari, S. L.; Watkin, K. L.; Cunningham, B. T., *Sensor Actuat B-Chem* **2008,** *132* (2), 418-425.

(32) Orosco, M. M.; Pacholski, C.; Miskelly, G. M.; Sailor, M. J., *Adv Mater* **2006,** *18* (11), 1393-+.

(33) Kilian, K. A.; Lai, L. M. H.; Magenau, A.; Cartland, S.; Bocking, T.; Di Girolamo, N.; Gal, M.; Gaus, K.; Gooding, J. J., *Nano Lett* **2009,** *9* (5), 2021-2025.

(34) Zhang, J. T.; Cai, Z. Y.; Kwak, D. H.; Liu, X. Y.; Asher, S. A., *Anal Chem* **2014,** *86* (18), 9036-9041.

(35) Cai, Z. Y.; Kwak, D. H.; Punihaole, D.; Hong, Z. M.; Velankar, S. S.; Liu, X. Y.; Asher, S. A., *Angew Chem Int Edit* **2015,** *53* (44), 13036-13040.

(36) Kado, S.; Otani, H.; Nakahara, Y.; Kimura, K., *Chem Commun* **2013,** *49* (9), 886-8.

(37) Li, X.; Peng, L.; Cui, J.; Li, W.; Lin, C.; Xu, D.; Tian, T.; Zhang, G.; Zhang, D.; Li, G., *Small* **2012,** *8* (4), 612-8.

(38) Pan, Z.; Ma, J. K.; Yan, J.; Zhou, M.; Gao, J. P., *J Mater Chem* **2012,** *22* (5), 2018-2025.

(39) Lee, Y. J.; Pruzinsky, S. A.; Braun, P. V., *Langmuir* **2004,** *20* (8), 3096-3106.

(40) Guo, C.; Zhou, C. H.; Sai, N.; Ning, B. A.; Liu, M.; Chen, H. S.; Gao, Z. X., *Sensor Actuat B-Chem* **2012,** *166*, 17-23.

(41) Fu, X. Q.; Guo, M.; Wu, J.; Zhan, S. X., *Acta Chim Sinica* **2012,** *70* (5), 611-616.

(42) Holtz, J. H.; Asher, S. A., *Nature* **1997,** *389* (6653), 829-832.

(43) Goponenko, A. V.; Asher, S. A., *J Am Chem Soc* **2005,** *127* (30), 10753-10759.

(44) Muscatello, M. M. W.; Stunja, L. E.; Thareja, P.; Wang, L. L.; Bohn, J. J.; Velankar, S. S.; Asher, S. A., *Macromolecules* **2009,** *42* (13), 4403-4406.

(45) Smith, N. L.; Hong, Z. M.; Asher, S. A., *Analyst* **2014,** *139* (24), 6379-6386.

(46) Alexeev, V. L.; Sharma, A. C.; Goponenko, A. V.; Das, S.; Lednev, I. K.; Wilcox, C. S.; Finegold, D. N.; Asher, S. A., *Anal Chem* **2003,** *75* (10), 2316-2323.

(47) Holtz, J. H.; Holtz, J. S. W.; Munro, C. H.; Asher, S. A., *Anal Chem* **1998,** *70* (4), 780-791.

(48) Chen, C.; Zhu, Y. H.; Bao, H.; Shen, J. H.; Jiang, H. L.; Peng, L. M.; Yang, X. L.; Li, C. Z.; Chen, G. R., *Chem Commun* **2011,** *47* (19), 5530-5532.

(49) Arunbabu, D.; Sannigrahi, A.; Jana, T., *Soft Matter* **2011,** *7* (6), 2592-2599.

(50) Baca, J. T.; Finegold, D. N.; Asher, S. A., *Analyst* **2008,** *133* (3), 385-390.

(51) Asher, S. A.; Sharma, A. C.; Goponenko, A. V.; Ward, M. M., *Anal Chem* **2003,** *75* (7), 1676-1683.

(52) Yan, F. Y.; Asher, S., *Anal Bioanal Chem* **2007,** *387* (6), 2121-2130.

(53) Ye, B. F.; Zhao, Y. J.; Cheng, Y.; Li, T. T.; Xie, Z. Y.; Zhao, X. W.; Gu, Z. Z., *Nanoscale* **2012,** *4* (19), 5998-6003.

(54) Sharma, A. C.; Jana, T.; Kesavamoorthy, R.; Shi, L. J.; Virji, M. A.; Finegold, D. N.; Asher, S. A., *J Am Chem Soc* **2004,** *126* (9), 2971-2977.

(55) Walker, J. P.; Kimble, K. W.; Asher, S. A., *Anal Bioanal Chem* **2007,** *389* (7-8), 2115-2124.

(56) Walker, J. P.; Asher, S. A., *Anal Chem* **2005,** *77* (6), 1596-1600.

(57) Lee, K.; Asher, S. A., *J Am Chem Soc* **2000,** *122* (39), 9534-9537.

(58) Xu, M.; Goponenko, A. V.; Asher, S. A., *J Am Chem Soc* **2008,** *130* (10), 3113-3119.

(59) Cui, Q. Z.; Wang, W.; Gu, B. H.; Liang, L. Y., *Macromolecules* **2012,** *45* (20), 8382-8386.

(60) Zhang, J. T.; Smith, N.; Asher, S. A., *Anal Chem* **2012,** *84* (15), 6416-6420.

(61) Asher, S. A.; Alexeev, V. L.; Goponenko, A. V.; Sharma, A. C.; Lednev, I. K.; Wilcox, C. S.; Finegold, D. N., *J Am Chem Soc* **2003,** *125* (11), 3322-3329.

(62) Reese, C. E.; Guerrero, C. D.; Weissman, J. M.; Lee, K.; Asher, S. A., *J Colloid Interf Sci* **2000,** *232* (1), 76-80.

(63) Rundquist, P. A.; Photinos, P.; Jagannathan, S.; Asher, S. A., *J Chem Phys* **1989,** *91* (8), 4932-4941.

(64) Tandon, S.; Kesavamoorthy, R.; Asher, S. A., *J Chem Phys* **1998,** *109* (15), 6490-6496.

(65) Asher, S. A.; Kesavamoorthy, R.; Jagannathan, S.; Rundquist, P., *Nonlinear Optics Iii* **1992,** *1626*, 238-242.

(66) Zhang, J. T.; Wang, L. L.; Luo, J.; Tikhonov, A.; Kornienko, N.; Asher, S. A., *J Am Chem Soc* **2011,** *133* (24), 9152-9155.

(67) Muscatello, M. M. W.; Asher, S. A., *Adv Funct Mater* **2008,** *18* (8), 1186-1193.

(68) Jiang, H. L.; Zhu, Y. H.; Chen, C.; Shen, J. H.; Bao, H.; Peng, L. M.; Yang, X. L.; Li, C. Z., *New J Chem* **2012,** *36* (4), 1051-1056.

(69) Okay, O., *Springer Ser Chem Se* **2009,** *6*, 1-14.

(70) Dusek, K.; Patterso.D, *J Polym Sci A2* **1968,** *6* (7pa2), 1209-&.

(71) Khokhlov, A. R.; Starodubtzev, S. G.; Vasilevskaya, V. V., *Adv Polym Sci* **1993,** *109*, 123-175.

(72) Kozlovskaya, V.; Chen, J.; Tedjo, C.; Liang, X.; Campos-Gomez, J.; Oh, J. W.; Saeed, M.; Lungu, C. T.; Kharlampieva, E., *J Mater Chem B* **2014,** *2* (17), 2494-2507.

(73) Best, J. P.; Neubauer, M. P.; Javed, S.; Dam, H. H.; Fery, A.; Caruso, F., *Langmuir* **2013,** *29* (31), 9814-9823.

(74) He, L. H.; Fullenkamp, D. E.; Rivera, J. G.; Messersmith, P. B., *Chem Commun* **2011,** *47* (26), 7497-7499.

(75) Yang, K. W.; Wan, S. C.; Chen, B. B.; Gao, W. X.; Chen, J. X.; Liu, M. C.; He, B.; Wu, H. Y., *Carbohyd Polym* **2016,** *136*, 300-306.

(76) Nemethy, A.; Solti, K.; Kiss, L.; Gyarmati, B.; Deli, M. A.; Csanyi, E.; Szilagyi, A., *Eur Polym J* **2013,** *49* (9), 2392-2403.

(77) Qiu, Y.; Park, K., *Adv Drug Deliver Rev* **2012,** *64*, 49-60.

(78) White, E. M.; Yatvin, J.; Grubbs, J. B.; Bilbrey, J. A.; Locklin, J., *J Polym Sci Pol Phys* **2013,** *51* (14), 1084-1099.

(79) Ifkovits, J. L.; Burdick, J. A., *Tissue Eng* **2007,** *13* (10), 2369-2385.

(80) Kopecek, J., *Biomaterials* **2007,** *28* (34), 5185-5192.

(81) Ahmed, E. M., *J Adv Res* **2015,** *6* (2), 105-121.

(82) Soppimath, K. S.; Aminabhavi, T. M.; Dave, A. M.; Kumbar, S. G.; Rudzinski, W. E., *Drug Dev Ind Pharm* **2002,** *28* (8), 957-974.

(83) Tanaka, T., *Sci Am* **1981,** *244* (1), 124-&.

(84) Shibayama, M.; Tanaka, T., *Adv Polym Sci* **1993,** *109*, 1-62.

(85) Buenger, D.; Topuz, F.; Groll, J., *Prog Polym Sci* **2012,** *37* (12), 1678-1719.

(86) Flory, P. J., *Principles of polymer chemistry*. Cornell University Press: Ithaca,, 1953; p 672 p.

(87) Alexeev, V. L.; Sharma, A. C.; Goponenko, A. V.; Das, S.; Lednev, I. K.; Wilcox, C. S.; Finegold, D. N.; Asher, S. A., *Anal Chem* **2003,** *75* (10), 2316-23.

(88) Reese, C. E.; Asher, S. A., *Anal Chem* **2003,** *75* (15), 3915-3918.

(89) Horkay, F.; Tasaki, I.; Basser, P. J., *Biomacromolecules* **2000,** *1* (1), 84-90.

(90) Brannonpeppas, L.; Peppas, N. A., *Chem Eng Sci* **1991,** *46* (3), 715-722.

(91) Ohshima, H.; Ohki, S., *Biophys J* **1985,** *47* (5), 673-678.

CHAPTER 3 – OBJECTIVE AND SPECIFIC AIMS

3.1 Objective

The overall objective of this research was to investigate the utility of using chemically and structurally modified photonic crystal hydrogels for the optical detection of enzyme activity, nucleic acids, and monitoring microbial fermentation. The first aim of this work was to demonstrate that CCA-based PC sensors are capable of label-free detection of kinase activity through altering the immobilized charge state of the hydrogel backbone. The natural evolution to the first aim was to then investigate the material and solution properties that influence the response of the CCA-based PC sensor to kinase activity. Due to the significant influence of solution ionic strength and immobilized charge concentration, it was then of interest to demonstrate the ability of CCA-based PC sensors for the detection of DNA hybridization events. Lastly, a temperature sensitive CCA-based PC sensor was developed for the detection of hydrophobic solvents and small molecules with the goal of monitoring microbial fermentation. Completion of these aims serves to increase the understanding of the capability of these materials as a biological sensing platform.

3.2 Specific Aims

3.2.1 Aim 1 – Development of a CCA-based PC sensor for the detection of kinase activity

Detection of post-translational modifications is an area of interest for the study of cellular mechanisms and disease pathways and for drug discovery. There are a variety of enzyme families that catalyze post-translational modifications and, of these, kinases are one of the most important and well understood. To develop a CCA-based PC sensing platform capable of detecting kinase activity we have: 1) fabricated a kinase-responsive optically diffracting

hydrogel through functionalization with a charged peptide substrate, 2) demonstrated the sensor response to enzyme activity both as a function of enzyme dose and reaction time, and 3) successfully used the sensing platform to detect a small molecule kinase inhibitor.

3.2.2 Aim 2 – Investigation of the material properties that influence sensor response to kinase activity.

The effectiveness of an assay is determined by the sensitivity and selectivity of the sensing platform. Sensor selectivity may be modulated through the analyte recognition mechanism and is largely determined by the selectivity of the catalytic domain of the enzyme. Response sensitivity is largely determined by the material properties of the sensor. To understand the factors that affect the sensitivity of the CCA-based PC sensing platform we implemented a theoretical model of the response based on Flory's description of swelling in polymer networks. Using the model, we modulated parameters such as charge density, Flory-Huggins interaction parameter, and the cross-link density of the materials to determine which properties may be rationally tuned to improve sensor response. Additionally, we experimentally altered and tuned the materials properties of the hydrogel and implemented the improved sensing platform for the detection of phosphorylation events in cell lysate.

3.2.3 Aim 3 – Demonstrate the utility of CCA-based PC sensors for the detection of DNA hybridization events.

Due to the sensitivity of the CCA-based PC sensor for the detection of changes in immobilized charge it was of interest to extend this sensing approach from sensing post-translational modifications to sensing binding of biomolecules. One binding event of particular interest is DNA hybridization. Development of a CCA-based PC sensing platform for the detection of DNA hybridization was achieved through the fabrication of a DNA-responsive optically diffracting hydrogel. The response of the DNA-responsive hydrogels was then investigated as a function of target DNA concentration and solution ionic strength. The platform

was then successfully shown to differentiate between a perfect match target, a single base pair mismatch target, and a methylated perfect match target.

3.2.4 Aim 4 – Development of a temperature sensitive CCA-based PC sensor for the detection of hydrophobic solvents and small molecules with the goal of high-throughput monitoring of microbial fermentation.

Engineering of microbial strains for the improved production of alcohols and other usable byproduct is of interest for use in renewable energy. Consequently, we developed a high-throughput platform for monitoring microbial fermentation. This platform was developed by fabricating thermal-responsive optically diffracting hydrogels in a 96-well plate format. We then investigated the sensitivity of the platform to ethanol and glucose as a function of both lower critical solution temperature (LCST) and measurement temperature. Lastly, we cultured wild-type (WT) *Saccharomyces cerevisiae* and used the sensing platform to monitor the depletion of glucose as a function of time along with an endpoint measurement of ethanol, the main fermentation product.

CHAPTER 4 – PHOTONIC CRYSTAL KINASE BIOSENSOR

4.1 Introduction

Protein kinases are a critical family of enzymes that modulate virtually all cellular processes, including differentiation, proliferation, motility, and apoptosis, and thus cell function.[1,2] Modulation of cell function by kinases is the result of the phosphorylation of target protein substrates that are involved in intracellular signaling pathways. At the molecular level, the phosphorylation of protein substrates provides a mechanism by which target proteins may be activated or deactivated. The resulting activation or deactivation of target proteins can, in turn, lead to aberrant signal transduction if levels of kinase activity are altered, as is the case in many disease states. Due to their central role in signal transduction, kinases have been implicated in a myriad of diseases, making kinases among the most important targets for therapeutic molecules.[3]

Despite the importance of kinases as potential drug targets, robust, high-throughput screening methods for kinase inhibitors and activators are sorely lacking. Kinases are inherently difficult to assay due to the lack of measurable signal (i.e., pH or color change) upon protein phosphorylation. Conventional biochemical methods to assay kinase activity nearly all use radiolabeled or fluorescent substrates or phospho-specific antibodies.[4-6] Such methods, while sensitive, require expensive reagents and frequently involve multiple steps. Notably, phospho-specific antibodies are also challenging to generate and of limited availability for phosphoserine and -threonine residues.[7] Additionally, fluorescent methods, which are widely based on quenching, polarization, or resonance energy transfer, are prone to signal interference by small molecules that may fluoresce or quench fluorescent signals. Kinase screening efforts may alternatively rely on biophysical binding techniques such as NMR,[8] surface plasmon resonance,[9] differential scanning fluorimetry (i.e., thermal shift assay),[10] and quartz crystal microbalance,[11]

although traditional binding assays are limited in their ability to measure changes in catalytic activity. More recently, screening methods based on improved mass spectroscopy techniques,[12] computational approaches,[13,14] and label-free nanoparticle aggregation assays[15-18] have been reported. Ultimately, the development of high-throughput kinase screening platforms would greatly facilitate the discovery of potential drug candidates as well as probes for studying cellular mechanisms involved in disease and, moreover, kinase profiling.

Here, we present a novel photonic crystal biosensor for the optical detection of peptide phosphorylation and, thus, kinase activity. The biosensor is composed of a crystalline colloidal array (CCA) polymerized into a hydrogel matrix. The photonic crystal, shown in Scheme, consists of negatively charged, vinyl-functionalized polystyrene particles that self-assemble into a pseudocrystal structure that diffracts light in the visible spectrum. Once polymerized, the hydrogel is functionalized with a kinase recognition sequence that is subject to phosphorylation, which alters the electrostatic environment within the hydrogel. The resulting change in the electrostatics induces a Donnan potential that causes the hydrogel to swell and, in turn, the lattice spacing of the CCA to increase and the wavelength of peak diffraction to red shift. Such an optical response can be monitored spectrophotometrically, after rinsing of mobile ions, to readily quantify the effect of kinase inhibitors and activators on phosphorylation activity. Incorporation of photonic crystals into swellable polymer networks has been reported previously for detecting pH changes and charged species, including small molecules and metal ions.[19-22] Importantly for biosensing applications, because the CCAs developed here diffract light at visible wavelengths ($\geq$400 nm), the adsorption of light by small molecules, which typically adsorb light in the UV range, will not interfere with the CCA signal. Additionally, because the sensing platform is

reagentless, kinase activity may be screened without exogenous labels or components, representing a significant advantage over conventional kinase assay methods.

4.2 Experimental Methods

4.2.1 Peptide Synthesis and Purification

LRRASLG was synthesized by standard solid-phase peptide synthesis methods. Fluorenylmethoxycarbonyl (Fmoc)-protected amino acids, MBHA Rink amide resin, and (2-(1H-benzotriazol-1-yl)-1,1,3,3-tetramethyluronium hexafluorophosphate (HBTU) were purchased from Chem-Impex International, Inc. Solvents (ACS grade) were purchased from Fisher Scientific and used as received without further purification. Manual solid-phase synthesis was performed under constant agitation at room temperature. Prior to each amino acid coupling step, a solution of 20 vol% piperidine in DMF was used for Fmoc deprotection of the N-terminal amine of the peptide. The amino acid to be coupled was pre-activated with HBTU and N,N-diisopropylethylamine (DIPEA) in DMF (4 mol eq. amino acid : 3.96 mol eq. HBTU : 6 mol eq. DIPEA) before being added to the reaction vessel. After addition of the final amino acid, the final N-terminus Fmoc group was removed and the peptide was cleaved from the resin through agitation in a solution of trifluoroacetic acid (TFA), water, and triisopropylsilane (95 vol eq.: 2.5 vol eq.: 2.5 vol eq.). The peptide was recovered by precipitation in ethyl ether and dried. Peptide was subsequently resuspended in water and 0.1 vol% TFA to a final concentration of 2 mg/mL and filtered prior to HPLC purification. The product was purified by reverse-phase HPLC (Agilent 1100) using a Phenomenex Jupiter column (stationary phase: 10 μm, dC_{12}) and linear gradient of 0% to 95% acetonitrile in water (HPLC grade), both with 0.1 vol% TFA. After purification, the peptide product was rotary evaporated to remove excess solvents and lyophilized. The mass and purity of the LRRASLG product were verified using matrix-assisted

laser desorption/ionization time-of-flight mass spectroscopy (MALDI-TOF, ABI Voyager-DE STR) at the University of Colorado Mass Spectrometry Central Analytical Lab. For control experiments using phosphorylated peptide, crude LRRApSLG was purchased from GenScript, Inc. and purified by HPLC following the same procedure as for non-phosphorylated LRRASLG.

4.2.2 Synthesis of Colloidal Suspensions of PS Spheres

Monodisperse, negatively-charged polystyrene (PS) spheres were synthesized by emulsion polymerization as described elsewhere.[23] The colloidal suspension of PS spheres utilized for the presented experiments contained 110 nm diameter PS particles with a polydispersity of ~4% at a concentration of ~11 wt% in water (**Figure 4.1**). Particles were stored with BioRad mixed bed resin (AG 501-X8) to remove ion impurities from the synthesis and to stabilize the colloidal suspension. The particle diameter and polydispersity were determined by dynamic light scattering measurements (Titan DynaPro with the Dyna V6.3.4 software package). Zeta potential was measured using a Malvern Zetasizer Nano ZS.

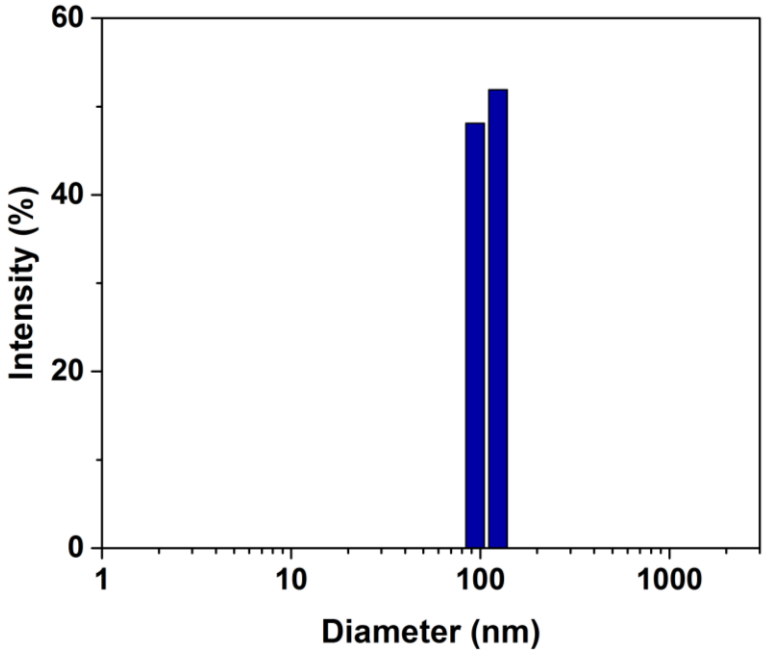

Figure 4.1 Dynamic light scattering data of PS particles with 110 nm diameter and a polydispersity of ~4%.

4.2.3 Polymerization of Hydrogel

Hydrogels were synthesized by free radical polymerization using Irgacure 2959 (BASF) as the photoinitiator. Solutions containing 0.1 g acrylamide monomer, 2.5 mg N,N,`-methylenebisacrylamide, and 1.5 g of the suspension of colloidal PS spheres were shaken with 0.1 g of ion exchange resin (BioRad AG 501-X8). The solution was centrifuged to remove resin and photoinitiator (at 10 wt% in DMSO) was added to an overall final concentration of 0.05 wt%. The solution was then injected into a cell composed of a vinyl support film (BioRad) and 2 clean microscope slides separated by a 126.4±0.7 μm parafilm spacer. Photopolymerization was performed by flood exposure of the sample to 365 nm light from a UV mercury lamp at an irradiance of 15 mW/cm^2 for 1 h. Films were rinsed and equilibrated with ultrapure water.

4.2.4 Peptide Functionalization of Hydrogel

The polyacrylamide hydrogel backbone was hydrolyzed for 4 h at room temperature using a solution of 10 vol% N,N,N',N'-tetramethylethylenediamine (TEMED) in a 0.1 M aqueous solution of NaOH. After extensive rinsing, the hydrogel was submerged in a 0.1 M MES buffer at pH 5 containing 0.1 M NaCl, 30 mM 1-ethyl-3-[d-dimethylaminopropyl] carbodiimide hydrochloride (EDC), and 50 mM N-hydroxysulfosuccinimide (Sulfo-NHS) for 20 min at 4 ℃.[24] The solution was then exchanged for a 0.1 M sodium phosphate buffer at pH 7.5 with 0.1 M NaCl and 100 mM LRRASLG or LRRApSLG, and allowed to react for 16 h at room temperature. Peptide loading in the hydrogel was increased by repeating the EDC/NHS and peptide treatments for a total of 4 reaction cycles. Functionalized samples were thoroughly rinsed with and stored in sodium phosphate buffer at 4 ℃.

4.2.5 Kinase Treatment

The hydrogel-encapsulated crystalline colloidal arrays were immersed in 50 mM tris-HCl buffer with 10 mM $MgCl_2$ and 1 mM ATP. The catalytic subunit of protein kinase A (New England Biolabs) was added in varying concentrations (0 – 25 U/μL) and incubated at 30 °C for varying times (0 – 8 h). The phosphorylation reaction was stopped by inactivating the kinase via submerging the samples in water at 65 °C for 20 min. For experiments in the presence of inhibitor, PKA was pre-incubated for 10 min at 30 °C in 50 mM tris-HCl buffer with 10 mM $MgCl_2$, 100 μM ATP, and varying concentrations of H-89 inhibitor (Cell Signaling Technologies, 0.1 nM– 100 μM). The CCA biosensors were incubated in the enzyme-inhibitor solution for 3 h at 30 °C and then the kinase was inactivated as described above.

4.2.6 Phosphatase Treatment

The hydrogel-encapsulated crystalline colloidal arrays were immersed in 50 mM bis-tris-propane HCl, at pH 6.0, with 1 mM $MgCl_2$ and 0.1 mM $ZnCl_2$. Antarctic phosphatase (New England Biolabs) was added at 0.1 U/μL and incubated at 37 °C for 16 h. The dephosphorylation reaction was stopped by inactivating the phosphatase via submerging the samples in water at 70 °C for 5 min.

4.2.7 Characterization of Immobilized Charge by Hydrogel Staining

Hydrogel staining was performed using toluidine blue O (Sigma-Aldrich) to stain for negative charges[25] and acid orange 7 (Sigma-Aldrich) to stain for positive charges.[26] Samples were stained with toluidine blue O by rinsing thoroughly with a 0.1 mM NaOH solution and incubating with 0.5 mM stain in 0.1 mM NaOH for 3 h at 25 °C. Samples were rinsed three times with the 0.1 mM NaOH solution and the dye adsorbed to the hydrogel was extracted by incubating at room temperature with a 50 vol% aqueous acetic acid solution for 15 min.

Absorbance measurements were taken at 633 nm and the dye concentration in the extracted solution was calculated using an absorptivity of $\varepsilon = 7x10^4\ cm^{-1}\ M^{-1}$. Samples were stained with acid orange 7 by rinsing thoroughly with a 1 mM HCl solution and incubating with 0.5 mM stain in 1 mM HCl for 3 h at 25 °C. Samples were rinsed three times with the 1 mM HCl solution and dye adsorbed into the hydrogel was extracted by incubating at room temperature with a 30 vol% aqueous ethanolamine solution for 20 min. Absorbance measurements were taken at 468 nm and the dye concentration in the extracted solution was calculated using an absorptivity of $\varepsilon = 1.6x10^4\ cm^{-1}\ M^{-1}$.

4.2.8 Diffraction Measurements

Optical diffraction from the hydrogel-encapsulated CCA was measured with an Ocean Optics USB-4000 fiber-optic spectrophotometer operating in reflectance mode (angle of incidence of 15° from the sample surface normal). Spectra were collected across the UV-visible range (375 - 850 nm). Samples were thoroughly rinsed with ultrapure water to remove all mobile ions and to achieve an equilibrium extent of hydrogel swelling before each optical measurement was performed.

4.3 Results and Discussion

Optically diffracting hydrogel thin films (126.4 ± 0.7 μm thick) were fabricated on vinyl-functionalized plastic substrates via the process outlined in **Figure 4.2**. Specifically, acrylamide was photopolymerized in the presence of a colloidal suspension of charged, vinyl-functionalized polystyrene (PS) latex spheres (10–12% w/w), resulting in the cross-linking of a stable CCA within the hydrogel network.

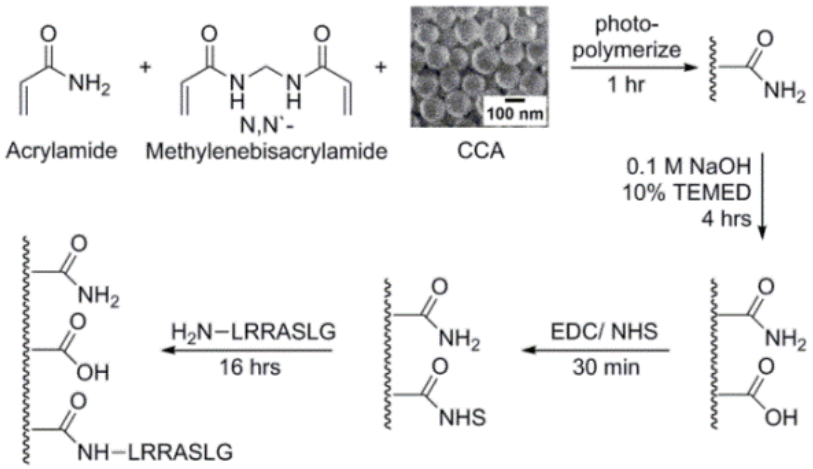

Figure 4.2 Fabrication of a kinase responsive CCA biosensor.

The negatively charged polystyrene particles were synthesized by emulsion polymerization in water using surfactants to stabilize the initial micelle formation and the polymer particles that were formed.[27, 28] Dynamic light scattering (**Figure 4.1**) and scanning electron microscopy were used to characterize the resulting spheres, which were found to pack into a dense array in thin films (see the scanning electron micrograph in **Figure 4.2** as well as to be monodisperse in size with a diameter of 110 ± 2 nm. In solution, the formation of the CCA is the result of the electrostatic forces between negatively charged sulfonate groups (zeta potential of −33 ± −2 mV) on the surface of the polystyrene particles. Electrostatic repulsion between the particles causes them to adopt a face-centered cubic lattice structure that has the lowest configurational energy. The crystal structure and thus volume of the hydrogel dictates the diffraction spectrum of the CCA sensor through Bragg's law.[29] **Figure 4.3** shows example diffraction spectra of hydrogel-encapsulated CCAs as a function of immobilized carboxylate groups, the concentration of which was controlled by varying the hydrolysis time. Reflectance spectroscopy is used to quantify the wavelength of peak diffraction, although distinct changes in film color can also be observed by eye. The photograph corresponding to a total negative-charge

concentration of 25 mM appears almost black due to excessive swelling of the hydrogel, which causes the hydrogel to diffract at wavelengths beyond the visible spectrum.

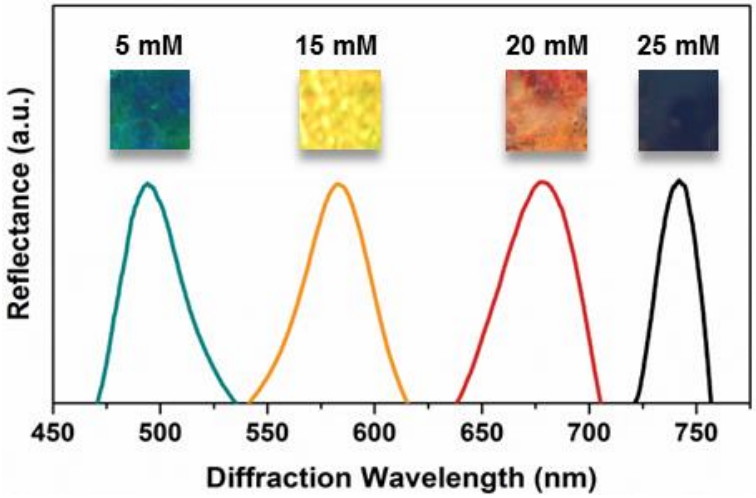

Figure 4.3 Redshift in peak optical reflectance of hydrogel-encapsulated CCAs with increasing concentrations of immobilized negatively charged groups (at pH 5.5). The inset images (~5x5 mm^2) show visual color changes of the hydrogels. The total concentrations of negative charge from 5 to 25 mM, as indicated above each image, were measured by colorimetric staining.

Upon preparation of the CCA-containing hydrogel, the hydrogel was functionalized with a peptide substrate (LRRASLG) for protein kinase A (PKA). The target LRRASLG peptide contains two positively charged arginine residues and has a net positive charge of +0.5 at neutral pH after phosphorylation of the serine. Briefly, peptide functionalization was enabled by converting free amide groups in the hydrogel to carboxylate groups through base hydrolysis. A two-step EDC/NHS reaction was subsequently used to form an amide linkage between the carboxylates in the hydrogel and the N-terminus amine of the peptide substrate. The functionalization reaction was performed in a high ionic strength environment to shield the immobilized negative charges, thus preventing excessive swelling and mechanical failure (i.e., delamination, fracturing, or wrinkling) of the hydrogel. Each step of the fabrication process was confirmed by diffraction measurements and the extent of reaction was quantified by staining for

immobilized charges. Prior to measuring optical diffraction, the hydrogels were rinsed extensively to remove free, mobile ions, which would interfere with the sensor's response. By rinsing the sensor, the structure and response of the CCA is dependent only on the immobilized charges. To stain the hydrogels for negative and positive charges, the gel was reacted with toluidine blue O and acid orange 7, respectively, as reported previously.[30, 31] The hydrogels were incubated in aqueous solutions containing each stain for 3 h to allow for complete dye adsorption, after which the hydrogels were rinsed to remove any loosely adsorbed dye. Following rinsing, the bound dye was extracted via treatment with a strong acid or base and quantified by UV–vis absorbance. For determination of immobilized charge concentrations in the hydrogel, the ratio of dye to immobilized charge was assumed to be 1:1.

The immobilized charge concentration in the hydrogel-encapsulated CCAs is shown in **Figure 4.4**, as quantified by charge staining, following the polymerization, hydrolysis, and peptide functionalization steps. Charge concentration was determined on a per unit volume basis of the unswollen hydrogel. The hydrogels had an initial wavelength of peak diffraction of 500 nm and a concentration of negative charge of 5 mM, which was due to the presence of the PS spheres. Hydrolysis increased the amount of negative charge immobilized in the hydrogel by 7-fold, although this represents a low overall conversion (<1 mol %) of the available amide groups to carboxylates. The larger concentration of immobilized charge increases the Donnan potential, causing the hydrogel to swell and the wavelength of peak diffraction to red shift to >800 nm. Functionalizing the hydrogel with LRRASLG reduced the concentration of negative charges, due to reactive coupling through the carboxylate groups, and increased the concentration of positive charges due to the two arginine residues (with pK_a's of 12.48) present in the peptide. Based on the charge concentration and an overall mole balance, the concentration of peptide immobilized

in the hydrogel was calculated to be ~10 mM (See **Appendix B.1** for details). The reduction in negative charge was more significant than that expected based on the corresponding increase in the concentration of positive charge. Peptide functionalization also caused a dramatic blue shift in the optical response to a wavelength of peak diffraction of 495 nm, which was less than that of the initial CCA. Likely these observed effects were due to the formation of ionic cross-links between positive and negative charges in the hydrogel, which reduced the concentrations of free charges and increased gel stiffness, resulting in less swelling. Potential cross-linking of immobilized charges was accounted for in the estimation of immobilized peptide concentration. In comparison, unhydrolyzed samples and samples without peptide showed no change in charge concentration.

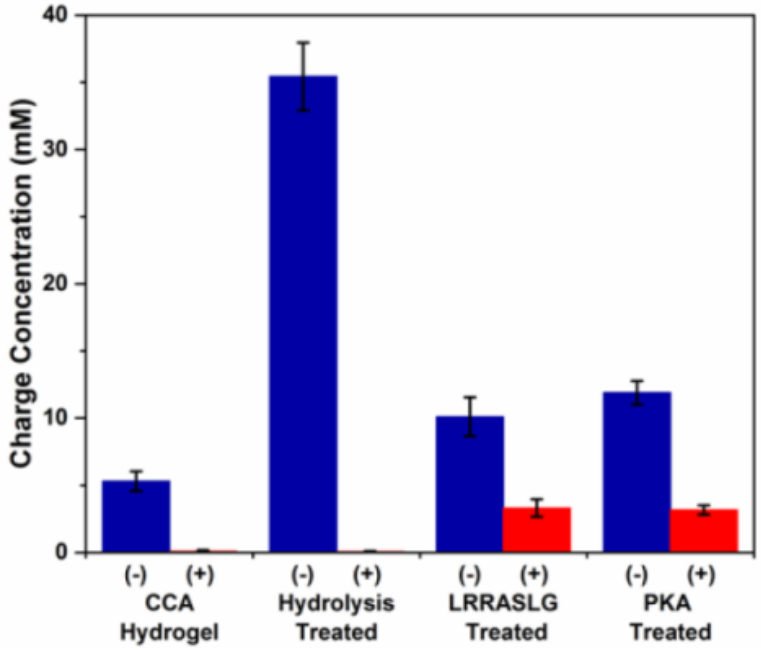

Figure 4.4 Concentration of immobilized charge in kinase responsive CCA-containing hydrogels characterized by colorimetric staining. The blue and red bars represent negative (-) and positive (+) charge concentrations, respectively. The positive charge concentrations in the CCA-containing hydrogel and the hydrolyzed hydrogel were determined to be negligible within error. Error bars represent ±1σ, as measured for the first three steps for 30 samples. The PKA treatment was performed at a concentration of 16 U/μL and 8 h and is reported for 3 independent samples.

The screening and quantification of kinase activity using the photonic crystal biosensor was demonstrated as a function of phosphorylation reaction time and enzyme concentration. Time course measurements (**Figure 4.5a)** were performed by incubating the biosensor at 30 °C in 0.5 mL of reaction buffer (50 mM Tris-HCl, pH 7.5, with 10 mM $MgCl_2$ and 1 mM ATP) with 16 U/μL of PKA. The reaction was quenched by heating the biosensor at 65 °C for 20 min to denature the enzyme. The biosensor was then thoroughly rinsed in water to remove any excess reactants or mobile ions that may reduce the extent of swelling. The red shift in the wavelength of peak diffraction is reported, representing the difference in Bragg diffraction between post- and pre-PKA treatment (see **Appendix B, Figure B.2** for raw spectra). The red shift in the wavelength of peak diffraction due to the increase in immobilized negative charge was detected in as short as 30 min and increased with reaction times from 0 to 4 h, whereas after 4 h a plateau in sensor response was observed. Control samples prepared with phosphorylated LRRASLG (LRRApSLG) indicated that a red shift in peak diffraction of 100 nm corresponded to 30% phosphorylation (**Appendix B, Figure B.1**). Based on this, the response of the sensor in the time course plot is presumably limited by the extent of phosphorylation of the immobilized peptide. Limitations in phosphorylation may result from the loss of PKA activity from enzyme instability as well as partial inaccessibility of the immobilized peptide. Inamori et al.[32] previously observed that phosphorylation of LRRASLG tethered to gold surfaces by PKA was limited to ~20 mol % of that in solution. Moreover, while it is also plausible that this plateau may result from diffusional limitations, this is unlikely based on previous literature that has shown that proteins of similar size were able to diffuse 50 μm into CCA-impregnated hydrogels within 20 min, which is much deeper than the optically active region of the film being probed here.[33, 34] Additionally, a dose response curve, showing red shift in peak diffraction as a function of PKA

concentration, is shown in **Figure 4.5b**. Phosphorylation of the peptide by PKA can also be detected by staining as a small increase in the immobilized negative charge concentration (**Figure 4.4**, PKA treated samples). However, this response is significantly weaker than that measured optically, indicating the higher sensitivity of the CCA's optical response as compared to that of the charge staining assay. Control samples (not shown) for both the time course and dose response data were incubated in the presence of PKA, but without ATP. Time course controls were incubated for 8 h (also with 16 U/μL enzyme), and dose response controls were incubated with 25 U/μL enzyme (also for 2 h). Both sets of controls showed a shift in the wavelength of peak diffraction of <1 nm upon enzyme treatment, confirming that the apparent response was due solely to phosphorylation. Moreover, the sensor showed no change in response in the presence of exogenous charged molecules, indicating that there is no interference from such molecules (**Appendix B, Figure B.3**).

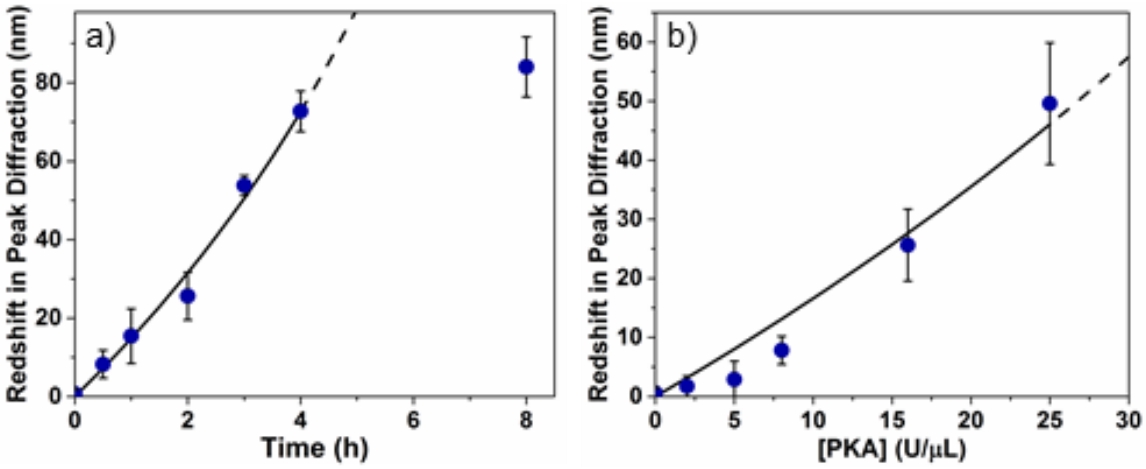

Figure 4.5 Redshift in the wavelength of peak diffraction as a function of (a) time upon treatment with 10 U/μL of PKA and (b) PKA concentration for 2 h treatments. The solid black curves represent model predictions over the range fitted, and the dashed curves are extrapolations from the model. Error bars represent ±1σ from the mean for 3 independent samples.

To demonstrate the utility of the CCA sensor to screen for kinase inhibitors, the sensor response to PKA activity in the presence of the small molecule kinase inhibitor H-89 was measured (**Figure 4.6**). The small molecule inhibitor H-89 competitively inhibits PKA by binding to the ATP binding cleft.[35] The activity of PKA in the presence of H-89 was measured by preincubating 16 U/μL of PKA with 0.1 nM–100 μM H-89 for 10 min in reaction buffer (50 mM Tris-HCl, pH 7.5, 10 mM $MgCl_2$, 100 μM ATP). Following incubation of PKA with H-89, the CCA sensor was immersed in the reaction solution for 3 h at 30 °C after which residual PKA activity was quenched as above and the system was rinsed with water. As expected, increasing the concentration of H-89 decreased the red shift in peak diffraction, which is attributed to decreasing PKA activity. Notably, the IC50 value of H-89 was determined to be 68 nM, which is in agreement with previously reported literature values.

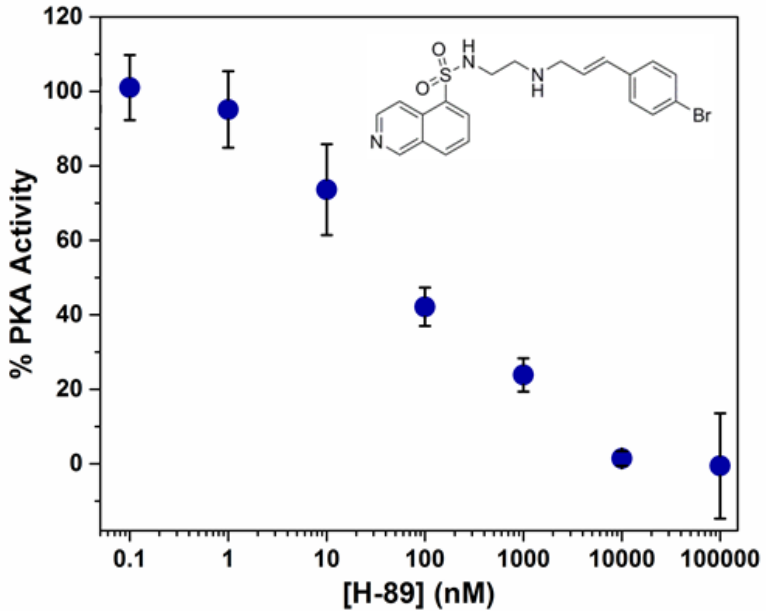

Figure 4.6 Sensitivity of kinase responsive CCA sensor to PKA inhibition by H-89 (inset structure). Inhibition of PKA by H-89 was measured with varying inhibitor concentrations (0-10^5 nM) and 16 U/μL of PKA. Hydrogel-encapsulated CCAs were incubated with the enzyme and inhibitor for 3 h at 30 °C. Error bars represent ±1σ from the mean for 3 independent samples.

The optical response of CCAs encapsulated in the kinase responsive hydrogel is dependent on not only the kinase activity but also (i) the material properties of the hydrogel, (ii) the immobilized charge distribution in the hydrogel, and (iii) the ionic character of the surrounding environment. A model of swelling in ionic polymer networks elucidates these dependencies and was used to fit the time course and dose response data in **Figure 4.5** (solid curves, for derivation see **Appendix A**). The model predictions fit the experimental data well and allow for quantification of the extent of phosphorylation and enzyme kinetics including k_{cat} from the optical response (**Appendix B, Figure B.4**). Deviation of the time course data from the model predictions at long incubation times (8 h) may be, as suggested previously, due in part to the loss in PKA activity over time or peptide inaccessibility. By elucidating the critical parameters that are associated with the diffraction of the biosensor in response to kinase activity, the model ultimately may be used to improve the sensitivity of the sensor and thus reduce the detection limit and permit shorter reaction times. For example, the model predicts that increased sensitivity may be achieved by increasing the concentration of accessible peptide, eliminating extraneous charges immobilized in the hydrogel (e.g., unreacted carboxylate functionalities), or by lowering the elastic restoring force upon swelling by reducing Young's modulus of the gel (i.e., cross-linking density). Excess negative charges in the polymer backbone may be eliminated by linking the peptide through chemistries that do not require hydrolysis of the hydrogel (e.g., click reactions). Furthermore, although diffusional limitations do not affect the response of the sensor toward PKA, such limitations, which impact sensor response, with larger enzymes or proteins may be reduced by altering cross-linking density.

4.4 Conclusion

In summary, novel photonic crystal-containing polymer hydrogels that are responsive to peptide phosphorylation were developed for assaying kinase activity. Such hydrogels may be used as a sensing platform to identify kinase inhibitors or activators of kinase pathways, as well as for assaying kinase selectivity. The lack of exogenous fluorescent reagents or labels, furthermore, enhances the potential utility of the hydrogels for high-throughput screening, which may be enabled through preparation of the hydrogels in a multiplex format. Though the photonic crystal biosensor was specifically developed for screening purified kinases, washing and detection in pure water will allow for assaying biologically complex samples as well. We have also demonstrated that the sensor can be used to detect the reverse (i.e., dephosphorylation) reaction, involving the removal of immobilized negative charges, by phosphatases (**Appendix B, Figure B.5**). More broadly, such hydrogels may be used to assay the activity of other enzymes that catalyze post-translational modifications that alter substrate charge (e.g., sulfonation, acetylation, carboxylation, or amidation), thus providing a platform to screen a broad spectrum of protein or biomolecule modifications.

4.5 References

(1) Hunter, T., *Cell* **2000,** *100* (1), 113-127.

(2) Miduturu, C. V.; Deng, X. M.; Kwiatkowski, N.; Yang, W. N. A.; Brault, L.; Filippakopoulos, P.; Chung, E.; Yang, Q. K.; Schwaller, J.; Knapp, S.; King, R. W.; Lee, J. D.; Herrgard, S.; Zarrinkar, P.; Gray, N. S., *Chem Biol* **2011,** *18* (7), 868-879.

(3) Cohen, P.; Alessi, D. R., *Acs Chem Biol* **2013,** *8* (1), 96-104.

(4) Ko, K. C.; Choi, M. H.; Rho, J. K.; Park, S. H., *Sensor Actuat B-Chem* **2013,** *178*, 434-442.

(5) Prevel, C.; Pellerano, M.; Van, T. N.; Morris, M. C., *Biotechnol J* **2013**.

(6) Jeong, H. J.; Ohmuro-Matsuyama, Y.; Ohashi, H.; Ohsawa, F.; Tatsu, Y.; Inagaki, M.; Ueda, H., *Biosens Bioelectron* **2013,** *40* (1), 17-23.

(7) Koerber, J. T.; Thomsen, N. D.; Hannigan, B. T.; Degrado, W. F.; Wells, J. A., *Nat Biotechnol* **2013,** *31* (10), 916-+.

(8) Masterson, L. R.; Shi, L.; Metcalfe, E.; Gao, J. L.; Taylor, S. S.; Veglia, G., *Proc Natl Acad Sci U S A* **2011,** *108* (17), 6969-6974.

(9) Takeda, H.; Goshima, N.; Nomura, N., *Surface Plasmon Resonance: Methods and Protocols* **2010,** *627*, 131-145.

(10) Fedorov, O.; Niesen, F. H.; Knapp, S., *Kinase Inhibitors: Methods and Protocols* **2012,** *795*, 109-118.

(11) Xu, X.; Zhou, J.; Liu, X.; Nie, Z.; Qing, M.; Guo, M.; Yao, S., *Anal Chem* **2012,** *84* (11), 4746-53.

(12) Zinn, N.; Hopf, C.; Drewes, G.; Bantscheff, M., *Methods* **2012,** *57* (4), 430-440.

(13) Metz, J. T.; Johnson, E. F.; Soni, N. B.; Merta, P. J.; Kifle, L.; Hajduk, P. J., *Nat Chem Biol* **2011,** *7* (4), 200-202.

(14) Shen, M. Y.; Zhou, S. Y.; Li, Y. Y.; Pan, P. C.; Zhang, L. L.; Hou, T. J., *Mol Biosyst* **2013,** *9* (3), 361-374.

(15) Oishi, J., Asami, Y.; Mori, T.; Kang, J.-H.; Tanabe, M.; Niidome, T.; Katayama, Y. *ChemBioChem* **2007**, 8 (8), 875.

(16) Kang, J. H.; Asami, Y.; Murata, M.; Kitazaki, H.; Sadanaga, N.; Tokunaga, E.; Shiotani, S.; Okada, S.; Maehara, Y.; Niidome, T.; Hashizume, M.; Mori, T.; Katayama, Y., *Biosens Bioelectron* **2010,** *25* (8), 1869-74.

(17) Asami, Y.; Oishi, J.; Kitazaki, H.; Kamimoto, J.; Kang, J. H.; Niidome, T.; Mori, T.; Katayama, Y., *Anal Biochem* **2011,** *418* (1), 44-9.

(18) Xu, X.; Liu, X.; Nie, Z.; Pan, Y.; Guo, M.; Yao, S. *Anal. Chem* **2011**, 83, 52.

(19) Arunbabu, D.; Sannigrahi, A.; Jana, T., *Soft Matter* **2011,** *7* (6), 2592-2599.

(20) Holtz, J. H.; Asher, S. A., *Nature* **1997,** *389* (6653), 829-832.

(21) Walker, J. P.; Asher, S. A., *Anal Chem* **2005,** *77* (6), 1596-1600.

(22) Sharma, A. C.; Jana, T.; Kesavamoorthy, R.; Shi, L. J.; Virji, M. A.; Finegold, D. N.; Asher, S. A., *J Am Chem Soc* **2004,** *126* (9), 2971-2977.

(23) Reese, C. E.; Guerrero, C. D.; Weissman, J. M.; Lee, K.; Asher, S. A., *J Colloid Interface Sci* **2000,** *232* (1), 76-80.

(24) Hermanson, G. T., *Bioconjugate techniques*. 2nd edition. ed.; p.219-223.

(25) Nakajima, N.; Ikada, Y., *Bioconjugate Chem* **1995,** *6* (1), 123-130.

(26) Uchida, E.; Uyama, Y.; Ikada, Y., *Langmuir* **1993,** *9* (4), 1121-1124.

(27) Arunbabu, D.; Sannigrahi, A.; Jana, T., *J Appl Polym Sci* **2008,** *108* (4), 2718-2725.

(28) Reese, C. E.; Guerrero, C. D.; Weissman, J. M.; Lee, K.; Asher, S. A., *J Colloid Interface Sci* **2000,** *232* (1), 76-80.

(29) Asher, S. A.; Holtz, J.; Liu, L.; Wu, Z. J., *J Am Chem Soc* **1994,** *116* (11), 4997-4998.

(30) Nakajima, N.; Ikada, Y., *Bioconjugate Chem* **1995,** *6* (1), 123-130.

(31) Uchida, E.; Uyama, Y.; Ikada, Y., *Langmuir* **1993,** *9* (4), 1121-1124.

(32) Inamori, K.; Kyo, M.; Matsukawa, K.; Inoue, Y.; Sonoda, T.; Tatematsu, K.; Tanizawa, K.; Mori, T.; Katayama, Y., *Anal Chem* **2008,** *80* (3), 643-65

(33) Baca, J. T.; Finegold, D. N.; Asher, S. A., *Analyst* **2008,** *133* (3), 385-390.

(34) Tong, J.; Anderson, J. L., *Biophys J* **1996,** *70* (3), 1505-1513.

(35) Lochner, A.; Moolman, J. A., *Cardiovasc Drug Rev* **2006,** *24* (3-4), 261-74.

CHAPTER 5 – OPTICALLY DIFFRACTING HYDROGELS FOR SCREENING KINASE ACTIVITY IN VITRO AND IN CELL LYSATE: IMPACT OF MATERIAL AND SOLUTION PROPERTIES

5.1 Introduction

Optically diffracting and responsive materials based on the polymerization of photonic crystals within hydrogels have considerable utility as label-free chemical sensors.[1-5] As chemical sensors, these materials provide a platform by which the presence of an analyte is detectable via changes in the hydrogel volume. The resulting change in hydrogel volume alters the lattice spacing and, in turn, the apparent diffraction spectrum of the embedded photonic crystal. This modulation in spectrum can be readily detected via reflectance spectroscopy and, depending on the characteristic dimensions of the crystal, as a color change at visible wavelengths that can qualitatively be ascertained by eye. A volume change in the hydrogel may be coupled to molecular recognition of the analyte through the conjugation of a ligand that is selective for the analyte within the hydrogel network. Such materials have previously been reported for the detection of various small molecules, including glucose,[6-8] ammonia,[9] surfactants,[10] creatinine,[11] and parathion,[12, 13] as well as metal ions,[14-18] including Cu^{2+}, Co^{2+}, Ni^{2+}, Zn^{2+}, Hg^{2+}, and Pb^{2+}. This sensing approach has also been demonstrated in the context of measuring changes in solution pH.[19-21]

We have recently extended this sensing approach to the detection of enzyme activity while developing a novel sensor for kinases.[22] The sensor is comprised of a hydrogel-encapsulated crystalline colloidal array (CCA) that contains a target peptide, which is a substrate for protein kinase A (PKA). Phosphorylation of the peptide (LRRASLG), which is tethered to the hydrogel network, results in the addition of negative charge in the hydrogel that modifies the Donnan potential with the environment and causes the hydrogel volume to change (**Figure 5.1**).

With this sensor, we were able to detect phosphorylation events in as short as 30 min and, moreover, PKA levels on the order of 4 U/μL in solution. Additionally, the utility of the sensor to discern differences in PKA activity in the presence of an inhibitor was demonstrated, highlighting the potential use of the sensor for screening modulators of kinase activity. The lack of required exogenous fluorescent reagents or labels represents a significant advantage over conventional methods for assaying kinase.[23, 24] To the best of our knowledge, this work represents the first use of such sensors for quantitatively screening enzyme activity.

The aim of this work was to understand the impact of material properties on the response of kinase responsive CCA-containing hydrogels with the goal of improving the sensitivity of these materials to the phosphorylation activity of kinases. Specifically, in this work, the dependence of the optical response of the kinase sensor on material properties was investigated by modeling the swelling behavior of ionic polymer networks. Of particular focus, the model was used to examine the influence of the shear modulus of the hydrogel and the Flory-Huggins interaction parameter (χ), which describes polymer-solvent mixing, on the theoretical shift in peak diffraction of an ideal hydrogel system. The model was, furthermore, used to investigate the role of the ionic character of the surrounding environment (*i.e.*, solution ionic strength) on peak diffraction. This understanding was subsequently exploited to experimentally show how varying material properties and solution conditions enables the sensor response to be rationally tuned and, ultimately, improved. As part of this effort, we have investigated an alternative approach to synthesis of the hydrogel network to eliminate extraneous charges in the polymer backbone that reduce the sensitivity of the sensor to phosphorylation. This approach entails use of click chemistry, rather than hydrolysis of the hydrogel, to link the peptide substrate within the hydrogel (**Figure 5.2**). Such use of click chemistry permits the rapid and facile functionalization

of CCA-containing hydrogels with multiple, distinct recognition motifs for sensing orthogonal analytes. Additionally, we also examined the utility of our sensing approach to assay the activity of PKA in cell lysate to demonstrate the feasibility of using this approach to quantify changes in PKA regulation.

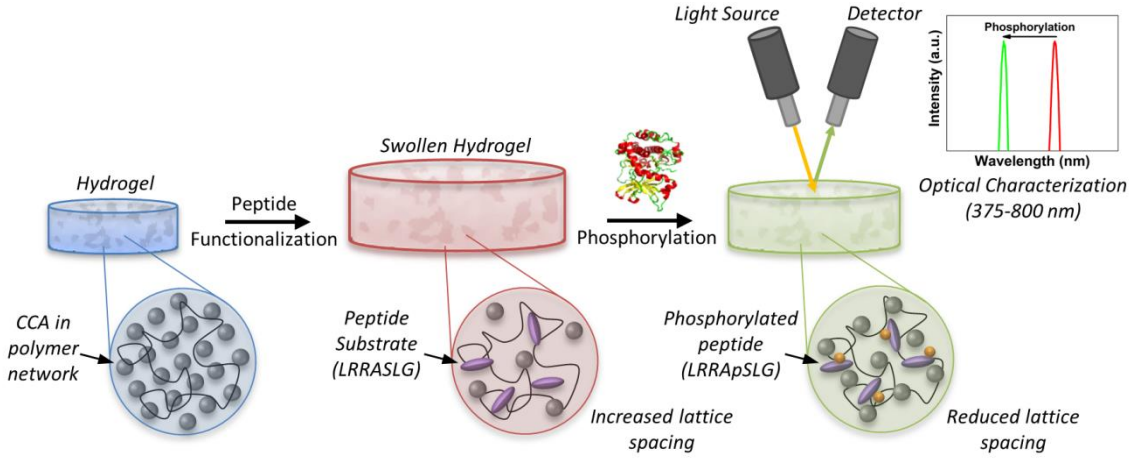

Figure 5.1 Schematic of the behavior of optically diffracting hydrogels in response to phosphorylation by kinase. The hydrogels undergo reversible swelling and change color as a function of altered lattice spacing due to peptide functionalization and phosphorylation.

5.2 Experimental Methods

5.2.1 Materials

Acrylamide (AA), *N,N'*-methylenebis(acrylamide) (BA), propargylamine, triethylamine, acryloyl chloride, and tris(3-hydroxypropyltriazolylmethyl)amine (THPTA) were purchased from Sigma-Aldrich (St. Louis, MO) and used without further purification. *N*-hydroxyethyl acrylamide (HEAA) and 2-hydroxyethyl acrylate (HEA) were purchased from Sigma-Aldrich and were purified over a column of basic alumina to remove inhibitors. Crude LRRASLG peptide was purchased from GenScript, Inc. (Piscataway, NJ) and purified via reverse-phase HPLC (Agilent 1100) using a Phenomenex (Torrance, CA) Jupiter column (stationary phase: 10 μm, dC_{12}). Azido-PEG4-NHS linker was purchased and used without further purification from

Conju-Probe (San Diego, CA). The catalytic subunit of protein kinase A (PKA) was purchase from New England Biolabs (Ipswich, MA).

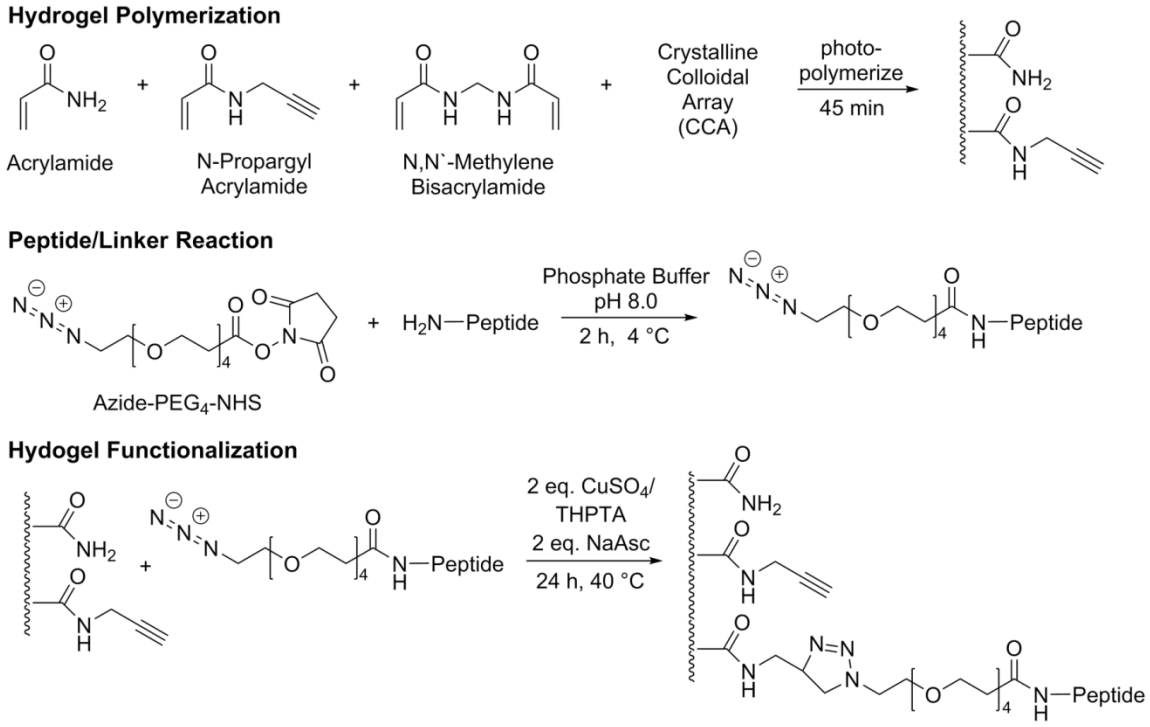

Figure 5.2 Preparation of optically diffracting kinase responsive hydrogels using click chemistry for peptide functionalization.

5.2.2 Synthesis of N-propargyl Acrylamide

N-propargyl acrylamide (PA) was synthesized according to a modified procedure described previously.[25, 26] Briefly, propargylamine (0.7 mL, 10.9 mmol) and triethylamine (1.83 mL, 13.1 mmol) were combined with anhydrous dichloromethane (DCM) (10 mL) in a flame dried round bottom flask under nitrogen. A solution of acryloyl chloride (1.02 mL, 12.6 mmol) and dry DCM (10 mL) was then added dropwise to the flask. The reaction was quenched with deionized water after reacting for 16 h at room temperature and washed three times with aqueous sodium bicarbonate, three times with deionized water, and once with a brine solution. The remaining organic phase was dried over anhydrous Na_2SO_4 and evaporated *in vacuo*. The

resulting product (yield: 403 mg, 34%), an off white crystalline solid, was characterized by NMR (Bruker Ascend^{TM} 400, 400 MHz).

5.2.3 Synthesis of Colloidal Suspensions of PS Spheres

Colloidal suspensions of monodisperse, negatively-charged polystyrene (PS) spheres were synthesized by emulsion polymerization following a previously described protocol.[27, 28] The colloidal suspension utilized for the presented experiments had a concentration of 11 wt% in water and contained 98 nm PS particles with a polydispersity of 1.1%, as determined by dynamic light scattering (Titan DynaPro with Dyna V6.3.4 software package). Particles were stored with a BioRad (Hercules, CA) mixed bed resin (AG 501-X8).

5.2.4 Hydrogel Polymerization

Hydrogels were photopolymerized by free radical polymerization using Irgacure 2959 (BASF; Florham Park, NJ) as the photoinitiator. Hydrogels were synthesized by solubilizing 0.025 - 0.1 g AA in 710 µL of the colloidal suspension. To this solution, a mixture of 1.25 mg BA and 5 mg PA in 40 µL of DMSO was added. The solution was then shaken with 0.1 g ion exchange resin and centrifuged to remove the resin. Photoinitiator (10 wt% in DMSO) was added to a final concentration of 0.05 wt%. The solution was then injected into a cell comprised of two clean microscope slides separated by a 273 ± 2 µm parafilm spacer. The samples were photopolymerized by flood exposure to 365 nm light from a UV mercury lamp with an irradiance of 15 mW/cm^2 for 45 min. Hydrogels with varying Flory-Huggins interaction parameters were prepared by substitution of 0-100% AA with HEA or HEAA monomer. All films were equilibrated in ultrapure water before use.

5.2.5 Hydrogel Functionalization with Peptide Substrate

The peptide LRRASLG was initially solubilized in 100 mM sodium phosphate buffer (pH 8.0) with 100 mM NaCl to a final concentration of 75 mM. One molar equivalent of azide-PEG4-NHS linker was dissolved in 20 µL DMSO and added to the peptide solution. The solution was reacted at 4°C for 2 h to completion, which was verified using matrix-assisted laser desorption ionization time-of-flight mass spectroscopy (MALDI-TOF, ABI Voyager-DE STR). Hydrogels to be functionalized were reacted with a solution containing 0.1 - 10 mM of linker-modified peptide and 2 equivalents each of $CuSO_4 \cdot 5H_2O$, THPTA, and sodium ascorbate (NaAsc) in ultrapure water. The reaction was incubated at 40°C for 24 h. Functionalization was verified by Raman spectroscopy (BioTools µ-BioRAMAN^{TM}) and detection of charged groups via hydrogel staining. Functionalized samples were thoroughly rinsed and stored in 100 mM sodium phosphate buffer (pH 8.0).

5.2.6 Characterization of Immobilized Charge by Colorimetric Hydrogel Staining

To detect the immobilization of positive charges after functionalization, hydrogels were stained with acid orange 7 (Sigma-Aldrich).[29] Samples were first rinsed thoroughly with 1 mM HCl and subsequently incubated with 0.5 mM stain in 1 mM HCl at 25 °C for 3 h. After incubation, samples were rinsed 3 times with HCl (1 mM) and adsorbed dye was extracted by incubating at room temperature with 30 vol% aqueous ethanolamine for 20 min. Absorbance of the extracted dye was measured at 468 nm from which the dye concentration was determined using the extinction coefficient of the dye ($\varepsilon = 1.6 \times 10^4$ cm^{-1} M^{-1}) and assuming that one dye molecule adsorbs to one positive charge.

5.2.7 Characterization of Modulus and Flory-Huggins Interaction Parameter of CCA-Containing Hydrogels

The shear modulus (*G'*) was measured with a TA Instruments (New Castle, DE) Ares series rheometer using parallel plate geometry. The modulus was measured both with a frequency-sweep from 0.1-100 rad/s with a fixed shear strain of 10% and a strain-sweep from 1-20% strain with a fixed frequency of 0.75 rad/s. The Flory-Huggins interaction parameter was calculated from the volume difference between non-strained and water equilibrated hydrogel, as measured by changes in the wavelength of peak diffraction. Buoyancy measurements in heptane, a non-solvent, were utilized to determine polymer volume fraction and dry hydrogel volume.

5.2.8 Kinase Treatment of Hydrogels

Hydrogels were immersed in 50 mM tris-HCl buffer (pH 7.5) with 10 mM $MgCl_2$ and 1 mM ATP. To initiate the kinase reaction, PKA was added in varying concentrations (0-10 U/µL), after which the hydrogel was incubated with PKA at 30°C for 2 h. The kinase reaction was terminated by inactivating the kinase by removing the hydrogels from the reaction solution and heating the hydrogels to 65°C for 20 min in 100 mM sodium phosphate buffer (pH 8.0).

5.2.9 Preparation of HEK293 Lysate

To collect cell lysate, human embryonic kidney 293 (HEK293) cells were seeded on 10 cm tissue culture-treated polystyrene plates in Dulbecco's Modified Eagle's Medium (DMEM) supplemented with 10% fetal bovine serum, 100 U/mL penicillin, 100 µg/mL streptomycin, and 1x GlutaMax (LifeTechnologies, Grand Island, NY) and incubated at 37 °C in 5% CO_2. Once the cells reached a confluence of approximately 90%, the media was replaced with serum-free DMEM in which the cells were incubated for 4 h. To stimulate PKA activation, 50 µM Forskolin (FSK) in DMSO (30 µL) was added to the media. Unstimulated samples were treated with DMSO in the absence of FSK. The cells were then incubated for 1 h and washed with

Dulbecco's phosphate-buffered saline. Cells were removed from plates by scraping in 300 µL of 50 mM Tris-HCl buffer (pH 7.5) containing 50 mM NaCl and 1.0 mM phenylmethanesulfonyl fluoride and lysed by sonication (200W and 10 s on ice). Cell lysate was clarified by centrifugation at 14,000 rpm for 15 min at 4 °C. Total protein concentration of the lysate was determined by Bradford assay.

5.2.10 Lysate Treatment of Hydrogels

Cell lysate was diluted in 50 mM tris-HCl buffer (pH 7.5) with 10 mM $MgCl_2$ and 1 mM ATP to a total protein concentration of 100 µg/mL. Samples containing the peptide PKI, which is a PKA specific inhibitor, were incubated on ice with 5 µM PKI for 10 min prior to hydrogel treatment. Hydrogels were immersed in the lysate samples and incubated at 30 °C for 4 h. The kinase reaction was terminated as described above.

5.2.11 Optical Diffraction Measurements

Optical diffraction measurements were taken with an Ocean Optics USB-4000 fiber-optic spectrophotometer operating in reflectance mode with an angle of incidence of 15° from the sample surface normal. Spectra were collected across the UV-visible range (375 -800 nm). Samples were thoroughly rinsed and equilibrated with either ultrapure water or varying ionic strength sodium phosphate buffer (pH 8.0) during characterization.

5.3 Results and Discussion

5.3.1 Hydrogel Functionalization with Peptide Substrate Using Click Chemistry Approach

To facilitate the investigation of hydrogel properties on the sensitivity of optically diffracting kinase responsive hydrogels, CCA-containing hydrogels were functionalized with LRRASLG via click modification. Copper (I)-catalyzed alkyne-azide cycloaddition (CuAAC) of the peptide substrate was enabled via copolymerization of an alkyne-containing monomer into

the hydrogel (**Figure 5.2**). CuAAC has previously be[3]en shown to be highly efficient at both tagging peptides and linking peptides to a variety of polymer systems.[30-39] Specifically, in this work, clickable photonic crystal biosensors were fabricated from AA and the alkyne-containing monomer PA, as well as low concentrations of the BA cross-linker. Because the hydrogel network is uncharged, the CCA is able to self-assemble without interference via electrostatic repulsions between the negatively-charged PS particles. Incorporation of the alkyne moiety in the hydrogel was confirmed with Raman spectroscopy (**Figure 5.3**), which showed a characteristic alkyne stretch at 2130 cm^{-1}. Notably, as expected, the stretch at 2130 cm^{-1} is absent in the spectra of CCA-containing hydrogels that were prepared with AA and BA only, serving as a control.

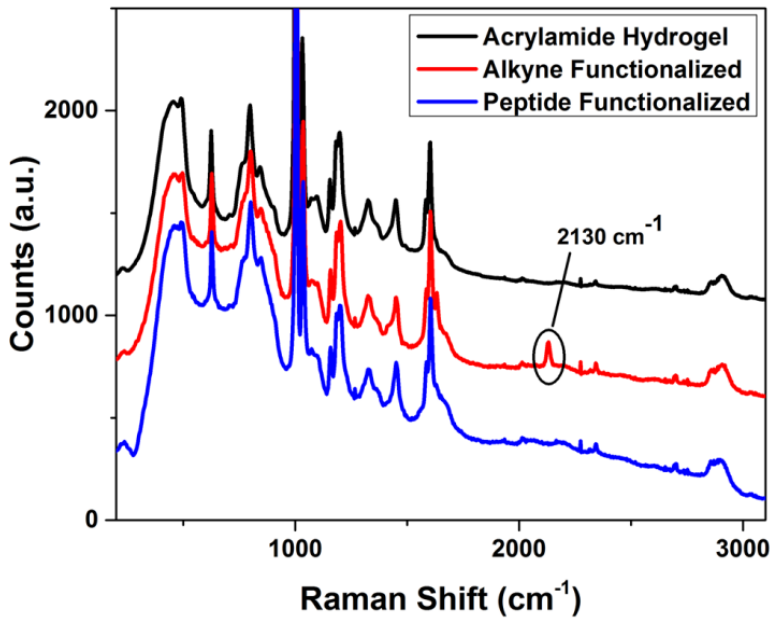

Figure 5.3 Raman spectra of an acrylamide CCA hydrogel (black), alkyne-functionalized CCA hydrogel (red), and peptide-functionalization CCA hydrogel (blue). An alkyne peak is seen at 2130 cm^{-1} in the hydrogel containing PA, which is not observed in hydrogels fabricated with acrylamide only. Peptide functionalization was performed by incubating the hydrogel with 2:1 H_2O:t-butanol in the absence of THPTA. After peptide functionalization, the alkyne peak is no longer detected indicating full conversion of the alkyne moieties.

For peptide attachment, LRRASLG was modified with a complementary reactive azide group by means of reaction of the N-terminal amino of the peptide with azide-PEG4-NHS. The reaction of the azide-modified peptide with the alkyne monomer in the hydrogel network was monitored through the disappearance of the alkyne stretch in the hydrogel. Under the reaction conditions used, the spectra of the peptide-functionalized hydrogels showed full conversion of the alkyne monomer. The immobilization of peptide within the hydrogel was further quantified by staining the hydrogel with a colorimetric dye that associates with positive charged residues in the peptide (the peptide contains two positively-charged arginine residues that, at neutral pH, can react with the dye). Charge staining indicated concentrations ranging from 0 - 21 mM of peptide immobilized in the hydrogel, as normalized to the unstrained volume of the hydrogel. At high peptide concentrations in the functionalization reaction (> 10 mM), the alkyne groups in the hydrogel were limiting relative to the concentration of azide groups in the reaction. It is plausible that a fraction of the alkyne groups may react with the acrylamide monomer during the formation of the hydrogel network,[40, 41] although the cross-linking densities of PA-containing hydrogels and hydrogels with only AA were similar when prepared with equivalent total concentrations of both monomers. Additionally, the alkyne groups may undergo dimerization as well as cycloisomerization, thereby also reducing the effective concentration of free alkynes.[42]

The CuAAC functionalization scheme that has been demonstrated allows for rapid incorporation of the target peptide, and also permits precise control over peptide concentration and thus the overall immobilized charge within the hydrogel. Additionally, this approach, which circumvents the need for hydrolysis of the hydrogel network for functionalization, eliminates extraneous charges in the hydrogel that alter sensitivity. The following sections present a simple model that describes the response of the peptide-functionalized biosensors to kinase activity, as

well as the experimental characterization of their behavior as a function of critical material properties and ionic character.

5.3.2 Theoretical Model of Optically Diffraction of Kinase Responsive CCA-Containing Hydrogels

Flory's description of swelling in ionic polymer networks[43] provides a theoretical basis to describe the optical response of hydrogel-encapsulated photonic crystals. At equilibrium, the total osmotic pressure $\Pi_T = \Pi_{ion} + \Pi_E + \Pi_M = 0$, where Π_{ion} is the osmotic pressure due to the Donnan potential, Π_E is the osmotic pressure due to the elastic restoring force, and Π_M is the osmotic pressure due to the free energy of mixing. Expressions for the individual terms of the overall pressure balance are given by:

$$\Pi_{ion} = RT\sum(c_x - c_x^*) \quad (1)$$

$$\Pi_E = -\frac{1}{2}RTv_e\left(\frac{V_m}{V}\right)^{1/3} \quad (2)$$

$$\Pi_M = -\frac{RT}{V_s}\left[ln\left(1-\frac{V_o}{V}\right)+\frac{V_o}{V}+\chi\left(\frac{V_o}{V}\right)^2\right] \quad (3)$$

where R is the universal gas constant and T is the system temperature. In the Donnan potential expression, c_x is the concentration of mobile ions of species x inside the hydrogel and c_x^* is the concentration of ions in the surrounding environment, and the summation is performed over all ionic species. Thus, the Donnan potential provides a driving force for swelling or shrinking the hydrogel depending on whether the net charge immobilized in the hydrogel increases or decreases, respectively, upon functionalization and kinase activity. In contrast, the elastic or mechanical term strictly resists deformation of the hydrogel from its undeformed state, with v_e representing the effective cross-linking density of the hydrogel, V_m is the unstrained hydrogel volume, and V is the actual hydrogel volume. The cross-linking density for the

materials used here was experimentally measured from the shear modulus, G', and the polymer volume fraction, ϕ.[43]

$$G' = v_e RT\phi^{1/3} \qquad (4)$$

The osmotic pressure for polymer-solvent mixing considers the thermodynamic preference of the polymer in the hydrogel to interact with itself relative to interacting with the solvent. This interaction strength is commonly described by χ between the polymer network and the solution, with larger values of χ indicating a greater dislike of the polymer for the surrounding environment and a preference of the hydrogel to contract and exclude solvent (*i.e.*, to minimize polymer-solvent interactions and to maximize polymer-polymer interactions). The variables V_s and V_o are the molar solvent volume and the dry hydrogel volume, respectively.

The optical response of hydrogel-encapsulated photonic crystals is directly related to volumetric changes in the hydrogel system described by Flory's description of swelling. The optical response in the photonic crystals detectors is dominated by Bragg diffraction, with the wavelength of peak diffraction being dictated by the lattice spacing of the crystal structure. Therefore a relationship between peak diffraction wavelength and the hydrogel volume can be defined:

$$\frac{\lambda}{\lambda_m} = \left(\frac{V}{V_m}\right)^{1/3} \qquad (5)$$

where λ is the peak diffraction wavelength from the hydrogel at volume $V$and λ_m is the peak diffraction wavelength of the unstrained volume V_m.

Figure 5.4 captures the optical response of hydrogel-encapsulated photonic crystals as function of the key material parameters, χ and the elastic modulus, of the hydrogel described by the Flory model for swelling. The model predicts that biosensors with such a design will be more sensitive (*i.e.*, displaying a larger optical response for a given stimulus) when materials are

selected to have smaller values of χ and the elastic modulus, such that the energetic penalty for hydrogel swelling is low. Moreover, the model suggests that the sensor response is more dependent on the magnitude of the interaction parameter rather than the elastic modulus. This prediction is a bit surprising and, although the elastic response of the hydrogel has been explored as a means to increase the sensitivity of detection, tuning the strength of the polymer-solvent interactions has not been carefully considered.

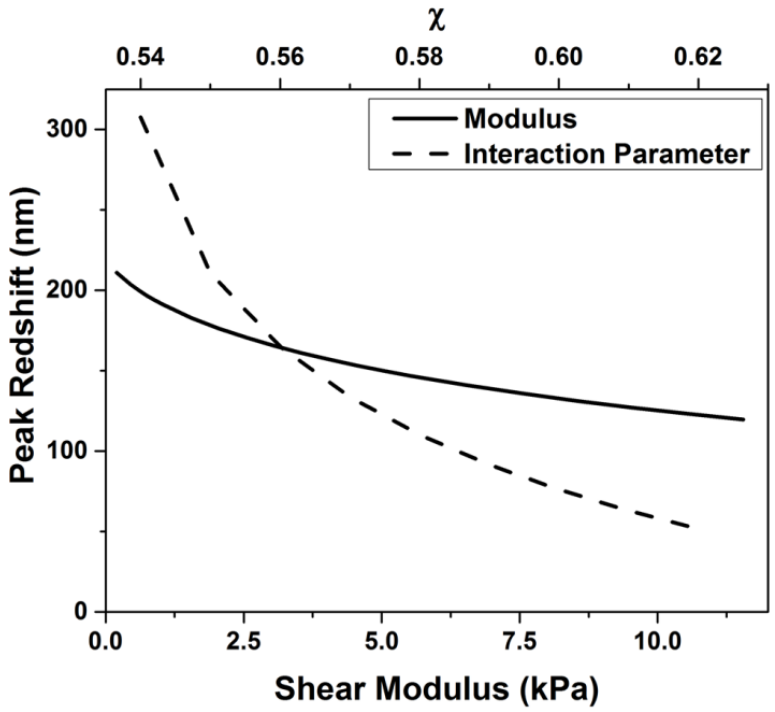

Figure 5.4 Theoretical peak redshift as a function of elastic modulus (solid curve) and χ (dashed curve) from Flory's description of swelling in ionic polymer networks. The theoretical redshifts were calculated assuming an immobilized charge concentration of 20 mM, immersion in a solution of ionic strength of 0 mM, an interaction parameter of 0.560 (for varying modulus values), and a modulus of 2.8 kPa (for varying χ values).

5.3.3 Effect of Hydrogel Elastic Modulus on Optical Response

Figure 5.5 shows the experimentally measured response of hydrogel-encapsulated photonic crystals as a function of elastic modulus from 0.7 to 6.2 kPa. The redshift in the

wavelength of peak diffraction, or peak redshift, is reported as the difference between the optical response post-peptide functionalization relative to the unfunctionalized state. As predicted by the model, hydrogels with small elastic moduli had a reduced elastic restoring force and were less resistant to deformation, such that greater peak redshifts and optical responses were observed. The moduli of the acrylamide hydrogels was controlled by varying the monomer concentration during photopolymerization. Hydrogels with moduli below 0.7 kPa were not characterized because they were too fragile to handle, which led to mechanical failure. Beside the varying elastic modulus, the hydrogels were prepared to be otherwise identical; the hydrogels were each functionalized with 10 mM of the azide modified peptide and diffraction measurements were performed in a 1.0 mM sodium phosphate buffer at a pH of 8.0.

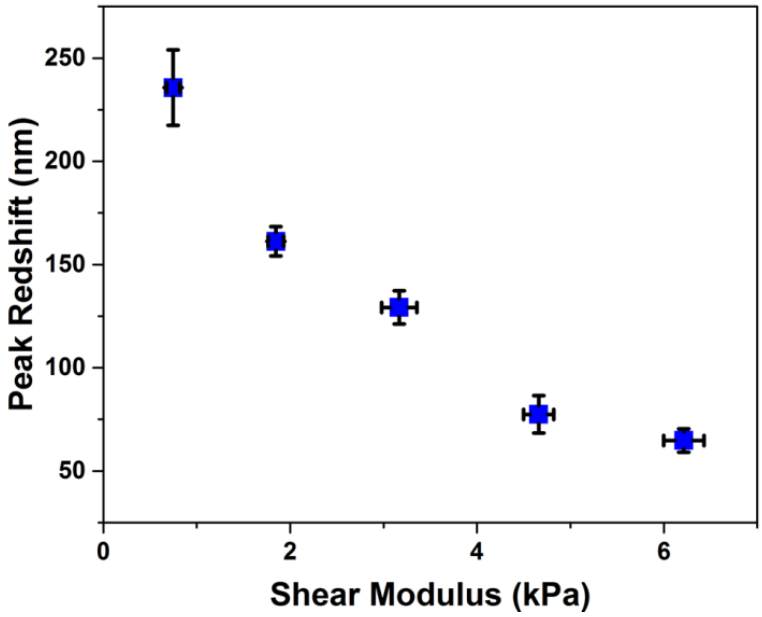

Figure 5.5 Peak redshift as a function of shear modulus for hydrogels (with $\chi = 0.609$) containing 21.4 ± 0.6 mM of peptide, as measured by charge staining. Diffraction measurements were taken in 1.0 mM sodium phosphate buffer at pH 8.0. Error bars represent ±1σ from the mean of 3-4 distinct samples.

5.3.4 Effect of Hydrogel-Solvent Flory-Huggins Interaction Parameter on Optical Response

The hydrogel swelling model predicts that the Flory-Huggins interaction parameter should have a substantial impact on the optical response of the sensor to the concentration of immobilized charge. One approach, as used here, to varying the polymer-solvent interaction parameter is by modifying the composition of the polymer hydrogel. The hydrogel composition was carefully tuned through the inclusion of comonomers, either HEA or HEAA (molecular structures shown in **Figure 5.6a**, insets), that were more hydrophilic than AA. By copolymerization of these monomeric units into the hydrogel, the overall polymer-solvent interaction parameter of the hydrogel was reduced from that of AA only hydrogels (χ = 0.609) as quantified in **Figure 5.6a**. The Flory-Huggins interaction parameter was calculated via the relationship between the interaction parameter and the equilibrium volume of the hydrogel:

$$\chi = -\left(\frac{V}{V_o}\right)^2 \left[ln\left(1-\frac{V_o}{V}\right) + \frac{V_o}{V} + V_s \frac{v_e}{2}\left(\frac{V_m}{V}\right)^{1/3}\right] \qquad (6)$$

Figure 5.6b shows the peak redshift in the optical response of the hydrogels upon peptide functionalization, and the associated inclusion of immobilized charge, as a function of χ. The interaction parameter was measured prior to peptide functionalization and ranged from 0.587 for pure HEA hydrogels to 0.609 for pure AA hydrogels. As anticipated, decreasing the polymer-solvent interaction parameter increased the peak redshift for a constant concentration of immobilized charge (10 mM azide modified peptide) and hydrogel elastic modulus (2.8 kPa). Importantly, the optical response for both the HEA and HEAA copolymerized hydrogels can be plotted as a single curve as function of χ. When plotted this way, the χ parameter effectively describes the ensemble polymer-solvent interactions while accounting for differences in chemical structure. Of note, the overall χ for the hydrogels varies during the course of

functionalization and as well as during phosphorylation by kinase. The optical response observed experimentally nevertheless corresponds well to the theoretical predictions (the dashed curved in Figure 4), in terms of both the trend and relative magnitude of the optical response over the range of χ that was investigated, regardless of the small variations in hydrogel composition that arise during peptide functionalization.

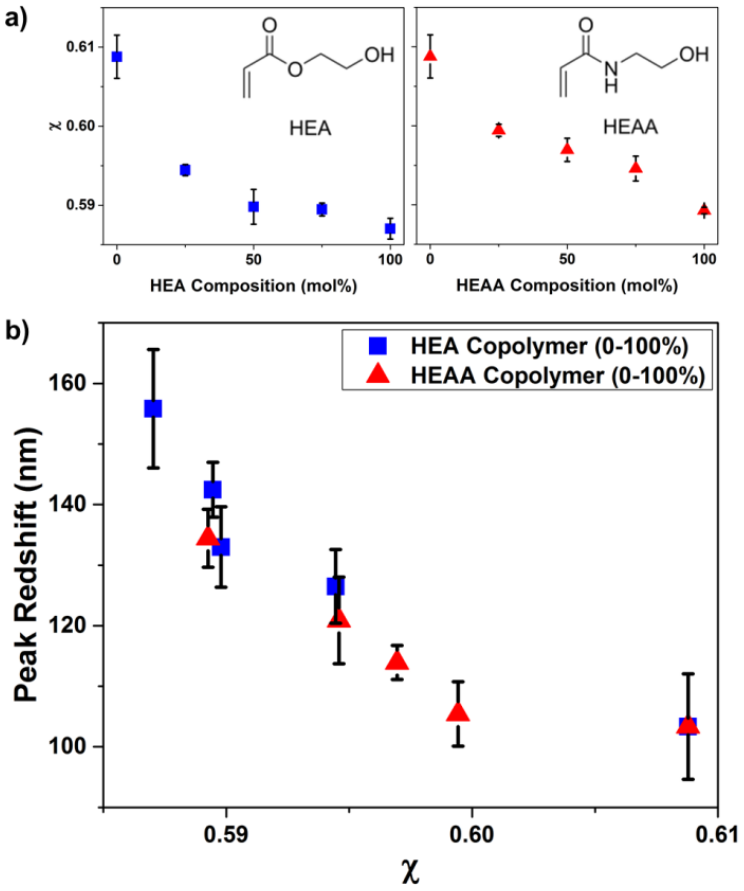

Figure 5.6 a) The variation of χ for hydrogels (with a modulus of 2.8 kPa) as a function composition for HEA (left panel) and HEAA (right panel) copolymerized with AA. b) Peak redshift as a function of χ for hydrogels containing 21.4 ± 0.6 mM peptide, as measured by charge staining. χ was calculated prior to peptide functionalization. Diffraction measurements were taken in 1 mM sodium phosphate buffer at pH 8.0. Error bars represent ±1σ from the mean of 3-4 distinct samples.

5.3.5 Effect of Free Ions in Solution

The ionic strength of the environment influences the optical response of the optical response of the hydrogel-encapsulated photonic crystals, with lower ionic strength conditions leading to greater sensitivity and dynamic range. The osmotic pressure due to the Donnan potential (Equation 1) between the hydrogel and the surrounding environment arises from a gradient in the concentration of mobile ions. Thus, the strength of the Donnan potential is dependent upon the concentration of ions immobilized in the hydrogel and the ionic strength of the surrounding environment. **Figure 5.7** shows the relative redshift in the wavelength of peak diffraction reported by the hydrogel-encapsulated photonic crystals as a function of the concentration of peptide immobilized in the hydrogel and the ionic strength of the buffer solution in which the sensor was immersed. Diffraction measurements were made after thoroughly rinsing and equilibrating the hydrogel sensors in the buffer solutions of the specified ionic strength. Increasing concentrations of immobilized peptide, which have a charge of +2, induce a larger influx of mobile ions from the buffer solution into the hydrogel. In high ionic strength environments, however, the gradient in the mobile ion concentrations in the hydrogel (c_x) and in the buffered environment (c_x^*) remained small and no change in the optical response was observed. All of the systems that were considered attained a minimum wavelength of peak diffraction at buffer ionic strengths above 25 mM, which effectively corresponds to the situation in which $c_x^* \to \infty$ and the hydrogel is not swollen. The absolute value of this minimum wavelength differed for each concentration of immobilized peptide, with the hydrogel systems functionalized with 0.1 and 10 mM peptide having the most blueshifted and redshifted responses, respectively. This variation in the minimum wavelength of peak diffraction was likely due to

differences in the effective Flory-Huggins interaction parameter that arise due to different extents of functionalization by the hydrophilic peptides that replace hydrophobic alkyne moieties.

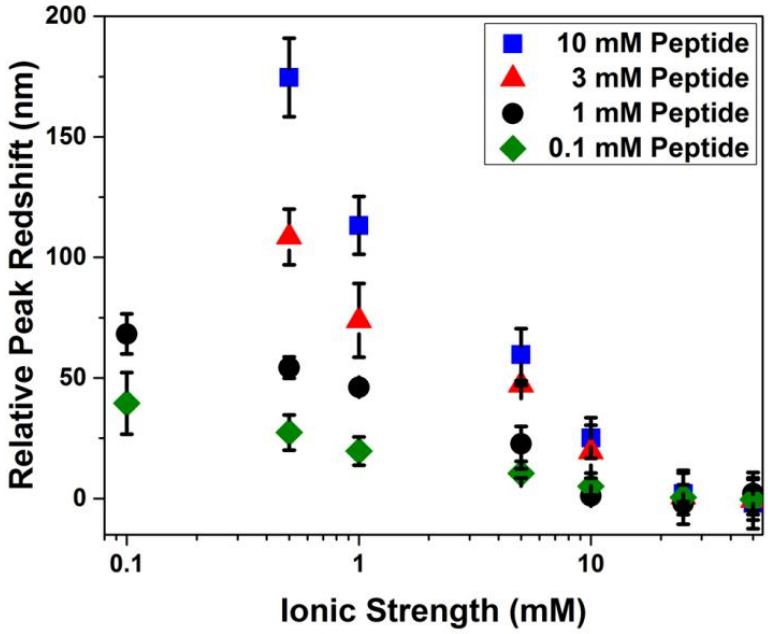

Figure 5.7 Relative peak redshift as a function of both buffer ionic strength and peptide concentration for hydrogels with a modulus of 2.8 kPa and χ of 0.609. The redshift represents the difference in the wavelength of peak diffraction of the sample in a given solution ionic strength relative to the sample in solution ionic strength >25 mM. The reported peptide concentrations correspond to the peptide concentration in the reaction mixture during hydrogel functionalization. The corresponding peptide concentrations in the hydrogel were measured by charge staining to be 21.4 ± 0.6, 15.6 ± 0.6, 9.3 ± 0.7, and 2.8 ± 0.4 mM for reaction concentrations of 10, 3, 1, and 0.1 mM, respectively. Error bars represent ±1σ from the mean of 3-4 distinct samples.

Decreasing the ionic strength of the environment in which the hydrogel-encapsulated photonic crystal was immersed increased the mobile ion gradient, thereby yielding enhanced optical responses. These optical responses were significant (up to 175 nm) and arose for environments reduced in ionic strength by two orders of magnitude. While in theory further reducing the ionic strength of the environment should lead to greater sensitivity and dynamic range, in practice challenges associated with the manipulation and characterization of extensively

swollen hydrogels must first be overcome. For example, hydrogels reacted with 3 and 10 mM modified peptide were not measured in solutions with ionic strengths lower than 0.5 mM due to excess swelling, which caused the gels to become too fragile to handle.

5.3.6 Characterization of Optical Sensitivity of Click-Modified Kinase Responsive CCA-Containing Hydrogels to PKA

The application of the optically responsive sensors to characterize peptide phosphorylation events and kinase activity was demonstrated by the acquisition of a dose-dependent response curve. **Figure 5.8** shows the peak blueshift as a function of PKA concentration for hydrogels treated with 1, 3, and 10 mM of the azide modified peptide. The hydrogel materials were specifically selected for this experiment to display a large optical response and to be sensitive to kinase activity, and therefore had an elastic modulus of 0.8 kPa (low modulus) and were comprised of 100% HEA (small χ). Phosphorylation due to kinase activity reduced the net charge, and thus the Donnan potential, in the hydrogel such that the material contracted (from the swollen state induced by functionalization with the positively charge peptide) and the wavelength of peak diffraction blueshifted. The azide-alkyne click chemistry approach to peptide functionalization of the hydrogel-encapsulated photonic crystals also significantly reduced the concentration of immobilized charge in the system and improved the sensitivity of detection. Here, with ~10 mM of peptide immobilized in the hydrogel (*i.e.*, the 1 mM treatment condition), a PKA sensitivity of 0.5 U/μL was determined. Increasing the peptide concentration immobilized in the gel by a factor of two (*i.e.*, the 10 mM condition in Figure 8) enabled the device sensitivity to be further improved to 0.1 U/μL. In comparison, a hydrogel-encapsulated photonic crystal containing similar peptide concentrations, but that was functionalized via an EDC/NHS pathway that left a high background concentration of

negatively-charged carboxylate functionalities in the hydrogel, had a sensitivity to PKA of only 4 U/μL.

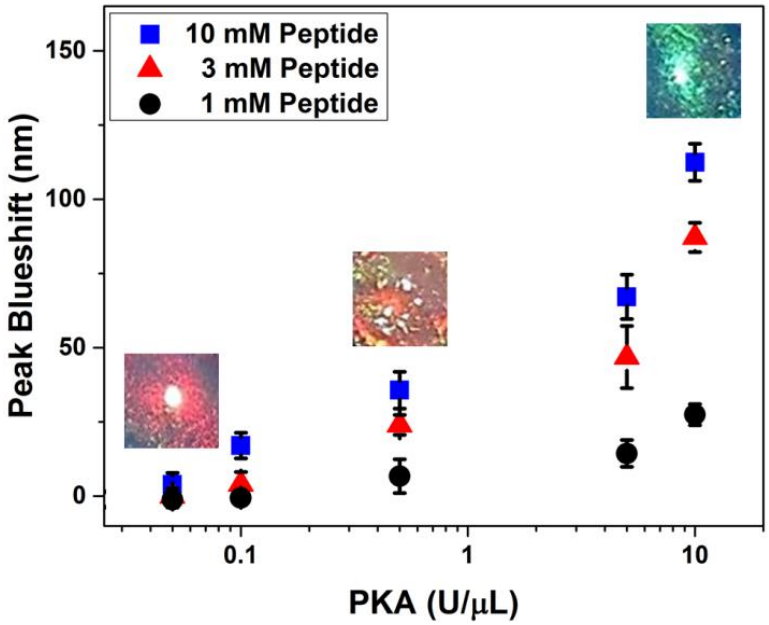

Figure 5.8. Biosensor response as a function of peptide and PKA concentrations for a 2 h reaction time for hydrogels with a modulus of 0.8 kPa and χ of 0.587. The reported peptide concentrations correspond to the peptide concentration in the reaction mixture during hydrogel functionalization. The corresponding peptide concentrations in the hydrogel were measured by charge staining to be 21.4 ± 0.6, 15.6 ± 0.6, and 9.3 ± 0.7 mM for reaction concentrations of 10, 3, and 1 mM, respectively. Control samples incubated in the absence of either PKA or cofactor ATP showed no change in diffraction. Inset images (~3x3 mm^2) show the visual color difference between hydrogels reacted with 10 mM peptide and treated with 0.05, 0.5, and 10 U/μL PKA. Diffraction measurements were measured in 1 mM sodium phosphate buffer at pH 8.0. Error bars represent ±1σ from the mean of 3-4 distinct samples.

5.3.7 Detection of FSK Induced Activation of PKA in Cell Lysate

Having demonstrated utility of our approach for the detection of purified PKA, of particular interest was to understand if this approach can quantify PKA activity in lysate from whole cells. To determine the feasibility of detecting PKA activity in cell lysate, HEK293 cells were stimulated with FSK, which activates PKA through elevating intracellular levels of cyclic AMP.[44, 45] Following stimulation, hydrogels were incubated in clarified lysate from the cells

under similar conditions (*i.e.*, 30 ºC for 4 h) as in the case for purified PKA. Notably, the lysate from FSK-treated cells produced a significantly larger (approximately 6-fold) blueshift relative to that produced by the lysate from unstimulated cells (**Figure 5.9**). To confirm that the response was indeed PKA specific, the shift in peak diffraction from the lysate from stimulated cells was also measured in the presence of the PKA inhibitor, PKI.[46] In the presence of PKI, as expected, the sensor response was significantly lower than that without PKI, which can be attributed to the inhibition of PKA. As an added control, the sensor response was also measured upon incubation of lysate from unstimulated cells to which PKI was also added. The shift in peak diffraction from these samples was statistically similar to that resulting from incubation with untreated cells only. Of note, the extent of blueshift due to FSK-stimulated lysate was several fold lower than that measured with purified PKA. This reduction may be due to lower overall PKA activity in the lysate as well as competing phosphatase activity, which can contribute to the dephosphorylation of the substrate. Additionally, this difference may arise from diffusional differences between full-length PKA from the lysate and the truncated catalytic subunit used in experiments with purified PKA. These results ultimately highlight the feasibility of using this sensing approach to quantify changes in PKA regulation and, in theory, expression in whole cell assays. Furthermore, these results support the use of our sensing approach for screening potential therapeutic molecules that alter intracellular PKA activity.

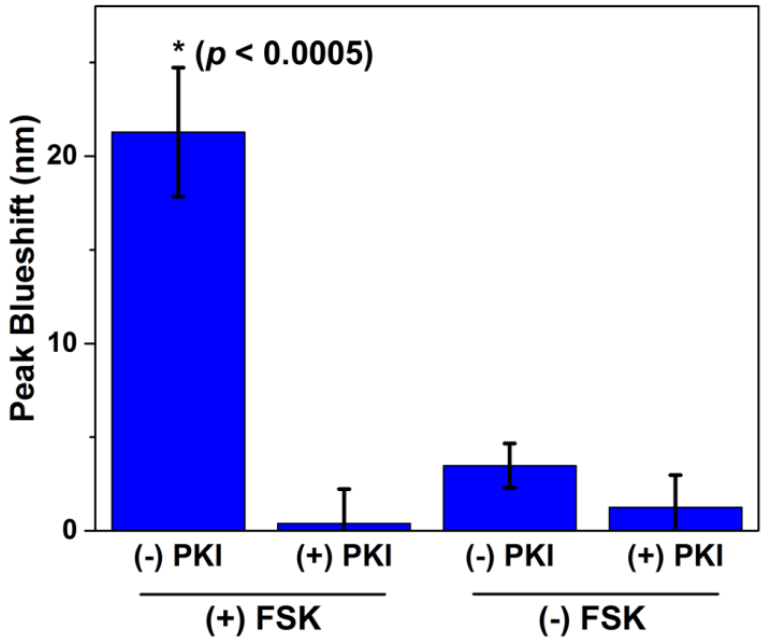

Figure 5.9 Optical response of PKA activity in FSK stimulated, non-stimulated and PKI inhibited lysate from HEK293 cells. The hydrogel samples used in cell lysate experiments had a modulus of 0.8 kPA and χ of 0.587. The peptide concentration in the hydrogels was 21.4 ± 0.6 mM, which was determined by charge staining. Diffraction measurements were measured in 1 mM sodium phosphate buffer at pH 8.0. (*) indicates $p < 0.0005$. Error bars represent ±1σ from the mean of 3-4 distinct samples.

5.4 Conclusion

Herein, we have investigated the development of optically diffracting materials that are responsive to the phosphorylation activity of kinases. The development of such materials was specifically investigated by theoretically and experimentally characterizing the influence of hydrogel properties and the local environment on optical sensitivity. Results of a theoretical model of swelling in ionic polymer networks and experiments, which were consistent, showed that optical sensitivity increases as shear modulus and Flory-Huggins interaction parameter between the hydrogel network and solvent decrease. Furthermore, the sensitivity of the responsive hydrogel network was shown to increase through the elimination of extraneous charges in the hydrogel by exploiting azide-alkyne click chemistry for functionalization.

Through tuning the hydrogel properties, the sensitivity of the optical response was sufficiently high enough to detect 0.1 U/μL PKA in 2 h. Such sensitivity limits are similar to those of conventional biochemical assays, highlighting the potential utility of this approach, which has added advantages that enable label-free detection. Further enhancements in sensitivity may be realized by the use of even more hydrophilic constituents and consideration of the impact of the assay temperature on the Flory-Huggins interaction parameter. The utility of this approach was also demonstrated through the application and selective detection of PKA in cell lysate. Given its advantages and utility, this approach is a highly attractive screening platform for the discovery of novel therapeutic molecules and probes for studying kinase regulation *in vivo*.

5.5 References

(1) Cui, Q. Z.; Wang, W.; Gu, B. H.; Liang, L. Y., *Macromolecules* **2012,** *45* (20), 8382-8386.

(2) Endo, T.; Yanagida, Y.; Hatsuzawa, T., *Sensor Actuat B-Chem* **2007,** *125* (2), 589-595.

(3) Holtz, J. H.; Asher, S. A., *Nature* **1997,** *389* (6653), 829-832.

(4) Holtz, J. H.; Holtz, J. S. W.; Munro, C. H.; Asher, S. A., *Anal Chem* **1998,** *70* (4), 780-791.

(5) Zhang, J. T.; Wang, L.; Luo, J.; Tikhonov, A.; Kornienko, N.; Asher, S. A., *J Am Chem Soc* **2011,** *133* (24), 9152-5.

(6) Alexeev, V. L.; Sharma, A. C.; Goponenko, A. V.; Das, S.; Lednev, I. K.; Wilcox, C. S.; Finegold, D. N.; Asher, S. A., *Anal Chem* **2003,** *75* (10), 2316-2323.

(7) Ben-Moshe, M.; Alexeev, V. L.; Asher, S. A., *Anal Chem* **2006,** *78* (14), 5149-5157.

(8) Muscatello, M. M. W.; Stunja, L. E.; Asher, S. A., *Anal Chem* **2009,** *81* (12), 4978-4986.

(9) Kimble, K. W.; Walker, J. P.; Finegold, D. N.; Asher, S. A., *Anal Bioanal Chem* **2006,** *385* (4), 678-685.

(10) Zhang, J. T.; Smith, N.; Asher, S. A., *Anal Chem* **2012,** *84* (15), 6416-6420.

(11) Sharma, A. C.; Jana, T.; Kesavamoorthy, R.; Shi, L.; Virji, M. A.; Finegold, D. N.; Asher, S. A., *J Am Chem Soc* **2004,** *126* (9), 2971-7.

(12) Walker, J. P.; Asher, S. A., *Anal Chem* **2005,** *77* (6), 1596-1600.

(13) Walker, J. P.; Kimble, K. W.; Asher, S. A., *Anal Bioanal Chem* **2007,** *389* (7-8), 2115-2124.

(14) Arunbabu, D.; Sannigrahi, A.; Jana, T., *Soft Matter* **2011,** *7* (6), 2592-2599.

(15) Asher, S. A.; Sharma, A. C.; Goponenko, A. V.; Ward, M. M., *Anal Chem* **2003,** *75* (7), 1676-1683.

(16) Baca, J. T.; Finegold, D. N.; Asher, S. A., *Analyst* **2008,** *133* (3), 385-90.

(17) Goponenko, A. V.; Asher, S. A., *J Am Chem Soc* **2005,** *127* (30), 10753-9.

(18) Yan, F.; Asher, S., *Anal Bioanal Chem* **2007,** *387* (6), 2121-30.

(19) Lee, K.; Asher, S. A., *J Am Chem Soc* **2000,** *122* (39), 9534-9537.

(20) Shin, J.; Braun, P. V.; Lee, W., *Sensor Actuat B-Chem* **2010,** *150* (1), 183-190.

(21) Xu, X.; Goponenko, A. V.; Asher, S. A., *J Am Chem Soc* **2008,** *130* (10), 3113-9.

(22) MacConaghy, K. I.; Geary, C. I.; Kaar, J. L.; Stoykovich, M. P., *J Am Chem Soc* **2014,** *136* (19), 6896-6899.

(23) Li, Y. J.; Xie, W. H.; Fang, G. J., *Anal Bioanal Chem* **2008,** *390* (8), 2049-2057.

(24) Olive, D. M., *Expert Rev Proteomics* **2004,** *1* (3), 327-41.

(25) Malkoch, M.; Thibault, R. J.; Drockenmuller, E.; Messerschmidt, M.; Voit, B.; Russell, T. P.; Hawker, C. J., *J Am Chem Soc* **2005,** *127* (42), 14942-14949.

(26) Welser, K.; Perera, M. D. A.; Aylott, J. W.; Chan, W. C., *Chem Commun* **2009,** (43), 6601-6603.

(27) Arunbabu, D.; Sannigrahi, A.; Jana, T., *J Appl Polym Sci* **2008,** *108* (4), 2718-2725.

(28) Reese, C. E.; Guerrero, C. D.; Weissman, J. M.; Lee, K.; Asher, S. A., *J Colloid Interf Sci* **2000,** *232* (1), 76-80.

(29) Uchida, E.; Uyama, Y.; Ikada, Y., *Langmuir* **1993,** *9* (4), 1121-1124.

(30) Wang, Q.; Chan, T. R.; Hilgraf, R.; Fokin, V. V.; Sharpless, K. B.; Finn, M. G., *J Am Chem Soc* **2003,** *125* (11), 3192-3193.

(31) Rostovtsev, V. V.; Green, L. G.; Fokin, V. V.; Sharpless, K. B., *Angew Chem Int Edit* **2002,** *41* (14), 2596-+.

(32) Kolb, H. C.; Finn, M. G.; Sharpless, K. B., *Angew Chem Int Edit* **2001,** *40* (11), 2004-+.

(33) Binder, W. H.; Sachsenhofer, R., *Macromol Rapid Comm* **2007,** *28* (1), 15-54.

(34) Liang, L. Y.; Astruc, D., *Coordin Chem Rev* **2011,** *255* (23-24), 2933-2945.

(35) Fuaad, A. A. H. A.; Azmi, F.; Skwarczynski, M.; Toth, I., *Molecules* **2013,** *18* (11), 13148-13174.

(36) Besanceney-Webler, C.; Jiang, H.; Zheng, T. Q.; Feng, L.; del Amo, D. S.; Wang, W.; Klivansky, L. M.; Marlow, F. L.; Liu, Y.; Wu, P., *Angew Chem Int Edit* **2011,** *50* (35), 8051-8056.

(37) Tang, W.; Becker, M. L., *Chem Soc Rev* **2014,** *43* (20), 7013-7039.

(38) Kakwere, H.; Chun, C. K. Y.; Jolliffe, K. A.; Payne, R. J.; Perrier, S., *Chem Commun* **2010,** *46* (13), 2188-2190.

(39) Chapman, R.; Jolliffe, K. A.; Perrier, S., *Polym Chem-Uk* **2011,** *2* (9), 1956-1963.

(40) Barson, C. A.; Bevington, J. C.; Huckerby, T. N., *Polym Bull* **1991,** *25* (1), 83-86.

(41) Yilmaz, G.; Kahveci, M. U.; Yagci, Y., *Macromol Rapid Comm* **2011,** *32* (23), 1906-1909.

(42) Yamazaki, S., *Inorg Chim Acta* **2011,** *366* (1), 1-18.

(43) Flory, P. J., *Principles of polymer chemistry*. Cornell University Press: Ithaca,, 1953; p 672

(44) Seamon, K. B.; Daly, J. W. J. *Cyclic Nucleotide Res.* **1981**, 7 (4), 201-224.

(45) Bachmann, B. A.; Riml, A.; Huber, R. G.; Baillie, G. S.; Liedl, K. R. ; Valovka, T.; Stefan, E. *Proc. natl. Acad. Sci. U. S. A.* **2013**, 110 (21), 8531-8536.

(46) Cheng, H. C.; Van Patten, S. M.; Smith, A. J.; Walsh, D. A. *Biochem. J.* **1985**, 231 (3), 655-661.

CHAPTER 6 – LABEL-FREE DETECTION OF MISSENSE MUTATIONS AND METHYLATION DIFFERENCES IN THE P53 GENE USING OPTICALLY DIFFRACTING HYDROGELS

6.1 Introduction

Due to the importance of DNA detection in a myriad of fields, including genetic screening, forensics, pathogen identification, and biotechnology (*e.g.*, genome engineering), the development of new technologies for DNA sensing is critical. Of particular interest is the development of new approaches that accelerate DNA detection with high fidelity and reduce the cost of traditional DNA sequencing. In addition to traditional DNA sequencing (*i.e.*, capillary electrophoresis), which, although precise, requires specialized instrumentation, other methods of detecting DNA include electrochemical impedance spectroscopy,[1-3] surface enhanced Raman spectroscopy,[4] nanoparticle aggregation assays,[5-7] analysis by quartz crystal microbalance,[8, 9] surface plasmon resonance,[10-12] and scanning tunneling spectroscopy.[13-15] Additionally, fluorescent[16, 17] and chemiluminescent[18, 19] based techniques for DNA sensing have been reported. However, many of these techniques, as with traditional sequencing, require highly specialized instrumentation as well as exogenous labels or reagents and, moreover, are unable to detect down to single nucleotide changes.[20, 21]

A novel approach for the detection of DNA, which may overcome many of the limitations of current sensing methods, entails combining DNA-responsive and optically diffracting materials. In one such approach, a photonic crystal may be polymerized within a hydrogel matrix that can swell or contract in response to the presence of an analyte. The hydrogel matrix can be rationally tuned to change volume in response to a specific analyte by tethering a receptor for the analyte within the hydrogel along with the photonic crystal.[22-25] Depending on the properties of the analyte (*i.e.*, charge or hydrophobic character), receptor

binding may trigger a volume change of the hydrogel by creating a Donnan potential or altering the interaction of the hydrogel with water. Changes in hydrogel volume are accompanied by an alteration in the lattice spacing of the photonic crystal that may be readily measured by reflectance spectroscopy or, if large enough, visually through changes in coloration of the hydrogel. We and others have previously exploited this approach to develop sensors for a broad spectrum of small molecule analytes,[26-28] metals,[29-31] changes in solution conditions,[32, 33] and, more recently, protein kinase activity.[34, 35] Notably, in all cases, this approach enabled the detection of environmental cues in the absence of exogenous reagents, using changes in optical properties of the hydrogel as the primary readout.

In this work, we explored the utility of this approach as a sensing platform for label-free DNA detection *via* encapsulation of a crystalline colloidal array (CCA) within a DNA-responsive hydrogel. Specifically, we fabricated DNA-responsive hydrogel films that alter the diffraction of light upon hybridization of a specific "target" DNA strand to a capture "probe" sequence (**Figure 6.1**). We reasoned that hybridization of the target strand would cause a change in the volume of the hydrogel network by increasing the concentration of immobilized negative charges within the hydrogel. The addition of negative charges upon hybridization is due to the backbone of the target DNA being comprised of negatively-charged phosphate groups. Once these charges become immobilized within the hydrogel network, the Donnan potential between the hydrogel and surrounding solution is modified, resulting in swelling of the hydrogel and ultimately a change in the diffraction spectrum of the encapsulated CCA.

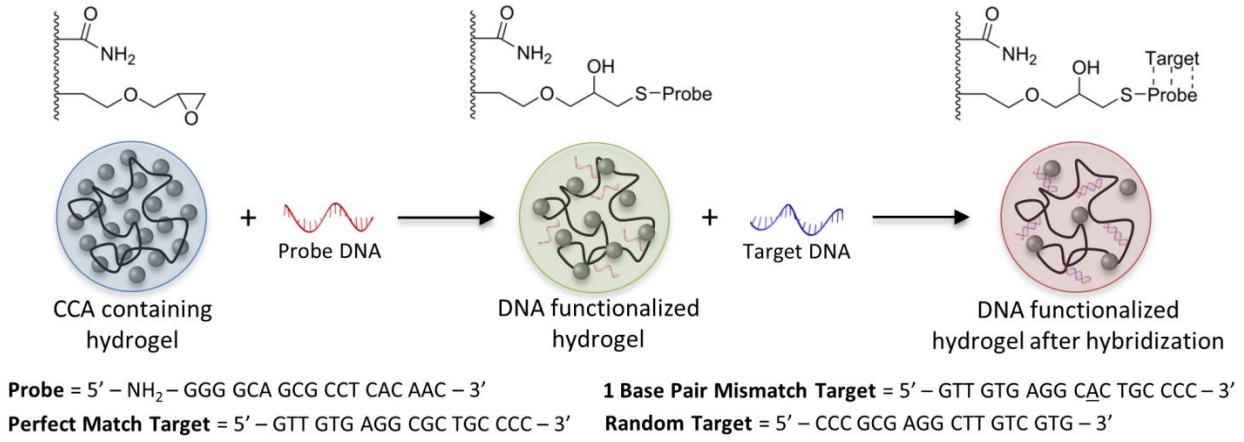

Figure 6.1 Schematic of hydrogel functionalization with "probe" DNA and subsequent hybridization of "target" DNA strands. Color changes in the optically diffracting hydrogel are representative of those observed upon functionalization and hybridization due to changes in the lattice spacing of the encapsulated CCA. The sequences of the probe and target DNA strands that were used are shown below the schematic.

The utility of this approach for DNA sensing was demonstrated *via* the detection of the gene for the major tumor suppressor protein p53. A key transcription factor involved in cell regulation, p53, which is inactivated in virtually all human cancers, is of specific interest as a marker for early cancer detection.[36-41] For sensing, a short 18-mer sequence that is complementary to the DNA-binding domain of the p53 gene was used as the capture probe and was conjugated to the hydrogel network (**Figure 6.1**). The perfect matching 18-mer sequence from the wild-type p53 gene was used as the target strand. Furthermore, we were interested in determining if the sensing approach was sensitive to mutations in p53, which is the most frequently mutated gene in cancer. To determine the sensitivity of the optical response of the detection approach to DNA mutations, a single base in the target strand was changed (G → A). This genetic alteration corresponds to mutation of arginine at position 175 to a histidine (*i.e.*, R175H), which is one of the more frequent oncogenic mutations in p53. Finally, we tested if the detection scheme was also sensitive to DNA methylation by using a methylated form of the wild-

type target strand (**Table 6.1**). We show that changes in methylation can also be readily detected, which may have additional implications in screening for epigenetic disease markers.

Table 6.16.1 Names and Sequences of DNA Oligos

Name	Sequence
Probe	5' –NH_2 - GGG GCA GCG CCT CAC AAC – 3'
Perfect Match (PM) Target	5' – GTT GTG AGG CGC TGC CCC – 3'
1 Base Pair Mismatch (1bpMM) Target	5' – GTT GTG AGG CAC TGC CCC – 3'
Random Target	5' – CCC GCG AGG CTT GTC GTG – 3'
Methylated Perfect Match (mPM)Target	5' – GTT GTG AGG $_{m}$CG$_{m}$C TG$_{m}$C $_{m}$C$_{m}$C$_{m}$C – 3'

6.2 Experimental Methods

6.2.1 Materials

Acrylamide (AA), *N*,*N*′-methylenebis(acrylamide) (BA), and allyl glycidyl ether (AGE) monomers were purchased from Sigma-Aldrich (St. Louis, MO) and used without further purification. DNA oligos (**Table 6.1**) were purchased and used as received from Integrated DNA Technologies (Coralville, IA). The linker SPDP-PEG4-NHS was purchased and used without further purification from Conju-Probe (San Diego, CA).

6.2.2 Synthesis of Polystyrene Nanospheres

Highly-charged polystyrene (PS) nanospheres were synthesized *via* emulsion polymerization as previously described.[42, 43] The PS nanospheres used in all experiments had a concentration of 12 wt% in water and were 87 nm in diameter with a polydispersity of 4.9%, as determined by dynamic light scattering (Titan DynaPro with Dyna V6.3.4 software package, Wyatt Technology, Inc.; Santa Barbara, CA). Particles were stored at room temperature in the presence of BioRad (Hercules, CA) AG501-X8 mixed bed resin.

6.2.3 Hydrogel Polymerization and Crystalline Colloidal Array Formation

Hydrogels were photopolymerized by solubilizing 35 mg (0.98 M) AA in 480 μL of the PS nanospheres. To this mixture, a solution of 1 mg (0.015 M) BA and 24 mg (0.42 M) AGE in 20 μL DMSO was added. The photoinitiator Irgacure 2959 (BASF; Florham Park, NJ) (10 wt% in DMSO) was added at a final concentration of 0.05 wt% to the CCA-monomer solution. The solution was then pipetted into a mold formed by two glass slides separated by a 273 ± 2 μm Parafilm spacer. Samples were flood exposed with 365 nm light at 15 mW cm^{-2} from a UV mercury lamp for 45 min. Films were subsequently equilibrated and stored in ultrapure water for a minimum of 24 h prior to DNA functionalization.

6.2.4 Hydrogel Functionalization with DNA Probe

DNA probe with a 5′-primary amine was solubilized in 100 mM $NaPO_4$ buffer, pH 8, at a concentration of 5 mM. A fifteen-fold molar excess of the SPDP-PEG4-NHS linker relative to the probe was solubilized in 10 μL DMSO and added to the DNA solution. The solution was incubated at 4 °C and reacted for 2 h. The solution was then desalted to remove excess linker after which 100 mM tris(2-carboxyethyl)phosphine (TCEP) was added and reacted at room temperature for 1 h to reduce the linker disulfide bond. To determine the amount of linker containing DNA, the absorbance of the cleaved pyridine-2-thione was measured at 343 nm. The concentration of the reduced linker was calculated using the pyridine-2-thione extinction coefficient of 8080 M^{-1} cm^{-1}.[44] After determining the linker concentration, a final desalt was performed to remove the cleaved pyridine-2-thione group.

Prior to functionalization, hydrogels were equilibrated in 100 mM $NaPO_4$ buffer, pH 8. To each sample, 25 μL of 75 μM linker-modified DNA probe in 100 mM $NaPO_4$ buffer was

added and reacted at room temperature for 36 h. Post-functionalization, the samples were thoroughly rinsed and stored in 100 mM NaCl, pH 6.

6.2.5 DNA Hybridization

Samples to be annealed were equilibrated in 100 mM NaCl solution, pH 6, prior to the addition of perfect match (PM), single base pair mismatch (1bpMM), random, or methylated perfect match (mPM) target DNA. Target DNA was added to the hydrogels at concentrations ranging from 0.5 to 1000 μM and annealed by heating the hydrogel samples to 85 °C, holding that temperature for 30 min, and ramping from 85 to 55 °C at rates ranging from 0.05 to 1 °C min^{-1}. Once the temperature reached 55 °C, the system temperature was no longer controlled and samples were permitted to naturally cool to room temperature.

6.2.6 Measurement of DNA Melting Point

The melting point for both the PM and 1bpMM samples was determined by first annealing samples with 50 μM PM target or 500 μM 1bpMM target in 100 mM NaCl followed by equilibration in 2.5 mM NaCl solution. Melting points were subsequently measured by submerging the hydrogels in a 2.5 mM NaCl solution and increasing the solution temperature from room temperature to 65 °C at a rate of 0.25 °C min^{-1}.

6.2.7 Optical Diffraction Measurements

The optical response of the equilibrated hydrogel-encapsulated CCA biosensors was measured with an Ocean Optics (Dunedin, FL) USB-4000 fiber-optic spectrophotometer operated in reflectance mode set to an angle of incidence of 15° from the sample surface normal. This optical setup allowed for characterization of the peak diffraction wavelength *in situ* and in real-time, enabling measurements as a function of temperature (*e.g.*, to generate melting curves). In all experiments, the hydrogels were initially rinsed with 100 mM NaCl solution, pH 6.0, to

remove non-hybridized DNA. For experiments utilizing a single ionic strength condition, samples were introduced to the desired ionic strength by a stepwise decrease in NaCl concentration. For experiments investigating sensor response to solution ionic strength, samples were first equilibrated and characterized in 10 mM NaCl, pH 6, followed by a stepwise reduction in ionic strength to 0.01 mM NaCl with measurements taken after equilibration at each condition.

6.3 Results and Discussion

6.3.1 Effect of Target DNA Concentration on Sensor Response

Upon hydrogel functionalization with the p53 probe strand, the sensitivity and selectivity of the sensing platform was investigated using a fully complementary (*i.e.*, perfect match) and random sequence. **Figure 6.2** shows the sensor response to concentrations of the perfect match (PM) and random sequence ranging from 0.5 to 1000 μM, which corresponds to 25 pmole to 50 nmole of target DNA. Addition of the PM caused a dose-dependent redshift in the diffraction peak with increasing target concentrations, resulting in a nearly 8-fold change in signal over the concentration range. Conversely, the random sequence, which has the same GC content as the PM, did not elicit a response at even the highest concentrations used. These results highlight the sensitivity and selectivity of the approach, which presumably are due to differences in the hybridization of the PM relative to the random sequence. Hybridization of the PM would result in the immobilization of negative charges from the target DNA strand within the hydrogel, triggering a change in the Donnan potential of the system. This change would, as a result, cause the hydrogel network to expand and, in turn, the lattice spacing of the embedded CCA to increase, leading to the observed redshift in peak diffraction. Accordingly, given that the random sequence would not be expected to hybridize with the capture probe, the lack of response that was generated by the random sequence is not surprising. In these measurements, the amount of

target DNA was less than that of the probe strand within the hydrogel such that the immobilization of additional probe would not enhance the response.

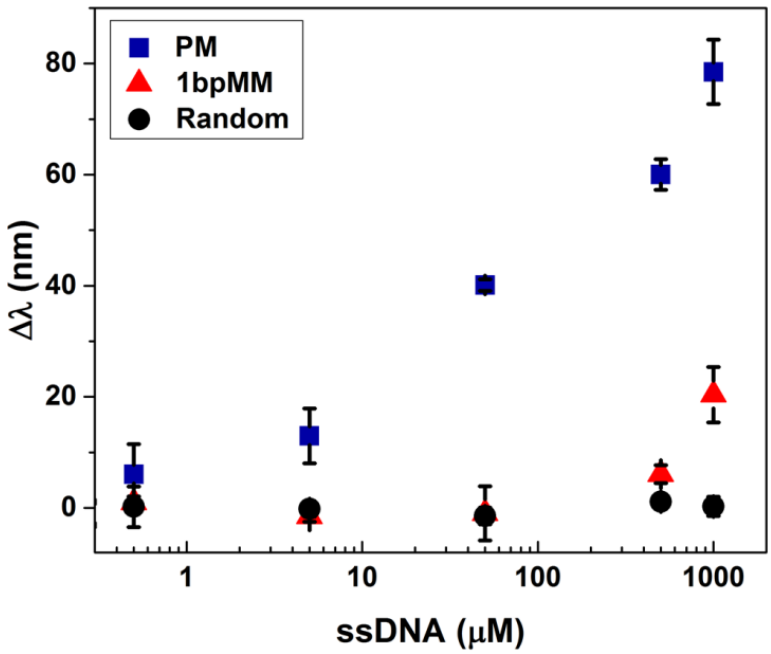

Figure 6.2 Change in wavelength of peak diffraction relative to that of the probe functionalized sensor as a function of the concentration of target ssDNA. Samples were annealed at a rate of 0.2 °C min^{-1} with PM, 1bpMM, or random target DNA concentrations ranging from 0.5 to 1000 μM. Diffraction measurements were taken in a 0.25 mM NaCl solution at pH 6 and at room temperature. Error bars represent ±1σ from the mean of 3 samples.

Due to the sensitivity of the approach to the hybridization between the target and probe strands, we also hypothesized that mutations in the target that weakened hybridization would be detectable. Of particular interest was if single base pair mutations could be detected using this approach. The detection of single base pair missense mutations is of practical importance for the identification and screening of genetic makers that are associated with various diseases. In the case of p53, screening for specific known hotspot mutations allows for the detection of genetic hallmarks of cancer, which permits rational treatment using cancer-specific therapies. To understand if our approach is sensitive to single base pair mutations, the optical response of

functionalized hydrogels to the target sequence with a base pair mismatch (1bpMM) was measured. Notably, the mutation that was introduced results in the hotspot mutation R175H, which perturbs the structure of the DNA binding domain of p53, resulting in a loss of p53 function.[45, 46] Although a redshift in the diffraction peak relative to the probe functionalized sensor (*i.e.*, the signal $\Delta\lambda$) was not observed at low concentrations of 1bpMM, a significant change in the diffraction peak was apparent at higher concentrations, indicating that, despite weaker affinity for the probe, a target with a single base pair substitution can be detected. Presumably, because the binding affinity would increase, the response to a base pair change in longer target and probe sequences would theoretically increase relative to the control. Moreover, the apparent selectivity of the approach for the PM relative to the 1bpMM suggests that, in principle, a target strand may be differentiated from similar sequences in complex DNA mixtures. Such mixtures may include a multitude of strands with differing sequences and lengths, which may arise, for example, from the digestion of cellular DNA.

6.3.2 Effect of Annealing Rate and Temperature on Sensor Response

Annealing conditions can greatly affect the ability of DNA to form the most thermodynamically favorable duplexes. Accordingly, the impact of annealing conditions on the sensitivity of the detection of the target sequence was investigated. The conditions for annealing were varied by heating hydrogels that contained the probe in the presence of the target DNA to approximately 10 °C above the theoretical T_m of the bound PM (~76 °C in 100 mM NaCl). After heating, the solution containing the free PM target and hydrogel was cooled to well below the T_m at different cooling rates. The final temperature to which the solution was cooled was 55 °C at which the PM sequence should be mostly bound within the hydrogel. As shown in **Figure 6.3a**, the magnitude of the redshift in diffraction is greatest at low cooling rates and drops off as the

rate of cooling increases beyond 0.2 °C min^{-1}. The decline in sensitivity at high cooling rates may be attributed to imperfect hybridization of the PM to the probe sequence, which would result in increased dissociation of the PM strand.

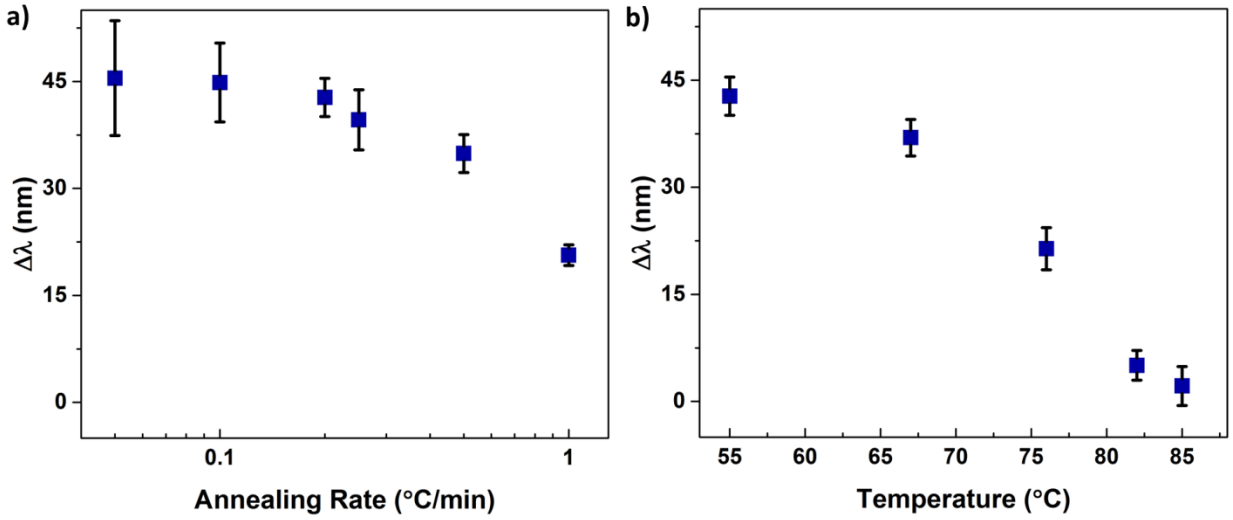

Figure 6.3 Optical response $\Delta\lambda$ observed for DNA hybridization as a function of (a) annealing rate and (b) annealing temperature. All samples were annealed in the presence of 50 μM PM target DNA at rates ranging from 0.05 to 1 °C min^{-1}. In (a) the annealing rate was maintained from 85 to 55 °C, followed by uncontrolled cooling from 55 °C to room temperature. Samples presented in (b) were annealed at a rate of 0.2 °C min^{-1} and, at the specified temperatures, were removed and immediately cooled in ice water followed by rinsing in 100 mM NaCl to quench hybridization. Diffraction measurements were taken in a 0.5 mM NaCl solution at pH 6 and at room temperature. Error bars represent $\pm 1\sigma$ from the mean of 3–6 samples.

The impact of annealing conditions on the sensitivity of target detection was also investigated by using a fixed cooling rate, but varying the annealing time. In this case, samples were heated to 85 °C and subsequently cooled at a rate of 0.2 °C min^{-1} for different times, which resulted in different final annealing temperatures, ranging from 85–55 °C. At the final annealing temperature, the hydrogels were quickly cooled in ice water followed by rinsing in 100 mM NaCl solution at room temperature to quench any further hybridization. **Figure 6.3b** shows the optical response to the PM sequence as a function of the final annealing temperature. As

anticipated, at high final annealing temperatures, where the amount of bound PM is expected to be low, the response of the sensing approach to the PM is low. A significant increase in the detection of the PM sequence is observed at longer times and thus lower final annealing temperatures. Annealing of the hydrogels below 55 °C resulted in no further change in the sensor response, indicating further lowering the annealing temperature has negligible impact on hybridization and sensitivity of the approach.

6.3.3 Characterization of the Critical Melting Temperature of Target DNA

A fundamentally interesting question related to DNA detection using our sensing approach is if the T_m of the bound target DNA is the same in the hydrogel as in solution. Dramatic changes in T_m of the bound target DNA, relative to the annealing or characterization temperatures, may significantly lower the magnitude of the observed response to the target and thus the detection limit. To determine the T_m of the target sequences used in this work, the PM (at 50 μM) and 1bpMM (at 500 μM) sequences were annealed at a cooling rate of 0.2 °C min^{-1} with the immobilized probe. For reference measurements, hydrogels were subject to annealing under identical conditions without target DNA. Of note, a larger concentration of the 1bpMM sequence relative to the PM sequence was used to obtain optical responses of similar magnitude for the two DNA targets. After annealing, the hydrogels were heated from room temperature to 65 °C at a rate of 0.25 °C min^{-1} and the diffraction response of each sample was measured over the entire temperature range. The diffraction response for the PM and 1bpMM sequences is reported as a normalized response, which was determined as the difference of the diffraction wavelength (*i.e.*, $\Delta\lambda$) of the sample with target DNA from that of the reference (with no target DNA) divided by the average maximum shift in peak diffraction wavelength (*i.e.*, $\Delta\lambda_{max,ave}$) from the PM or 1bpMM. By reporting the normalized difference in diffraction wavelength, volume changes in

the hydrogel related to temperature increases and DNA denaturation could be decoupled. In this case, changes in the equilibrium volume of the hydrogel at elevated temperatures may be attributed to changes in the solvent density and Flory–Huggins interaction parameter that alters the free energy of mixing of the system.[47]

From the melting curve of the normalized diffraction response for the PM and 1bpMM sequences (**Figure 6.4**), the T_m of bound PM and 1bpMM could be approximated. The approximated T_m of the bound PM and 1bpMM were 43.5 and 34.3 °C, respectively, as determined from linear interpolation of the melting curves. For comparison, the theoretical T_m of bound PM and 1bpMM in solution are 43 and 35 °C, respectively,[48] which are in good agreement with the experimentally determined values when bound in the hydrogel. This close agreement implies that the hybridization of the target DNA in the hydrogel is nearly identical to that in solution and, moreover, that the theoretical T_m of the target DNA-probe duplex in solution can be used to rationally design the probe strand to enhance sensitivity as well as to optimize the annealing and characterization temperatures.

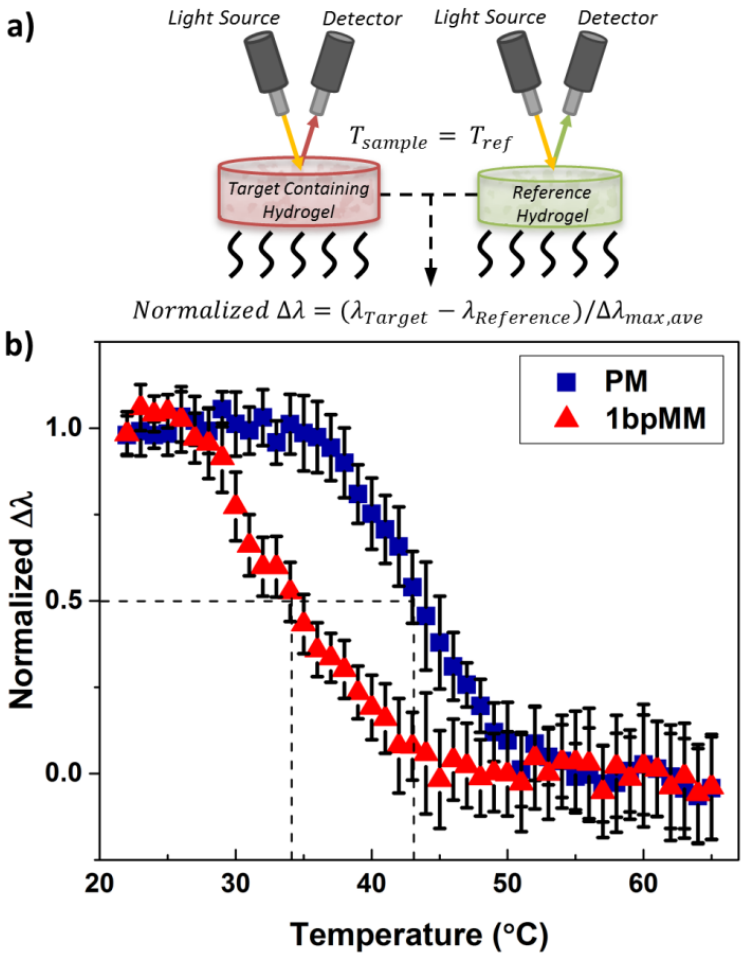

Figure 6.4 (a) Schematic of the optical setup for characterizing melting curves and (b) normalized melting curves for samples annealed with PM or 1bpMM target DNA. The normalized optical response was calculated as the difference in peak diffraction between the target containing samples and reference samples, normalized to the average maximum shift for the PM and 1bpMM samples. The T_m for the hybridized PM (blue squares) and 1bpMM (red triangles) was found to be 43.5 and 34.3 °C, respectively. Sample annealing was performed prior to melting with 50 μM PM or 500 μM 1bpMM target DNA at a rate of 0.2 °C min^{-1}. Melting was performed by ramping samples from room temperature to 65 °C at a rate of 0.25 °C min^{-1}. Diffraction measurements were taken in a 2.5 mM NaCl solution at pH 6. Error bars represent ±1σ from the mean of 3 samples.

6.3.4 Characterization of Sensor Response to Solution Ionic Strength

Due to the effect of ionic strength on DNA melting and the Donnan potential between the hydrogel and the surrounding environment, the detection of target DNA is strongly dependent on

ionic strength during the diffraction measurements. To understand the magnitude of this effect, the sensor response as a function of ionic strength of the optical characterization solution was investigated for PM, 1bpMM, and control samples (**Figure 6.5**). For both PM and 1bpMM samples, starting at high ionic strengths, the response of the sensor increased significantly as the ionic strength of the characterization solution was lowered. However, as the ionic strength was further lowered, the sensor response decreased, resulting in two discernable regimes that describe the effect of ionic strength on the sensor response.

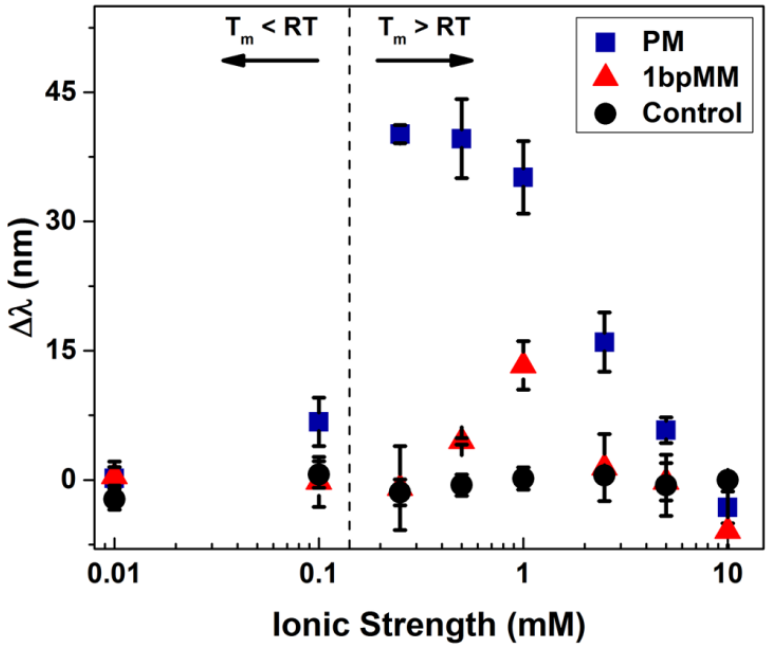

Figure 6.5 Optical response $\Delta\lambda$ as a function of ionic strength for samples annealed with 50 μM PM (blue squares) or 1bpMM (red triangles) target DNA annealed at a ramp rate of 0.2 °C min^{-1}. Control samples (black circles) included probe functionalized hydrogels annealed in the absence of target DNA and hydrogels that were not functionalized with probe but annealed in the presence of target DNA. The vertical dashed line indicates the ionic strength conditions at which the melting temperature of the PM target DNA is equal to the optical characterization temperature. Diffraction measurements were taken after sample equilibration in 0.01 to 10 mM NaCl solutions at pH 6 and at room temperature. Error bars represent $\pm 1\sigma$ from the mean of 3–6 samples.

The distinction between these regimes is most notable for the PM sequence for which a maximum response was observed at an ionic strength of ~0.25 mM. A decrease in the sensor response below this ionic strength is presumably due to the reduction in T_m for the hybridized PM to less than the characterization temperature, which results in weaker binding of the target strand. Notably, the predicted salt adjusted T_m for the hybridized PM is equivalent to room temperature at 0.15 mM salt (dashed line), which corresponds to the characterization temperature for these samples. As such, at ionic strengths less than 0.15 mM, one would expect that the amount of bound PM within the hydrogel at room temperature is very low. Despite the formation of the duplex being favored, the decrease in sensor response above the optimum ionic strength can be explained by a reduction in Donnan potential upon hybridization. This reduction is due to a smaller gradient in the concentration of mobile ions from the interior to the exterior of the hydrogel with increasing ionic strength. For the 1bpMM sample, the optimum ionic strength for detection was significantly higher than for the PM as expected given that the T_m for bound 1bpMM is lower (than for bound PM) at all ionic strengths.

These results ultimately show the importance of considering ionic strength and characterization temperature, which are intimately related, when expanding this sensing approach to other sequences and mutations. For example, for probe and target strands with a lower GC content, that when hybridized have a lower T_m, a lower characterization temperature or ionic strength could be used. Similarly, if longer probe and target strands are used, the characterization temperature or ionic strength (or both) could be increased to enable detection. However, the use of shorter probe and target strands enables a wider range of characterization conditions due to a greater difference in the T_m between a strand that is a perfect match and one that has a base pair mutation. The flexibility to rationally alter the characterization conditions for

the detection of virtually any sequence or length target strand represents a major strength of the approach. In the case of longer target strands that form secondary structures (*e.g.*, hairpin loops), the annealing conditions could be altered to ensure melting of the target and hybridization with the probe. Additionally, the location of a base pair mutation has little effect on the T_m of hybridization unless the mutation is present at one of the end positions. The location of the mutation at an end position would, in theory, result in a decrease in the difference in the response between the perfect match and mutated target strands. As such, this suggests that the probe strand should be designed such that the anticipated mutation is internal within the probe sequence.

6.3.5 Detection of Methylated DNA

Having demonstrated the utility of our sensing approach to detect single base pair mutations, an interesting question to ask is if this approach is also sensitive to epigenetic DNA modifications. Such modifications include DNA methylation and hydroxymethylation, which play a crucial role in gene regulation and thus the development and progression of a variety of diseases.[49, 50] Currently, the primary methods for detecting such modifications include mass spectrometry[51, 52] and methylation-specific PCR,[53, 54] although newer methods, including photopolymerization-based amplification,[55] have recently been reported. For conventional DNA sensing methods, these modifications are difficult to detect due to the often negligible impact these modifications generally have on DNA melting and thus hybridization.[56, 57]

To explore the question of sensitivity to epigenetic changes, we characterized the optical response using our approach to the fully methylated form of the PM sequence (mPM). The PM sequence, when fully methylated, contains six methylated cytosine bases (**Table 6.2.1**). We hypothesized that the methylated moieties in the mPM sequence would reduce the relative

hydrophilicity of the hydrogel (*i.e.*, increase the strength of the Flory–Huggins interaction parameter χ) and the extent of mixing in water, thereby causing the hydrogel to contract, rather than swell. As expected, a dose-dependent response to the addition of the mPM target sequence annealed at a rate of 0.2 °C min^{-1} was observed when measured at 10 mM ionic strength and room temperature. This response, which is shown in **Figure 6.6**, is reported as the difference between the optical peak shift due to hybridization of the mPM target strand and hybridization of the PM target strand ($|\Delta\Delta\lambda|$). The raw response generated by the addition of the mPM sequence is shown in the inset. Of note, optical characterization was performed in a high ionic strength solution to minimize the electrostatic contributions to the observed response upon hybridization of the mPM and PM sequences. By minimizing the contribution of electrostatics, the response that is observed is primarily due to volume changes arising from modulation of the $\chi$and the addition of the methyl groups to the target DNA. Moreover, as anticipated, the response generated by the addition of the mPM sequence resulted in a blueshift in the diffraction peak of the encapsulated CCA, which is consistent with the hydrogel shrinking.

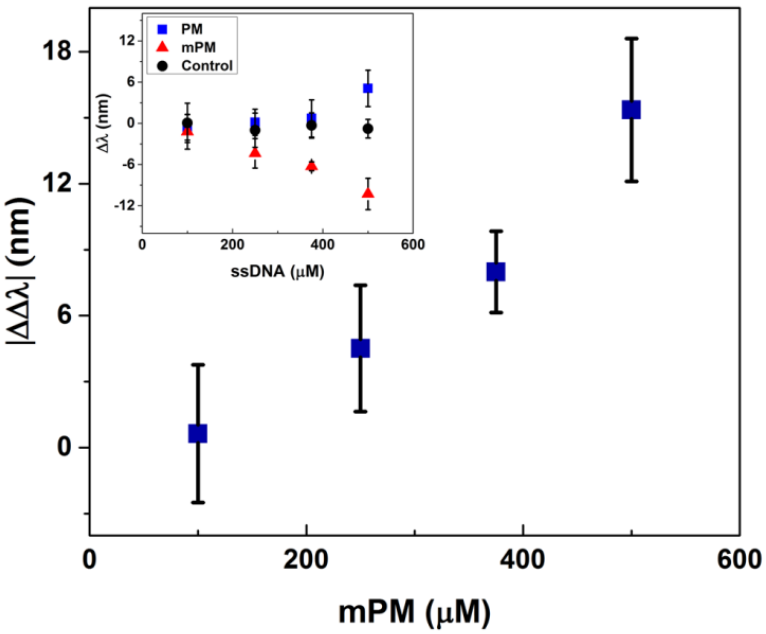

Figure 6.6 Optical response as a function of the concentration of methylated DNA target. The reported response ($|\Delta\Delta\lambda|$) is the difference between the optical shift in the wavelength of peak diffraction upon hybridization of the methylated target and the detected shift upon hybridization of the PM target. The inset shows the raw response generated by hybridization of the mPM target. Samples were annealed from 85 to 55 °C utilizing a ramp rate of 0.2 °C min^{-1} and target DNA concentrations ranging from 100 to 500 μM. Diffraction measurements were taken in a 10 mM NaCl solution at pH 6 and at room temperature. Error bars represent $\pm 1\sigma$ from the mean of 3–6 samples.

The relative impact of even a single methylation site on the target DNA may be predicted based on a theoretical model for hydrogel swelling,[47] in which the osmotic pressure term associated with hydrogel mixing in an aqueous solution scales as $\Pi_M \propto \chi$. To the simplest approximation $\chi_{\text{water-hydrogel}} \propto (\delta_{\text{water}} - \delta_{\text{hydrogel}})^2$ where δ are semi-empirical solubility parameters related to the cohesive energy density as based on the approaches of Hildebrand or Hansen.[58, 59] Often, solubility parameters for polymers may be well estimated by using a group contribution approach, in which $\delta = (\sum F)/V$ where F are tabulated values of the molar attraction constants for common functional groups[60] and V is the molar volume of the repeat unit. Therefore, the dependence of the interaction parameter on the number of methylation sites n on the DNA target

may be estimated by $\chi_{\text{methylated}} \approx \chi_{\text{unmethylated}} + 2n\delta_{CH3}\chi_{\text{unmethylated}}^{1/2}$, and assuming a linear dependence of the optical response on χ (a reasonable approximation for small changes in χ, see **Chapter 5**), the blueshift in optical response based on a single methyl group may be estimated to be 2–3 nm. Given the error of the optical response in **Figure 6.6,** the methylation of as few as two sites may be reasonably detected. One way to potentially enhance the response to a single methylation site may be to encapsulate the CCA in a hydrogel with a lower inherent χ.

Similarly, it may be predicted that other chemical modifications to DNA, including hydroxymethylation or more significantly functionalities that are highly hydrophobic, will also be readily detectable using this approach. For example, a single phenyl modification is predicted to have approximately three times the effect as a methyl modification. Chemical carcinogens that form DNA adducts may likewise be detected, including the classic example of benzo[*a*]pyrene which through a series of chemical reactions may be covalently linked to guanines in DNA.[61-63] In fact, the effect of benzo[*a*]pyrene on the p53 oncogene has been shown to lead to transversion mutations, such as the single base pair mutation considered here.[64] The DNA biosensing scheme presented here may then also provide opportunities to screen for chemical carcinogens and DNA adducts that lead to mutations from which cancer originates.

6.4 Conclusions

In summary, we have developed and demonstrated the utility of optically diffracting hydrogels for the label-free detection of DNA, as well as missense mutations and methylated sites ubiquitous to genes associated with a variety of diseases. Specifically, we showed that a short target DNA sequence from p53 could be readily distinguished from an analogous sequence that has a single base pair mutation that corresponds with the cancer hotspot mutation R175H in a highly selective and dose-dependent manner. Furthermore, methylation of the native target

sequence could be detected, indicating the feasibility of using this approach to screen for epigenetic modifications. Differences in the detection of the native *versus* mutant and methylated sequences can be attributed to alterations in hybridization and polymer-solvent interactions, respectively, and are sensitive to changes in ionic strength and hybridization conditions. This approach ultimately represents a new paradigm for screening oncogenic hotspot mutations in p53 and other cancer-associated proteins. More broadly, this approach may be extended to screen for genetic markers for other diseases as well as nucleotide modifications, stemming from epigenetic changes or chemical modification. The high selectivity in differentiating between a target strand and similar sequences would, in principle, permit the detection of the target strand from complex DNA mixtures.

6.5 References

(1) Benvidi, A.; Firouzabadi, A. D.; Moshtaghiun, S. M.; Mazloum-Ardakani, M.; Tezerjani, M. D., *Anal Biochem* **2015**.

(2) Ianeselli, L.; Grenci, G.; Callegari, C.; Tormen, M.; Casalis, L., *Biosens Bioelectron* **2014,** *55*, 1-6.

(3) Zhu, B. C.; Booth, M. A.; Shepherd, P.; Sheppard, A.; Travas-Sejdic, J., *Biosens Bioelectron* **2015,** *64*, 74-80.

(4) Barhoumi, A.; Halas, N. J., *J Am Chem Soc* **2010,** *132* (37), 12792-12793.

(5) Chak, C. P.; Lai, J. M. Y.; Sham, K. W. Y.; Cheng, C. H. K.; Leung, K. C. F., *Rsc Adv* **2011,** *1* (7), 1342-1348.

(6) Bu, T.; Zako, T.; Fujita, M.; Maeda, M., *Chem Commun* **2013,** *49* (68), 7531-7533.

(7) Wu, S.; Liang, P. P.; Yu, H. X.; Xu, X. W.; Liu, Y.; Lou, X. H.; Xiao, Y., *Anal Chem* **2014,** *86* (7), 3461-3467.

(8) Yeri, A. S.; Gao, L. Z.; Gao, D., *J Phys Chem B* **2010,** *114* (2), 1064-1068.

(9) Li, H.; Xiao, S. Y.; Yao, D. B.; Lam, M. H. W.; Liang, H. J., *Chem Commun* **2015,** *51* (22), 4670-4673.

(10) Cheng, X. R.; Hau, B. Y.; Endo, T.; Kerman, K., *Biosens Bioelectron* **2014,** *53*, 513-518.

(11) Ding, X. J.; Yan, Y. R.; Li, S. Q.; Zhang, Y.; Cheng, W.; Cheng, Q.; Ding, S. J., *Anal Chim Acta* **2015,** *874*, 59-65.

(12) Zagorodko, O.; Spadavecchia, J.; Serrano, A. Y.; Larroulet, I.; Pesquera, A.; Zurutuza, A.; Boukherroub, R.; Szunerits, S., *Anal Chem* **2014,** *86* (22), 11211-11216.

(13) Shapir, E.; Cohen, H.; Calzolari, A.; Cavazzoni, C.; Ryndyk, D. A.; Cuniberti, G.; Kotlyar, A.; Di Felice, R.; Porath, D., *Nat Mater* **2008,** *7* (1), 68-74.

(14) Ryndyk, D. A.; Shapir, E.; Porath, D.; Calzolari, A.; Di Felice, R.; Cuniberti, G., *Acs Nano* **2009,** *3* (7), 1651-1656.

(15) Tanaka, H.; Kawai, T., *Nat Nanotechnol* **2009,** *4* (8), 518-522.

(16) Sun, W.; Yao, J.; Yao, T.; Shi, S., *Analyst* **2013,** *138* (2), 421-424.

(17) Qiu, S.; Li, X.; Xiong, W.; Xie, L.; Guo, L.; Lin, Z.; Qiu, B.; Chen, G., *Biosens Bioelectron* **2013,** *41*, 403-408.

(18) Wang, F.; Ma, C.; Zeng, X.; Li, C.; Deng, Y.; He, N., *J Biomed Nanotechnol* **2012,** *8* (5), 786-790.

(19) Freeman, R.; Liu, X.; Willner, I., *J Am Chem Soc* **2011,** *133* (30), 11597-11604.

(20) Sassolas, A.; Leca-Bouvier, B. D.; Blum, L. J., *Chem Rev* **2008,** *108* (1), 109-139.

(21) Tosar, J. P.; Branas, G.; Laiz, J., *Biosens Bioelectron* **2010,** *26* (4), 1205-1217.

(22) Cai, Z.; Smith, N. L.; Zhang, J. T.; Asher, S. A., *Anal Chem* **2015,** *87* (10), 5013-5025.

(23) Zhang, J. T.; Wang, L.; Luo, J.; Tikhonov, A.; Kornienko, N.; Asher, S. A., *J Am Chem Soc* **2011,** *133* (24), 9152-9155.

(24) Kamenjicki, M.; Kasavamoorthy, R.; Asher, S., *Ionics* **2005,** *10*, 233-236.

(25) Nair, R. V.; Vijaya, R., *Prog Quant Electron* **2010,** *34* (3), 89-134.

(26) Sharma, A. C.; Jana, T.; Kesavamoorthy, R.; Shi, L.; Virji, M. A.; Finegold, D. N.; Asher, S. A., *J Am Chem Soc* **2004,** *126* (9), 2971-2977.

(27) Alexeev, V. L.; Sharma, A. C.; Goponenko, A. V.; Das, S.; Lednev, I. K.; Wilcox, C. S.; Finegold, D. N.; Asher, S. A., *Anal Chem* **2003,** *75* (10), 2316-2323.

(28) Tian, E. T.; Wang, J. X.; Zheng, Y. M.; Song, Y. L.; Jiang, L.; Zhu, D. B., *J Mater Chem* **2008,** *18* (10), 1116-1122.

(29) Yan, F. Y.; Asher, S., *Anal Bioanal Chem* **2007,** *387* (6), 2121-2130.

(30) Asher, S. A.; Sharma, A. C.; Goponenko, A. V.; Ward, M. M., *Anal Chem* **2003,** *75* (7), 1676-1683.

(31) Arunbabu, D.; Sannigrahi, A.; Jana, T., *Soft Matter* **2011,** *7* (6), 2592-2599.

(32) Xu, M.; Goponenko, A. V.; Asher, S. A., *J Am Chem Soc* **2008,** *130* (10), 3113-3119.

(33) Lee, K.; Asher, S. A., *J Am Chem Soc* **2000,** *122* (39), 9534-9537.

(34) MacConaghy, K. I.; Geary, C. I.; Kaar, J. L.; Stoykovich, M. P., *J Am Chem Soc* **2014,** *136* (19), 6896-6899.

(35) MacConaghy, K. I.; Chadly, D. M.; Stoykovich, M. P.; Kaar, J. L., *Anal Chem* **2015,** *87* (6), 3467-3475.

(36) Joerger, A. C.; Fersht, A. R., *Annu Rev Biochem* **2008,** *77*, 557-582.

(37) Joerger, A. C.; Fersht, A. R., *Oncogene* **2007,** *26* (15), 2226-2242.

(38) Freed-Pastor, W. A.; Prives, C., *Genes Dev* **2012,** *26* (12), 1268-1286.

(39) Lane, D. P.; Benchimol, S., *Genes Dev* **1990,** *4* (1), 1-8.

(40) Steele, R. J.; Thompson, A. M.; Hall, P. A.; Lane, D. P., *Br J Surg* **1998,** *85* (11), 1460-1467.

(41) Soussi, T.; Wiman, K. G., *Cancer Cell* **2007,** *12* (4), 303-312.

(42) Arunbabu, D.; Sannigrahi, A.; Jana, T., *J Appl Polym Sci* **2008,** *108* (4), 2718-2725.

(43) Reese, C. E.; Guerrero, C. D.; Weissman, J. M.; Lee, K.; Asher, S. A., *J Colloid Interf Sci* **2000,** *232* (1), 76-80.

(44) Stuchbury, T.; Shipton, M.; Norris, R.; Malthouse, J. P. G.; Brocklehurst, K.; Herbert, J. A. L.; Suschitzky, H., *Biochem J* **1975,** *151* (2), 417-432.

(45) Liu, D. P.; Song, H.; Xu, Y., *Oncogene* **2010,** *29* (7), 949-956.

(46) Soussi, T.; Lozano, G., *Biochem Biophys Res Commun* **2005,** *331* (3), 834-42.

(47) Flory, P. J., *Principles of polymer chemistry*. Cornell University Press: Ithaca, 1953.

(48) Howley, P. M.; Israel, M. A.; Law, M. F.; Martin, M. A., *Journal of Biological Chemistry* **1979,** *254* (11), 4876-4883.

(49) Robertson, K. D., *Nat Rev Genet* **2005,** *6* (8), 597-610.

(50) Shukla, A.; Sehgal, M.; Singh, T. R., *Gene* **2015,** *564* (2), 109-118.

(51) Ehrich, M.; Nelson, M. R.; Stanssens, P.; Zabeau, M.; Liloglou, T.; Xinarianos, G.; Cantor, C. R.; Field, J. K.; van den Boom, D., *Proc Natl Acad Sci U S A* **2005,** *102* (44), 15785-15790.

(52) Coolen, M. W.; Statham, A. L.; Gardiner-Garden, M.; Clark, S. J., *Nucleic Acids Res* **2007,** *35* (18), e119.

(53) Herman, J. G.; Graff, J. R.; Myohanen, S.; Nelkin, B. D.; Baylin, S. B., *Proc Natl Acad Sci U S A* **1996,** *93* (18), 9821-9826.

(54) Evron, E.; Dooley, W. C.; Umbricht, C. B.; Rosenthal, D.; Sacchi, N.; Gabrielson, E.; Soito, A. B.; Hung, D. T.; Ljung, B.; Davidson, N. E.; Sukumar, S., *Lancet* **2001,** *357* (9265), 1335-1336.

(55) Heimer, B. W.; Shatova, T. A.; Lee, J. K.; Kaastrup, K.; Sikes, H. D., *Analyst* **2014,** *139* (15), 3695-3701.

(56) Severin, P. M.; Zou, X.; Gaub, H. E.; Schulten, K., *Nucleic Acids Res* **2011,** *39* (20), 8740-8751.

(57) Dahl, C.; Guldberg, P., *Biogerontology* **2003,** *4* (4), 233-250.

(58) Hildebrand, J. H.; Scott, R. L., *Regular solutions*. Prentice-Hall: Englewood Cliffs, N.J., 1962.

(59) Hansen, C., *Hansen Solubility Parameters - A User's Handbook*. CRC Press: 1999.

(60) Cowie, J. M. G.; Arrighi, V., *Polymers: Chemistry and Physics of Modern materials*. 3 ed.; CRC Press: 2008.

(61) Jeffrey, A. M.; Jennette, K. W.; Blobstein, S. H.; Weinstein, I. B.; Beland, F. A.; Harvey, R. G.; Kasal, H.; Miura, I.; Nakanishi, K., *J Am Chem Soc* **1976,** *98* (18), 5714-5715.

(62) Osborne, M. R.; Harvey, R. G.; Brookes, P., *Chem Biol Interact* **1978,** *20* (1), 123-130.

(63) Kriek, E.; Den Engelse, L.; Scherer, E.; Westra, J. G., *Biochim Biophys Acta* **1984,** *738* (4), 181-201.

(64) Denissenko, M. F.; Pao, A.; Tang, M.; Pfeifer, G. P., *Science* **1996,** *274* (5286), 430-432.

CHAPTER 7 – DEVELOPMENT OF A THERMAL-RESPONSIVE PHOTONIC CRYSTAL HYDROGEL FOR THE HIGH-THROUGHPUT DETECTION OF SOLVENTS AND SMALL MOLECULES PRODUCED DURING MICROBIAL FERMENTATION

7.1 INTRODUCTION

In order to combat climate change and counteract diminishing supplies of fossil fuels, there is significant interest in research directed towards renewable and carbon-neutral energy sources such as biofuels. Biofuels are a renewable source of energy derived from a biological precursor.[1] In the simplest terms, there are three routes for the conversion of renewable biological materials into fuel-like molecules: 1) direct production by photosynthetic organisms such as plants and algae; 2) fermentative or nonfermentative production by heterotrophic organisms such as bacteria or yeast; and 3) chemical conversion of biomass to fuel.[2] At first glance, production of fuels direction from CO_2 via photosynthetic metabolism appears to be highly promising, however this approach faces major difficulties in terms of scalability and available land.[3-4] Chemical conversion of biomass to fuel also faces potentially insurmountable hurdle of requiring energy intensive and caustic pretreatment steps, making this process prohibitively expensive.[5-6]

Microbes, on the other hand, have been utilized in industrial processes for centuries. Some of the most successful examples include alcohol fermentation by *Saccharomyces cerevisiae* and bioplastic production by *Escherichia coli*.[7-8] However, though there are instances of effective industrial use of microbes, the expensive of feedstocks remain a major prohibitive factor to producing biofuels from microbes and, therefore, fermentation processes must be as carbon efficient as possible.[2] Methods for improving the efficiency of the fermentation process include reducing inhibitor sensitivity, increasing product tolerance, and increasing specific yields through directed evolution.[9-10] One difficulty of evolving more efficient microbial strains is time

consuming nature of the selection process. For example, if a microbial strain is being evolved to increase accumulation of an alcohol it is necessary to perform a comprehensive screen to quantify the production yields. Traditionally, this is performed by HPLC analysis, which, though automated, is extremely time-intensive.[11]

To alleviate this problem, we have developed a high-throughput photonic crystal hydrogel sensing platform capable of monitoring carbohydrate consumption during fermentation and, via an increase in measurement temperature, an endpoint measurement of ethanol production. Photonic crystal hydrogels, which are comprised of a photonic material embedded into a hydrogel network, have shown great utility in detecting solvent conditions,[12-14] small molecules,[15-18] and biomolecules.[19-20] The photonic crystal hydrogel used here is comprised of a crystalline colloidal array (CCA), a solution of highly charged nanoparticles, polymerized into an N-isopropylacrylamide (PNIPAM) hydrogel. The charged nanoparticles electrostatically repel each other in solutions, forming a 3-dimensional photonic crystal that Bragg diffracts visible light.[21] The diffraction wavelength is dependent upon the particle spacing which is modulated through volume transitions in the hydrogel. PNIPAM, a well-known thermal-responsive polymer, has a distinct lower critical solution temperature (LCST) where it exhibits a sharp volumetric transition due to hydrogen bonding and hydrophobic interactions inside the gel.[22-23] At temperatures below the LCST, the functional groups of the polymer hydrogen bond strongly with water molecules and the hydrogel remains the hydrophilic or swollen state. At temperature above the LCST, the hydrogen bonds between the functional groups and water are broken and the polymer undergoes a collapse into a reduced volume hydrophobic state.[24-26] Due to the strong dependence of the polymer state on hydrophobic and hydrogen bonding interactions, solvents

can also induce the same type of phase transition,[25, 27-28] which, because of the presence of the CCA, is seen as a color change of the hydrogel.

The PNIPAM photonic hydrogels were polymerized into a 96-well plate to facilitate high-throughput detection of glucose and ethanol, main components of a fermentation system. The presence of glucose or ethanol in solution acts to disrupt the hydrogen bonds between the PNIPAM and water,[29-30] thereby reducing the LCST, shrinking the hydrogel, and inducing a blueshift in the diffraction peak (**Figure 7.1**). Through the addition of hydrophobic and hydrophilic co-monomers we are able to tune the LCST of the material and, therefore, the response sensitivity to the target molecules. Furthermore, we can alter the measurement temperature to expand the detectable range and allow for the detection of molecules of differing hydrophobic character with the same polymer composition. Lastly, we used the developed sensing platform to monitor glucose consumption during *Saccharomyces cerevisiae* growth and ethanol accumulation after reaching the diauxic shift.

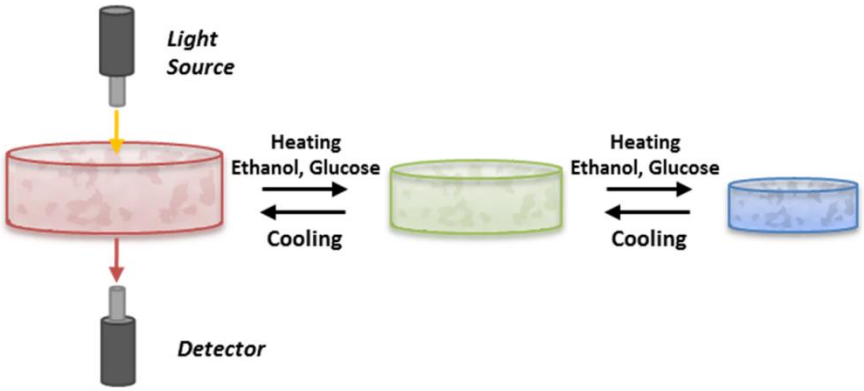

Figure 7.1 Schematic of photonic hydrogel response to temperature, glucose, and ethanol. Detection is preformed via high-throughput transmission spectroscopy with a conventional plate reader.

7.2 EXPERIMENTAL METHODS

7.2.1 Materials

N-isopropylacrylamide (NIPAM) was purchased from Sigma-Aldrich (St. Louis, MO) and purified by solubilizing in hexane at 60 °C followed by precipitation in an ice bath. White solid was filtered and stored at 4 °C for up to 2 wks. *N,N'*-methylenebis(acrylamide) (BA), and N-tert-butylacrylamide (tBA), and N-hydroxyethyl acrylamide (HEAA) monomers were purchased from Sigma-Aldrich and used without further purification. Wild-type (BY4709) *Saccharomyces cerevisiae* was purchased from ATCC (Manassas, VA). Half-are UV bottom 96-well plates (#3679) were purchased from Corning, Inc. (Corning, NY).

7.2.2 Synthesis of Colloidal Suspension of Nanospheres

As previously described, the colloidal suspension of highly-charged polystyrene (PS) nanospheres were synthesized via emulsion polymerization.[31] The colloidal suspension used had a concentration of 11 wt% in water and were ~110 nm in diameter with a polydispersity of 3.4%, as determined by dynamic light scattering (Titan DynaPro with Dyna V6.3.4 software package, Wyatt Technology, Inc.; Santa Barbara, CA). The suspension was stored at room temperature with BioRad (Hercules, CA) AG501-X8 mixed bed resin.

7.2.3 Hydrogel Polymerization and Crystalline Colloidal Array Formation

Hydrogels were photopolymerized by solubilizing 50-56 mg NIPAM (0.9-1 M) and 1.2 mg (0.015 M) BA in 480 µL of the CCA solution. The hydrophobic monomer (tBA) and hydrophilic monomer (HEAA) were dissolved in DMSO at 1 M and added to the NIPAM/BA solution to a final concentration of 0-0.1 M. The photoinitiator Irgacure 2959 (BASF; Florham Park, NJ) (10 wt% in DMSO) was added at a final concentration of 0.03 wt% to the CCA-monomer solution. For all hydrogels fabricated, the final monomer concentration was maintained

constant at 1 M. 4 µL of the solution was then pipetted into the center of each well of UV clear 96-well acrylic plate and an acrylic mold was placed into the wells to create hydrogels of approximately 175 µm in thickness. Samples were flood exposed with 365 nm light at 6 mW/cm^2 from a handheld UV mercury lamp for 90 min at 4 °C. It was necessary to cool samples during polymerization to prevent phase separation of the monomers. Films were subsequently rinsed and stored in ultrapure water for a minimum of 24 h prior to use.

7.2.4 LCST Determination and Diffraction Shift as a Function of Temperature

The LCST of the copolymer was determined by differential scanning calorimetry (TA DSC Q2000, Dallas, TX). Approximately 10 mg of water equilibrated hydrogel was tested. Samples were equilibrated at 15 °C for 10 minutes prior to ramping from 15 °C to 60 °C at 3 °C/min. LCST values were measured by the peak position of the endotherm. The diffraction shift do to the polymer collapse was measured in pure water after a 24 h equilibrium period. The temperature profiles were measured from 26 to 32 °C with a step size of 1 °C. Prior to measurement, the micro-well plate was incubated for 30 min at the desired temperature to ensure equilibrium had been reached.

7.2.5 Saccharomyces cerevisiae Culture

Wild-type (WT) *S. cerevisiae* was cultured in 25 mL of complete synthetic media with added yeast nitrogen base and glucose concentrations ranging from 0 to 20 g/L at 30 °C and 200 rpm. OD600 measurements were taken every 1.5 h and samples were centrifuged at 4000 x g for 10 minutes to pellet the cells. The supernatant was then removed and 160 µL was added to each well. The 96-well plate was then incubated at the desired temperature for 30 min before measurement to reach equilibrium.

7.2.6 Optical Diffraction Measurements

The optical response of the equilibrated hydrogel-encapsulated CCA biosensors was measured with a TECAN (Winooski, VT) Infinite 200 Pro series plate reader. After gels equilibrated at the desired temperature for 30 min, the absorbance spectrum was scanned from 300 to 800 nm. Diffraction shifts were calculated as the difference between the sample measurements and the reference measurements. For the glucose response curve and glucose depletion studies, reference samples of glucose in synthetic complete media were used. For the ethanol response curve and endpoint ethanol values, reference samples of synthetic complete media in the absence of glucose were used.

7.2.7 Endpoint Ethanol Measurement via HPLC

HPLC measurements were taken using a Biorad (Hercules, CA) Amine HPX-87H ion exclusion column with a Shimadazu (Kyoto, Japan) 10avp HPLC system. Mobile phase consisted of 5 mM aqueous sulfuric acid at a flow rate of 0.6 mL/min. Column temperature was maintained at 50 °C throughout analysis. Injection volumes were 40 µL and the run time was 35 min per sample.

7.3 RESULTS AND DISCUSSION

7.3.8 Fabrication of Photonic Crystal Hydrogels in a 96-well Plate Format for High-throughput Detection

Photonic crystal hydrogels were developed to be compatible with half-area UV transparent 96-well plates (**Figure 7.2**) to allow for high-throughput detection of the diffraction shift with a conventional microplate reader. Hydrogels were fabricated directly into the microwell plate by adding 4 µL of monomer containing CCA solution to the center of each well. An acrylic mold consisting of 96 pins, roughly the same diameter as the well, was pushed into

the plate, effectively compressing the monomer solution to the bottom of the wells. The mold was specifically designed to have pins that are approximately 175 μm shorter than the well depth to ensure uniform hydrogel thickness. The solution was then polymerized by exposing to 365 nm light through the bottom of the plate. Because polymerization was performed through the bottom of the plate, it was necessary to use UV transparent microplates, which have a thin and semi-flexible bottom. Fabrication of photonic hydrogels within a standard, full area, UV transparent 96-well plate was also attempted. However, the bottom of the larger wells flexed much more during the application of the mold, disrupting the self-assembly of the CCA. Due to the response mechanism of the system, the key capabilities of the plate reader include temperature control and the ability to perform spectral absorbance scans from 300 to 800 nm. Depending on the plate reader used, scanning each well takes on the order of 30 s, meaning that an entire plate can be read in ~45 min which is comparable to the time it takes to run a single sample on a conventional HPLC system.

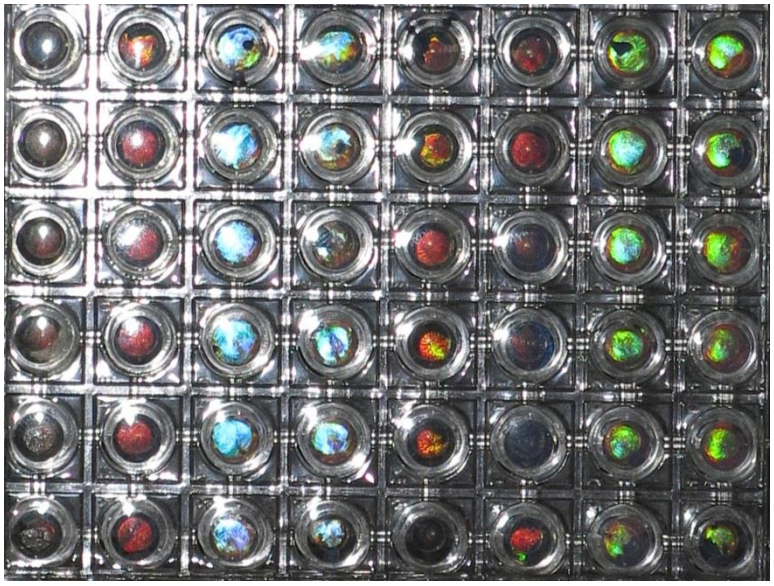

Figure 7.2 Image of photonic crystal hydrogels fabricated in a 96-well plate. From left to right in two column sections samples contain: 5 mol% HEAA, 5 mol% tBA, 2.5 mol% HEA, and 2.5 mol% tBA. Image was taken at 30 °C.

7.3.1 LCST Determination and Response as a Function of Temperature

Figure 7.3a shows the LCST of PNIPAM and PNIPAM co-polymers as a function of polymer composition, as measured by DSC. Photonic crystal hydrogel co-polymers were fabricated through blending 0 to 10 mol% of a hydrophobic (tBA) and hydrophilic (HEAA) monomer into the NIPAM monomer solution prior to polymerization. Hydrogels containing tBA showed decrease in LCST that is proportional to the molar increase of co-polymer concentration. Conversely, hydrogels containing HEAA show the opposite trend. Increasing the co-polymer concentration increases the LCST of the hydrogel. Inclusion of hydrophilic and hydrophobic co-monomers into a PNIPAM hydrogel affects the LCST of the resulting hydrogel via altering the polymer-water hydrogen bonds. The inclusion of a hydrophobic co-monomer acts to reduce the hydrogen bonding between PNIPAM and the water molecules, thereby stabilizing the hydrophobic or collapsed state of the hydrogel and lowering the LCST. Conversely, inclusion of

hydrophilic monomers increases the amount of hydrogen bonds between the polymer and solvent, resulting in a more swollen hydrogel and increased LCST.[22, 24]

This phenomena was further verified by monitoring the diffraction shift as a function of temperature for pure PNIPAM hydrogels and hydrogels containing 2.5% tBA and 2.5% HEA (**Figure 7.3b**). For all polymer compositions investigated, increasing the measurement temperature dramatically blueshifted the diffraction peak, indicating a reduction in hydrogel volume. Samples containing 2.5 mol% tBA, the hydrophobic monomer, exhibited a more rapid reduction in volume as the temperature is increased. Pure PNIPAM gels exhibited a transition between the hydrophobic and hydrophilic monomer. The hydrophilic monomer exhibited the lowest response to temperature over the range tested and the maximum diffraction shift that is a quarter the magnitude of the hydrophobic monomer. It is important to note that it was not possible to capture the entire thermal transition for any of the co-polymers investigated. The low end of the range, 26 °C, was chosen because this was the lowest temperature that the plate reader used could accurately control. At this temperature, both the tBA containing and PNIPAM hydrogels were already within the transition range. It also was not possible to capture the upper range of the transition because the hydrogels had collapsed to a state where the diffraction was below 300 nm and, therefore, no longer detectable.

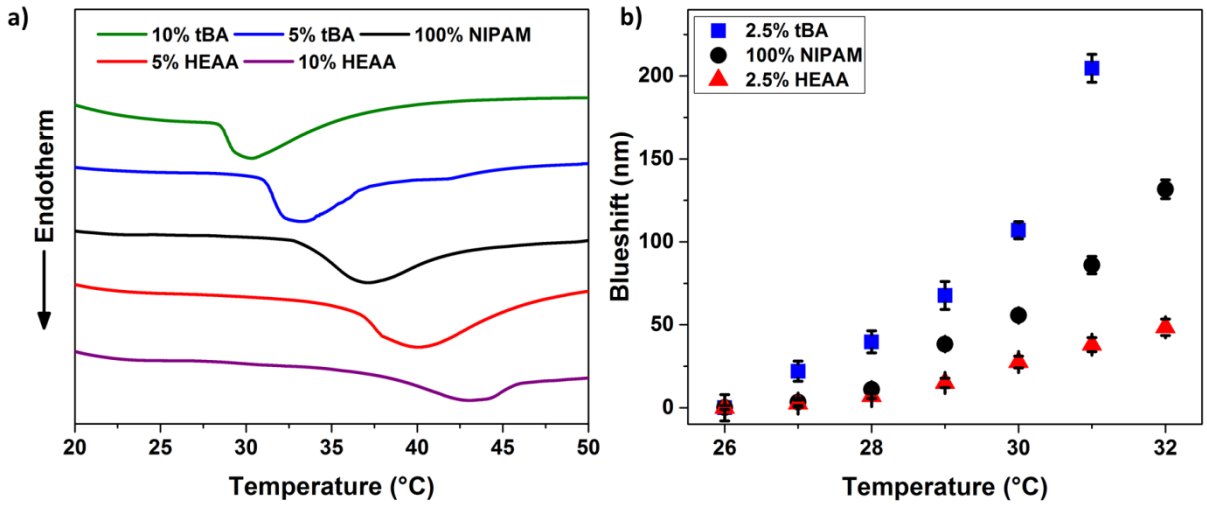

Figure 7.3 LCST as a function of polymer composition from DSC measurements (a) and hydrogel optical response as a function of polymer composition and temperature (b). DSC data was acquired by equilibrating samples at 15 °C for 10 minutes prior to ramping from 15 °C to 60 °C at a rate of 3 °C/min. Optical response data was performed in pure water. Error bars represent ± 1 σ from the mean of 4 distinct samples.

7.3.2 Sensor Response as a Function of Glucose Concentration in Synthetic Media

Due to the goal of detecting glucose consumption during microbial fermentation, it was necessary to choose a polymer composition with an LCST above the measurement temperature for samples equilibrated with synthetic complete media and 20 g/L of glucose. For the purpose of this study, a measurement temperature of 30 °C was chosen because that is a common temperature for culturing yeast. Because of the relatively high temperature, media, and glucose concentration, it was necessary to choose a hydrogel composition with a fairly high LCST to ensure that the diffraction wavelength was within the detection range (300 – 800 nm) across all applicable glucose concentrations (0 to 20 g/L). In theory, if different glucose concentrations or growth conditions were required, complete glucose detection could be achieved by selecting the polymer conditions that fit the temperature and media requirements (*e.g.* more HEAA for higher temperature or glucose concentrations).

Figure 7.4 is the redshift as a function of decreasing glucose concentration for polymers containing 2.5 mol% HEAA. Two conditions were tested: 1) varying glucose concentration in synthetic media and, 2) varying glucose with ethanol supplemented at 0.5 g ethanol/ g glucose consumed (*e.g.* 5 g ethanol/ 10 g glucose). As glucose is consumed the hydrogel redshifts because less glucose is available to disrupt the hydrogen bonding of the polymer and water. Therefore, the amount of hydrogen bonds increases, the LCST increases, and the diffraction peak redshifts. In a system that undergoes ethanol production from the consumptions of glucose, there is a competing response because ethanol accumulation disrupts the hydrogen bonding and lowers the LCST. An ethanol concentration of 0.5 g ethanol / g glucose was chosen because it is close to the theoretical maximum ethanol production of *S. cerevisiae*. At the theoretical maximum ethanol production, the difference between the glucose only control and the ethanol containing samples should be maximized. Though a slight difference is seen between the glucose standard and the ethanol containing samples, this difference is not large enough to differentiate between small variations in ethanol production rates that are expected from directed evolution of microbial strains. This lack of sensitivity is due to the fact that the measurement temperature is significantly lower than the LCST, which is approximately 38 °C in pure water for the polymer system used. It is necessary to measure the glucose consumption at such a low temperature for two reasons. One, there is significantly more initial glucose than final ethanol concentration (> 2 times) and measuring at a higher temperature would saturate the signal due to collapse of the polymer. Two, the hydrogel exhibits a larger response to glucose than to ethanol. This is likely due to the fact that glucose is a larger, more hydrophobic molecule that is better able to disrupt hydrogen bonding.

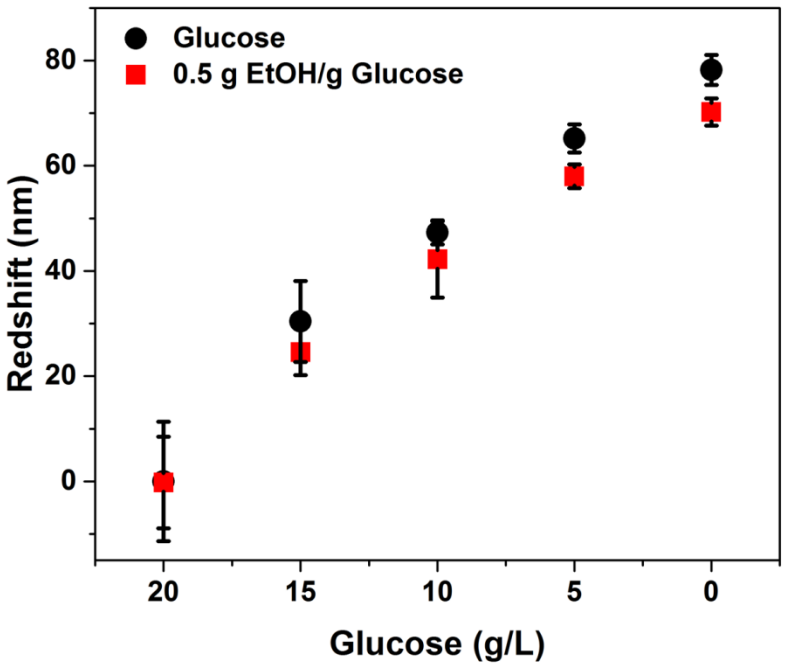

Figure 7.4 Redshift as a function of glucose in synthetic complete media and mixture of glucose and ethanol in synthetic media. Redshift was calculated as the difference between samples and reference samples containing 20 g/L glucose in synthetic media. Hydrogels contain 2.5 mol% HEAA and were measured at 30 °C. Error bars represent ± 1 σ from the mean of 4 distinct samples.

7.3.3 Sensor Response to Ethanol as a Function of Temperature and Concentration

To increase the sensitivity to ethanol is it necessary to measure the ethanol response at a temperature closer to the LCST of the material in the absence of glucose. **Figure 7.5** is the hydrogel response to ethanol in synthetic complete media as a function of temperature. Over the investigated range, which spans no ethanol production to the theoretical maximum, the response sensitivity dramatically increases as a function of temperature. As indicated by the glucose data, at 30 °C the sensor is not able to differentiate between no ethanol and 10 g/L ethanol. When the temperature is increased to 31 °C, the sensor can differentiate ethanol concentrations greater that 8 g/L. At 32 °C, the lower detection limit is 2 g/L ethanol. Though higher temperatures would allow for more sensitive detection, this range was selected because it is highly applicable for monitoring yeast fermentation. It is interesting to note that for the majority of the samples a 1 °C

increase (from 32 °C to 33 °C) shifted the response outside of the lower end of the detection range (*i. e.* below 300 nm). Though it is not possible to use this sensing platform to simultaneously measure glucose and ethanol concentration on the same hydrogel and in the same micro well, data suggests that glucose concentration may be monitored over the course of microbial fermentation and that, after all the glucose is depleted, it is possible to measure the ethanol accumulation.

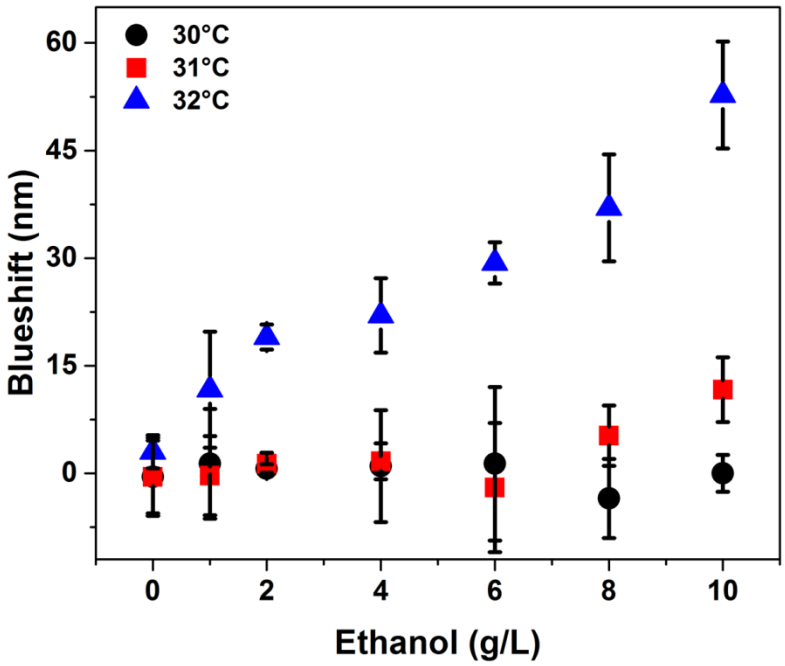

Figure 7.5 Blueshift as a function of both ethanol concentration and temperature. Sample contains synthetic complete media and ethanol. Blueshift was calculated as the difference between samples and reference samples containing synthetic complete media in the absence of glucose. Hydrogels contain 2.5 mol% HEAA. Error bars represent ± 1 σ from the mean of 4 distinct samples.

7.3.4 Application of the Photonic Hydrogel for Monitoring Microbial Fermentation

Wild-type *S. cerevisiae* was cultured for 15 h in synthetic complete media with yeast nitrogen base and 20 g/L glucose added. Reference measurements of media with 20 g/L glucose and media only were taken before measurement of the fermentation products. At the determined time points, samples were removed, the cells were centrifuged, and the glucose concentration of

the supernatant was measured. It was found that the redshift, due to consumption of glucose, closely matches the growth curve (**Figure 7.6a**). In the initial time points, there appears to be a slight lag phase before the response enters an exponential phase that mirror the exponential phase of the growth curve. After 13.5 hrs, the stationary phase was reached and growth halted. At the same time point, no further increase in response was seen, indicating that glucose consumption was complete. It is of interest to note that diffraction measurements were also attempted with samples containing microbial cells in the microplate wells. However, the noise was much greater than the signal and no clear trend could be elucidated. Likely, the noise was due to a localized response of the hydrogel to cells, sedimentation of the cells onto the hydrogel surface reducing the signal, or a combination of both factors.

After the growth had reached the stationary phase it was assumed that the glucose had been fully consumed. The samples were then heated to 32 °C and diffraction measurements were taken to determine the accumulation of ethanol (**Figure 7.6b**). The diffraction shift was found to be approximately 25 nm, which correlates to between 4 and 6 g/L ethanol. The concentration of glucose and ethanol were verified using HPLC. It was found that glucose had been completely consumed and the sample contained 7.9 g/L ethanol. Both the hydrogel sensor and HPLC indicated no ethanol in the media only control sample. The discrepancy between the hydrogel response and the HPLC results are likely due to interactions of other fermentation product within the hydrogel. HPLC analysis showed prominent acetic acid and glycol peaks. It is feasible that the presence of one or both of those small molecules act to reduce the sensor response to ethanol.

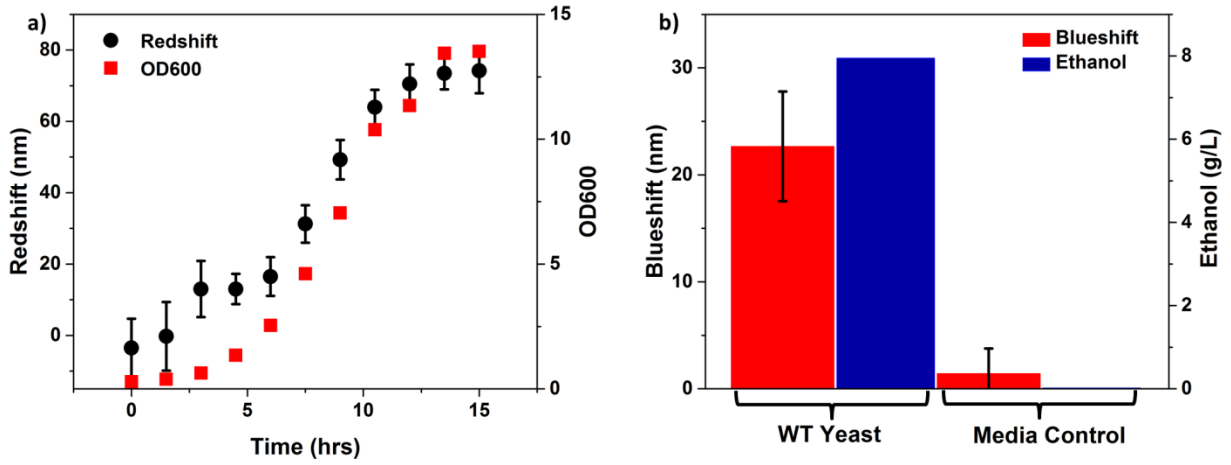

Figure 7.6 Redshift as a function of time during fermentation with *S. cerevisiae* (a) and blueshift as a function of sample for stationary phase growth (b). Redshift was calculated as the difference between samples and reference samples containing 20 g/L glucose in synthetic complete media and is due to consumption of glucose. Blueshift was calculated as the difference between samples and reference samples containing synthetic complete media in the absence of glucose. Ethanol concentration was determined via HPLC analysis. Hydrogels contain 2.5 mol% HEAA and were measured at 30 °C for (a) and 32 °C for (b). Error bars represent ± 1 σ from the mean of 4 distinct samples.

7.4 CONCLUSIONS

We developed a high-throughput photonic crystal hydrogel sensor responsive to both ethanol and glucose. The photonic crystal hydrogel is comprised of PNIPAM co-polymerized with hydrophobic and hydrophilic monomers to alter the LCST. Addition of either glucose or ethanol acts to reduce the hydrogen bonding between the polymer and solvent which, in turn, lowers the LCST, reduces the hydrogel volume, and blueshifts the diffraction peak. With this platform, we were able to detect glucose as a function of time during microbial fermentation. After consumption of glucose, we then increased the measurement temperature and were able to detect relevant concentrations of produced ethanol. Further study is still required to show that this platform can be used to detect modulations in ethanol accumulation after fermentation is complete. This will be accomplished by altering the growth conditions (*e.g.* reduced glucose concentration) to obtain cultures with differing endpoint ethanol accumulation. Lastly, expansion

of this platform to other microbial systems that produce other biofuels such as isobutanol or isopropanol is of interest.

7.5 REFERENCES

(1) Demirbas, A., *Appl Energ* **2009,** *86*, S108-S117.

(2) Rude, M. A.; Schirmer, A., *Curr Opin Microbiol* **2009,** *12* (3), 274-281.

(3) Chisti, Y., *Biotechnology Advances* **2007,** *25* (3), 294-306.

(4) Hu, Q.; Sommerfeld, M.; Jarvis, E.; Ghirardi, M.; Posewitz, M.; Seibert, M.; Darzins, A., *Plant Journal* **2008,** *54* (4), 621-639.

(5) Demirbas, A., *Prog Energ Combust* **2007,** *33* (1), 1-18.

(6) Huber, G. W.; Iborra, S.; Corma, A., *Chem Rev* **2006,** *106* (9), 4044-4098.

(7) Li, R.; Zhang, H. X.; Qi, Q. S., *Bioresource Technol* **2007,** *98* (12), 2313-2320.

(8) Li, R.; Chen, Q.; Wang, P. G.; Qi, Q. S., *Appl Microbiol Biot* **2007,** *75* (5), 1103-1109.

(9) Antoni, D.; Zverlov, V. V.; Schwarz, W. H., *Appl Microbiol Biot* **2007,** *77* (1), 23-35.

(10) Fortman, J. L.; Chhabra, S.; Mukhopadhyay, A.; Chou, H.; Lee, T. S.; Steen, E.; Keasling, J. D., *Trends Biotechnol* **2008,** *26* (7), 375-381.

(11) Shen, Y.; Chen, X.; Peng, B. Y.; Chen, L. Y.; Hou, J.; Bao, X. M., *Appl Microbiol Biot* **2012,** *96* (4), 1079-1091.

(12) Chen, C.; Zhu, Y.; Bao, H.; Shen, J.; Jiang, H.; Peng, L.; Yang, X.; Li, C.; Chen, G., *Chem Commun* **2011,** *47* (19), 5530-2.

(13) Zhang, Y. Q.; Fu, Q. Q.; Ge, J. P., *Nat Commun* **2015,** *6*.

(14) Wang, F. Y.; Zhu, Z. G.; Xue, M.; Xue, F.; Wang, Q. H.; Meng, Z. H.; Lu, W.; Chen, W.; Qi, F. L.; Yan, Z. Q., *Sensor Actuat B-Chem* **2015,** *220*, 222-226.

(15) Alexeev, V. L.; Sharma, A. C.; Goponenko, A. V.; Das, S.; Lednev, I. K.; Wilcox, C. S.; Finegold, D. N.; Asher, S. A., *Anal Chem* **2003,** *75* (10), 2316-23.

(16) Arunbabu, D.; Sannigrahi, A.; Jana, T., *Soft Matter* **2011,** *7* (6), 2592-2599.

(17) Walker, J. P.; Kimble, K. W.; Asher, S. A., *Anal Bioanal Chem* **2007,** *389* (7-8), 2115-2124.

(18) Zhang, J. T.; Smith, N.; Asher, S. A., *Anal Chem* **2012,** *84* (15), 6416-6420.

(19) MacConaghy, K. I.; Geary, C. I.; Kaar, J. L.; Stoykovich, M. P., *J Am Chem Soc* **2014,** *136* (19), 6896-9.

(20) Zhang, J. T.; Cai, Z. Y.; Kwak, D. H.; Liu, X. Y.; Asher, S. A., *Anal Chem* **2014,** *86* (18), 9036-9041.

(21) Rundquist, P. A.; Photinos, P.; Jagannathan, S.; Asher, S. A., *J Chem Phys* **1989,** *91* (8), 4932-4941.

(22) Pagonis, K.; Bokias, G., *Polym Bull* **2007,** *58* (1), 289-294.

(23) Ruel-Gariepy, E.; Leroux, J. C., *Eur J Pharm Biopharm* **2004,** *58* (2), 409-426.

(24) Yildiz, B.; Isik, B.; Kis, M., *Eur Polym J* **2002,** *38* (7), 1343-1347.

(25) Liu, L.; Song, X. L.; Ju, X. J.; Xie, R.; Liu, Z.; Chu, L. Y., *The journal of physical chemistry. B* **2012,** *116* (3), 974-9.

(26) Caykara, T.; Kiper, S.; Demirel, G., *Eur Polym J* **2006,** *42* (2), 348-355.

(27) Li, P. F.; Xie, R.; Fan, H.; Ju, X. J.; Chen, Y. C.; Meng, T.; Chu, L. Y., *Ind Eng Chem Res* **2012,** *51* (28), 9554-9563.

(28) Zhi, D. Y.; Huang, Y. M.; Han, X.; Liu, H. L.; Hu, Y., *Chem Eng Sci* **2010,** *65* (10), 3223-3230.

(29) Zhu, P. W.; Napper, D. H., *J Colloid Interf Sci* **1996,** *177* (2), 343-352.

(30) Xu, X. P.; Huther, A.; Maurer, G., *Chinese J Chem Eng* **2003,** *11* (3), 264-268.

(31) Reese, C. E.; Guerrero, C. D.; Weissman, J. M.; Lee, K.; Asher, S. A., *J Colloid Interf Sci* **2000,** *232* (1), 76-80.

BIBLIOGRAPHY

1) Ahmed, E. M., *J Adv Res* **2015,** *6* (2), 105-121.

2) Alexeev, V. L.; Sharma, A. C.; Goponenko, A. V.; Das, S.; Lednev, I. K.; Wilcox, C. S.; Finegold, D. N.; Asher, S. A., *Anal Chem* **2003,** *75* (10), 2316-2323.

3) Antoni, D.; Zverlov, V. V.; Schwarz, W. H., *Appl Microbiol Biot* **2007,** *77* (1), 23-35.

4) Arunbabu, D.; Sannigrahi, A.; Jana, T., J Appl Polym Sci **2008**, 108 (4), 2718-2725.

5) Arunbabu, D.; Sannigrahi, A.; Jana, T., *Soft Matter* **2011,** *7* (6), 2592-2599.

6) Asami, Y.; Oishi, J.; Kitazaki, H.; Kamimoto, J.; Kang, J. H.; Niidome, T.; Mori, T.; Katayama, Y., Anal Biochem 2011, 418 (1), 44-49.

7) Asher, S. A.; Alexeev, V. L.; Goponenko, A. V.; Sharma, A. C.; Lednev, I. K.; Wilcox, C. S.; Finegold, D. N., *J Am Chem Soc* **2003,** *125* (11), 3322-3329.

8) Asher, S. A.; Holtz, J.; Liu, L.; Wu, Z. J., J Am Chem Soc **1994**, 116 (11), 4997-4998.

9) Asher, S. A.; Kesavamoorthy, R.; Jagannathan, S.; Rundquist, P., *Nonlinear Optics Iii* **1992,** *1626*, 238-242.

10) Asher, S. A.; Sharma, A. C.; Goponenko, A. V.; Ward, M. M., *Anal Chem* **2003,** *75* (7), 1676-1683.

11) Babacan, S.; Pivarnik, P.; Letcher, S.; Rand, A. G., *Biosens Bioelectron* **2000,** *15* (11-12), 615-21.

12) Baca, J. T.; Finegold, D. N.; Asher, S. A., *Analyst* **2008,** *133* (3), 385-390.

13) Bachmann, B. A.; Riml, A.; Huber, R. G.; Baillie, G. S.; Liedl, K. R. ; Valovka, T.; Stefan, E. Proc. natl. Acad. Sci. U. S. A. **2013**, 110 (21), 8531-8536.

14) Barson, C. A.; Bevington, J. C.; Huckerby, T. N., Polym Bull **1991**, 25 (1), 83-86.

15) Ben-Moshe, M.; Alexeev, V. L.; Asher, S. A., Anal Chem **2006**, 78 (14), 5149-5157.

16) Besanceney-Webler, C.; Jiang, H.; Zheng, T. Q.; Feng, L.; del Amo, D. S.; Wang, W.; Klivansky, L. M.; Marlow, F. L.; Liu, Y.; Wu, P., Angew Chem Int Edit **2011,** 50 (35), 8051-8056.

17) Best, J. P.; Neubauer, M. P.; Javed, S.; Dam, H. H.; Fery, A.; Caruso, F., *Langmuir* **2013,** *29* (31), 9814-9823.

18) Binder, W. H.; Sachsenhofer, R., Macromol Rapid Comm **2007**, 28 (1), 15-54.

19) Blanco, A.; Chomski, E.; Grabtchak, S.; Ibisate, M.; John, S.; Leonard, S. W.; Lopez, C.; Meseguer, F.; Miguez, H.; Mondia, J. P.; Ozin, G. A.; Toader, O.; van Driel, H. M., *Nature* **2000,** *405* (6785), 437-440.

20) Brannonpeppas, L.; Peppas, N. A., *Chem Eng Sci* **1991,** *46* (3), 715-722.

21) Buenger, D.; Topuz, F.; Groll, J., *Prog Polym Sci* **2012,** *37* (12), 1678-1719.

22) Cai, Z. Y.; Kwak, D. H.; Punihaole, D.; Hong, Z. M.; Velankar, S. S.; Liu, X. Y.; Asher, S. A., *Angew Chem Int Edit* **2015,** *53* (44), 13036-13040.

23) Cai, Z. Y.; Smith, N. L.; Zhang, J. T.; Asher, S. A., *Anal Chem* **2015,** *87* (10), 5013-5025.

24) Carlson, R. J.; Asher, S. A., *Appl Spectrosc* **1984,** *38* (3), 297-304.

25) Caykara, T.; Kiper, S.; Demirel, G., *Eur Polym J* **2006,** *42* (2), 348-355.

26) Chan, L. L.; Gosangari, S. L.; Watkin, K. L.; Cunningham, B. T., *Sensor Actuat B-Chem* **2008,** *132* (2), 418-425.

27) Chapman, R.; Jolliffe, K. A.; Perrier, S., Polym Chem-Uk **2011**, 2 (9), 1956-1963.

28) Chen, C.; Zhu, Y. H.; Bao, H.; Shen, J. H.; Jiang, H. L.; Peng, L. M.; Yang, X. L.; Li, C. Z.; Chen, G. R., *Chem Commun* **2011,** *47* (19), 5530-5532.

29) Cheng, H. C.; Van Patten, S. M.; Smith, A. J.; Walsh, D. A. Biochem. J. **1985**, 231 (3), 655-661.

30) Chisti, Y., *Biotechnology Advances* **2007,** *25* (3), 294-306.

31) Choi, S. Y.; Mamak, M.; von Freymann, G.; Chopra, N.; Ozin, G. A., *Nano Lett* **2006,** *6* (11), 2456-2461.

32) Cohen, P.; Alessi, D. R., Acs Chem Biol **2013**, 8 (1), 96-104.

33) Colodrero, S.; Ocana, M.; Miguez, H., *Langmuir* **2008,** *24* (9), 4430-4434.

34) Cox, W. G.; Singer, V. L., *Biotechniques* **2004,** *36* (1), 114-+.

35) Cui, Q. Z.; Wang, W.; Gu, B. H.; Liang, L. Y., *Macromolecules* **2012,** *45* (20), 8382-8386.

36) Cunningham, B. T.; Laing, L., *Expert Rev Proteomic* **2006,** *3* (3), 271-281.

37) Cunningham, B. T.; Li, P.; Schulz, S.; Lin, B.; Baird, C.; Gerstenmaier, J.; Genick, C.; Wang, F.; Fine, E.; Laing, L., *J Biomol Screen* **2004,** *9* (6), 481-490.

38) Darragh, P. J.; Gaskin, A. J.; Terrell, B. C.; Sanders, J. V., *Nature* **1966,** *209* (5018), 13-&.

39) Demirbas, A., *Appl Energ* **2009,** *86*, S108-S117.

40) Demirbas, A., *Prog Energ Combust* **2007,** *33* (1), 1-18.

41) Dusek, K.; Patterso.D, *J Polym Sci A2* **1968,** *6* (7pa2), 1209-&.

42) Endo, T.; Yanagida, Y.; Hatsuzawa, T., Sensor Actuat B-Chem **2007**, 125 (2), 589-595.

43) Fan, X.; White, I. M.; Shopova, S. I.; Zhu, H.; Suter, J. D.; Sun, Y., *Anal Chim Acta* **2008,** *620* (1-2), 8-26.

44) Fedorov, O.; Niesen, F. H.; Knapp, S., Kinase Inhibitors: Methods and Protocols **2012**, 795, 109-118.

45) Flory, P. J., *Principles of polymer chemistry*. Cornell University Press: Ithaca,, **1953**

46) Fortman, J. L.; Chhabra, S.; Mukhopadhyay, A.; Chou, H.; Lee, T. S.; Steen, E.; Keasling, J. D., *Trends Biotechnol* **2008,** *26* (7), 375-381.

47) Fu, X. Q.; Guo, M.; Wu, J.; Zhan, S. X., *Acta Chim Sinica* **2012,** *70* (5), 611-616.

48) Fuaad, A. A. H. A.; Azmi, F.; Skwarczynski, M.; Toth, I., Molecules **2013**, 18 (11), 13148-13174.

49) Ge, J. P.; Yin, Y. D., *Angew Chem Int Edit* **2011,** *50* (7), 1492-1522.

50) Gerlach, G.; Arndt, K. F., *Springer Ser Chem Se* **2009,** *6*.

51) Global Industry Analysts, I. *Biosensors - A Global Strategic Business Report*; San Jose, 2014; p 287.

52) Goponenko, A. V.; Asher, S. A., *J Am Chem Soc* **2005,** *127* (30), 10753-10759.

53) Grieshaber, D.; MacKenzie, R.; Voros, J.; Reimhult, E., *Sensors (Basel)* **2008,** *8* (3), 1400-1458.

54) Guo, C.; Zhou, C. H.; Sai, N.; Ning, B. A.; Liu, M.; Chen, H. S.; Gao, Z. X., *Sensor Actuat B-Chem* **2012,** *166*, 17-23.

55) Guo, X. W., *J Biophotonics* **2012,** *5* (7), 483-501.

56) Haake, H. M.; Schutz, A.; Gauglitz, G., *Fresenius J Anal Chem* **2000,** *366* (6-7), 576-85.

57) He, L. H.; Fullenkamp, D. E.; Rivera, J. G.; Messersmith, P. B., *Chem Commun* **2011,** *47* (26), 7497-7499.

58) Hermanson, G. T., Bioconjugate techniques. 2nd edition. ed.; p.219-223.

59) Holtz, J. H.; Asher, S. A., *Nature* **1997,** *389* (6653), 829-832.

60) Holtz, J. H.; Holtz, J. S. W.; Munro, C. H.; Asher, S. A., *Anal Chem* **1998,** *70* (4), 780-791.

61) Horkay, F.; Tasaki, I.; Basser, P. J., *Biomacromolecules* **2000,** *1* (1), 84-90.

62) Hu, Q.; Sommerfeld, M.; Jarvis, E.; Ghirardi, M.; Posewitz, M.; Seibert, M.; Darzins, A., *Plant Journal* **2008,** *54* (4), 621-639.

63) Huber, G. W.; Iborra, S.; Corma, A., *Chem Rev* **2006,** *106* (9), 4044-4098.

64) Hunter, T., Cell **2000**, 100 (1), 113-127.

65) Ifkovits, J. L.; Burdick, J. A., *Tissue Eng* **2007,** *13* (10), 2369-2385.

66) Inamori, K.; Kyo, M.; Matsukawa, K.; Inoue, Y.; Sonoda, T.; Tatematsu, K.; Tanizawa, K.; Mori, T.; Katayama, Y., *Anal Chem* **2008**, 80 (3), 643-65

67) Ispas, C. R.; Crivat, G.; Andreescu, S., *Anal Lett* **2012,** *45* (2-3), 168-186.

68) Jeong, H. J.; Ohmuro-Matsuyama, Y.; Ohashi, H.; Ohsawa, F.; Tatsu, Y.; Inagaki, M.; Ueda, H., *Biosens Bioelectron* **2013**, 40 (1), 17-23.

69) Jiang, H. L.; Zhu, Y. H.; Chen, C.; Shen, J. H.; Bao, H.; Peng, L. M.; Yang, X. L.; Li, C. Z., *New J Chem* **2012,** *36* (4), 1051-1056.

70) Joannopoulos, J. D.; Villeneuve, P. R.; Fan, S. H., *Nature* **1997,** *386* (6621), 143-149.

71) John, S., *Nat Mater* **2012,** *11* (12), 997-999.

72) John, S., *Phys Rev Lett* **1987,** *58* (23), 2486-2489.

73) Kado, S.; Otani, H.; Nakahara, Y.; Kimura, K., *Chem Commun* **2013,** *49* (9), 886-8.

74) Kakwere, H.; Chun, C. K. Y.; Jolliffe, K. A.; Payne, R. J.; Perrier, S., *Chem Commun* **2010**, 46 (13), 2188-2190.

75) Kang, J. H.; Asami, Y.; Murata, M.; Kitazaki, H.; Sadanaga, N.; Tokunaga, E.; Shiotani, S.; Okada, S.; Maehara, Y.; Niidome, T.; Hashizume, M.; Mori, T.; Katayama, Y., *Biosens Bioelectron* **2010,** 25 (8), 1869-74.

76) Karra, S.; Gorski, W., *Anal Chem* **2013,** *85* (21), 10573-10580.

77) Khokhlov, A. R.; Starodubtzev, S. G.; Vasilevskaya, V. V., *Adv Polym Sci* **1993,** *109*, 123-175.

78) Kilian, K. A.; Lai, L. M. H.; Magenau, A.; Cartland, S.; Bocking, T.; Di Girolamo, N.; Gal, M.; Gaus, K.; Gooding, J. J., *Nano Lett* **2009,** *9* (5), 2021-2025.

79) Kimble, K. W.; Walker, J. P.; Finegold, D. N.; Asher, S. A., *Anal Bioanal Chem* **2006**, 385 (4), 678-685.

80) Kinoshita, S.; Yoshioka, S., *Chemphyschem* **2005,** *6* (8), 1442-1459.

81) Ko, K. C.; Choi, M. H.; Rho, J. K.; Park, S. H., *Sensor Actuat B-Chem* **2013**, 178, 434-442.

82) Koerber, J. T.; Thomsen, N. D.; Hannigan, B. T.; Degrado, W. F.; Wells, J. A., *Nat Biotechnol* **2013**, 31 (10), 916-924

83) Kolb, H. C.; Finn, M. G.; Sharpless, K. B., *Angew Chem Int Edit* **2001**, 40 (11), 2004-2036.

84) Kopecek, J., *Biomaterials* **2007,** *28* (34), 5185-5192.

85) Kotanen, C. N.; Moussy, F. G.; Carrara, S.; Guiseppi-Elie, A., *Biosens Bioelectron* **2012,** *35* (1), 14-26.

86) Kozlovskaya, V.; Chen, J.; Tedjo, C.; Liang, X.; Campos-Gomez, J.; Oh, J. W.; Saeed, M.; Lungu, C. T.; Kharlampieva, E., *J Mater Chem B* **2014,** *2* (17), 2494-2507.

87) Law, W. C.; Yong, K. T.; Baev, A.; Prasad, P. N., *Acs Nano* **2011,** *5* (6), 4858-4864.

88) Lee, K.; Asher, S. A., *J Am Chem Soc* **2000,** *122* (39), 9534-9537.

89) Lee, Y. J.; Pruzinsky, S. A.; Braun, P. V., *Langmuir* **2004,** *20* (8), 3096-3106.

90) Li, P. F.; Xie, R.; Fan, H.; Ju, X. J.; Chen, Y. C.; Meng, T.; Chu, L. Y., *Ind Eng Chem Res* **2012,** *51* (28), 9554-9563.

91) Li, R.; Chen, Q.; Wang, P. G.; Qi, Q. S., *Appl Microbiol Biot* **2007,** *75* (5), 1103-1109.

92) Li, R.; Zhang, H. X.; Qi, Q. S., *Bioresource Technol* **2007,** *98* (12), 2313-2320.

93) Li, X.; Peng, L.; Cui, J.; Li, W.; Lin, C.; Xu, D.; Tian, T.; Zhang, G.; Zhang, D.; Li, G., *Small* **2012,** *8* (4), 612-8.

94) Li, Y. J.; Xie, W. H.; Fang, G. J., *Anal Bioanal Chem* **2008,** *390* (8), 2049-2057.

95) Liang, L. Y.; Astruc, D., *Coordin Chem Rev* **2011**, 255 (23-24), 2933-2945.

96) Liu, L.; Song, X. L.; Ju, X. J.; Xie, R.; Liu, Z.; Chu, L. Y., *The journal of physical chemistry. B* **2012,** *116* (3), 974-9.

97) Liu, Y.; Yu, X.; Zhao, R.; Shangguan, D. H.; Bo, Z. Y.; Liu, G. Q., *Biosens Bioelectron* **2003,** *19* (1), 9-19.

98) Lochner, A.; Moolman, J. A., *Cardiovasc Drug Rev* **2006**, 24 (3-4), 261-74.

99) Lou, S.; Guo, X. M.; Fan, T. X.; Zhang, D., *Energ Environ Sci* **2012,** *5* (11), 9195-9216.

100) Ma, H. C.; Deacon, S.; Horiuchi, K., *Expert Opin Drug Dis* **2008,** *3* (6), 607-621.

101) Ma, X. Y.; Yan, Z. J., *Int J Mod Phys B* **2007,** *21* (16), 2761-2768.

102) MacConaghy, K. I.; Geary, C. I.; Kaar, J. L.; Stoykovich, M. P., *J Am Chem Soc* **2014,** *136* (19), 6896-6899.

103) Malkoch, M.; Thibault, R. J.; Drockenmuller, E.; Messerschmidt, M.; Voit, B.; Russell, T. P.; Hawker, C. J., *J Am Chem Soc* **2005**, 127 (42), 14942-14949.

104) Markets&Markets *In Vitro Diagnostic (IVD) Market, Technique, & Applications - Forecast to 2017*; Pune, **2013.**

105) Marrazza, G., *Biosensors (Basel)* **2014,** *4* (3), 301-17.

106) Masterson, L. R.; Shi, L.; Metcalfe, E.; Gao, J. L.; Taylor, S. S.; Veglia, G., *Proc Natl Acad Sci U S A* **2011,** 108 (17), 6969-6974.

107) Metz, J. T.; Johnson, E. F.; Soni, N. B.; Merta, P. J.; Kifle, L.; Hajduk, P. J., *Nat Chem Biol* **2011**, 7 (4), 200-202.

108) Miduturu, C. V.; Deng, X. M.; Kwiatkowski, N.; Yang, W. N. A.; Brault, L.; Filippakopoulos, P.; Chung, E.; Yang, Q. K.; Schwaller, J.; Knapp, S.; King, R. W.; Lee, J. D.; Herrgard, S.; Zarrinkar, P.; Gray, N. S., *Chem Biol* **2011**, 18 (7), 868-879.

109) Moerner, W. E., *P Natl Acad Sci USA* **2007,** *104* (31), 12596-602.

110) Muscatello, M. M. W.; Asher, S. A., *Adv Funct Mater* **2008,** *18* (8), 1186-1193.

111) Muscatello, M. M. W.; Stunja, L. E.; Thareja, P.; Wang, L. L.; Bohn, J. J.; Velankar, S. S.; Asher, S. A., *Macromolecules* **2009,** *42* (13), 4403-4406.

112) Nair, R. V.; Vijaya, R., *Prog Quant Electron* **2010,** *34* (3), 89-134.

113) Nakajima, N.; Ikada, Y., *Bioconjugate Chem* **1995,** 6 (1), 123-130.

114) Narsaiah, K.; Jha, S. N.; Bhardwaj, R.; Sharma, R.; Kumar, R., *J Food Sci Tech Mys* **2012,** *49* (4), 383-406.

115) Nemethy, A.; Solti, K.; Kiss, L.; Gyarmati, B.; Deli, M. A.; Csanyi, E.; Szilagyi, A., *Eur Polym J* **2013,** *49* (9), 2392-2403.

116) Ohshima, H.; Ohki, S., *Biophys J* **1985,** *47* (5), 673-678.

117) Oishi, J., Asami, Y.; Mori, T.; Kang, J.-H.; Tanabe, M.; Niidome, T.; Katayama, Y. *ChemBioChem* **2007**, 8 (8), 875.

118) Okay, O., *Springer Ser Chem Se* **2009,** *6*, 1-14.

119) Olive, D. M., *Expert Rev Proteomics* **2004**, 1 (3), 327-41.

120) Orosco, M. M.; Pacholski, C.; Miskelly, G. M.; Sailor, M. J., *Adv Mater* **2006,** *18* (11), 1393-+.

121) Pagonis, K.; Bokias, G., *Polym Bull* **2007,** *58* (1), 289-294.

122) Pan, Z.; Ma, J. K.; Yan, J.; Zhou, M.; Gao, J. P., *J Mater Chem* **2012,** *22* (5), 2018-2025.

123) Paquet, C.; Kumacheva, E., *Mater Today* **2008,** *11* (4), 48-56.

124) Parker, A. R.; McPhedran, R. C.; McKenzie, D. R.; Botten, L. C.; Nicorovici, N. A. P., *Nature* **2001,** *409* (6816), 36-37.

125) Perkel, J. M., *Science* **2009,** *324* (5928), 815-817.

126) Prevel, C.; Pellerano, M.; Van, T. N.; Morris, M. C., *Biotechnol J* **2014,** *9* (2), 253-65.

127) Qiu, Y.; Park, K., *Adv Drug Deliver Rev* **2012,** *64*, 49-60.

128) Ramadan, K. S.; Sameoto, D.; Evoy, S., *Smart Mater Struct* **2014,** *23* (3).

129) Reese, C. E.; Asher, S. A., *Anal Chem* **2003,** *75* (15), 3915-3918.

130) Reese, C. E.; Guerrero, C. D.; Weissman, J. M.; Lee, K.; Asher, S. A., *J Colloid Interf Sci* **2000,** *232* (1), 76-80.

131) Rostovtsev, V. V.; Green, L. G.; Fokin, V. V.; Sharpless, K. B., *Angew Chem Int Edit* **2002**, 41 (14), 2596-2601.

132) Rude, M. A.; Schirmer, A., *Curr Opin Microbiol* **2009,** *12* (3), 274-281.

133) Ruel-Gariepy, E.; Leroux, J. C., *Eur J Pharm Biopharm* **2004,** *58* (2), 409-426.

134) Rundquist, P. A.; Photinos, P.; Jagannathan, S.; Asher, S. A., *J Chem Phys* **1989,** *91* (8), 4932-4941.

135) Sagadevan, S.; Periasamy, M., *Rev Adv Mater Sci* **2014,** *36* (1), 62-69.

136) Saha, K.; Agasti, S. S.; Kim, C.; Li, X.; Rotello, V. M., *Chem Rev* **2012,** *112* (5), 2739-79.

137) Sang, S.; Wang, Y.; Feng, Q.; Wei, Y.; Ji, J.; Zhang, W., *Crit Rev Biotechnol* **2015**, 1-17.

138) Seamon, K. B.; Daly, J. W. J. *Cyclic Nucleotide Res*. **1981**, 7 (4), 201-224.

139) Shamah, S. M.; Cunningham, B. T., *Analyst* **2011,** *136* (6), 1090-1102.

140) Sharma, A. C.; Jana, T.; Kesavamoorthy, R.; Shi, L. J.; Virji, M. A.; Finegold, D. N.; Asher, S. A., *J Am Chem Soc* **2004,** *126* (9), 2971-2977.

141) Shen, M. Y.; Zhou, S. Y.; Li, Y. Y.; Pan, P. C.; Zhang, L. L.; Hou, T. J., *Mol Biosyst* **2013**, 9 (3), 361-374.

142) Shen, Y.; Chen, X.; Peng, B. Y.; Chen, L. Y.; Hou, J.; Bao, X. M., *Appl Microbiol Biot* **2012,** *96* (4), 1079-1091.

143) Shibayama, M.; Tanaka, T., *Adv Polym Sci* **1993,** *109*, 1-62.

144) Shin, J.; Braun, P. V.; Lee, W., *Sensor Actuat B-Chem* **2010**, 150 (1), 183-190.

145) Smith, N. L.; Hong, Z. M.; Asher, S. A., *Analyst* **2014,** *139* (24), 6379-6386.

146) Soper, S. A.; Brown, K.; Ellington, A.; Frazier, B.; Garcia-Manero, G.; Gau, V.; Gutman, S. I.; Hayes, D. F.; Korte, B.; Landers, J. L.; Larson, D.; Ligler, F.; Majumdar, A.; Mascini, M.; Nolte, D.; Rosenzweig, Z.; Wang, J.; Wilson, D., *Biosens Bioelectron* **2006,** *21* (10), 1932-42.

147) Soppimath, K. S.; Aminabhavi, T. M.; Dave, A. M.; Kumbar, S. G.; Rudzinski, W. E., *Drug Dev Ind Pharm* **2002,** *28* (8), 957-974.

148) Stradiotto, N. R.; Yamanaka, H.; Zanoni, M. V. B., *J Brazil Chem Soc* **2003,** *14* (2), 159-173.

149) Takeda, H.; Goshima, N.; Nomura, N., *Surface Plasmon Resonance: Methods and Protocols* **2010**, 627, 131-145.

150) Tanaka, T., *Sci Am* **1981,** *244* (1), 124-&.

151) Tandon, S.; Kesavamoorthy, R.; Asher, S. A., *J Chem Phys* **1998,** *109* (15), 6490-6496.

152) Tang, W.; Becker, M. L., *Chem Soc Rev* **2014**, 43 (20), 7013-7039.

153) Threm, D.; Nazirizadeh, Y.; Gerken, M., *J Biophotonics* **2012,** *5* (8-9), 601-616.

154) Tong, J.; Anderson, J. L., Biophys J 1996, 70 (3), 1505-1513.

155) Turner, A. P. F., *Chem Soc Rev* **2013,** *42* (8), 3184-3196.

156) Turner, A. P., *Biosens Bioelectron* **2013,** *40* (1), 1-2.

157) Tzou, H. S.; Tseng, C. I., *J Sound Vib* **1990,** *138* (1), 17-34.

158) Uchida, E.; Uyama, Y.; Ikada, Y., *Langmuir* **1993**, 9 (4), 1121-1124.

159) Vukusic, P., *Phys World* **2004,** *17* (2), 35-39.

160) Vukusic, P.; Sambles, J. R., *Nature* **2003,** *424* (6950), 852-5.

161) Walker, J. P.; Asher, S. A., *Anal Chem* **2005,** *77* (6), 1596-1600.

162) Walker, J. P.; Kimble, K. W.; Asher, S. A., *Anal Bioanal Chem* **2007,** *389* (7-8), 2115-2124.

163) Wang, F. Y.; Zhu, Z. G.; Xue, M.; Xue, F.; Wang, Q. H.; Meng, Z. H.; Lu, W.; Chen, W.; Qi, F. L.; Yan, Z. Q., *Sensor Actuat B-Chem* **2015,** *220*, 222-226.

164) Wang, H.; Zhang, K. Q., *Sensors (Basel)* **2013,** *13* (4), 4192-4213.

165) Wang, J. Y.; Cao, Y.; Feng, Y.; Yin, F.; Gao, J. P., *Adv Mater* **2007,** *19* (22), 3865-3876.

166) Wang, J., *Biosens Bioelectron* **2006,** *21* (10), 1887-1892.

167) Wang, J., *J Pharm Biomed Anal* **1999,** *19* (1-2), 47-53.

168) Wang, Q.; Chan, T. R.; Hilgraf, R.; Fokin, V. V.; Sharpless, K. B.; Finn, M. G., *J Am Chem Soc* **2003**, 125 (11), 3192-3193.

169) Welser, K.; Perera, M. D. A.; Aylott, J. W.; Chan, W. C., *Chem Commun* **2009**, (43), 6601-6603.

170) White, E. M.; Yatvin, J.; Grubbs, J. B.; Bilbrey, J. A.; Locklin, J., *J Polym Sci Pol Phys* **2013,** *51* (14), 1084-1099.

171) Whitney, H. M.; Kolle, M.; Andrew, P.; Chittka, L.; Steiner, U.; Glover, B. J., *Science* **2009,** *323* (5910), 130-133.

172) Xu, M.; Goponenko, A. V.; Asher, S. A., *J Am Chem Soc* **2008,** *130* (10), 3113-3119.

173) Xu, X. P.; Huther, A.; Maurer, G., *Chinese J Chem Eng* **2003,** *11* (3), 264-268.

174) Xu, X.; Liu, X.; Nie, Z.; Pan, Y.; Guo, M.; Yao, S. *Anal. Chem* **2011**, 83, 52.

175) Xu, X.; Zhou, J.; Liu, X.; Nie, Z.; Qing, M.; Guo, M.; Yao, S., *Anal Chem* **2012**, 84 (11), 4746-53.

176) Yablonovitch, E., *Phys Rev Lett* **1987,** *58* (20), 2059-2062.

177) Yamazaki, S., *Inorg Chim Acta* **2011**, 366 (1), 1-18.

178) Yan, F. Y.; Asher, S., *Anal Bioanal Chem* **2007,** *387* (6), 2121-2130.

179) Yan, Q. F.; Wang, L. K.; Zhao, X. S., *Adv Funct Mater* **2007,** *17* (18), 3695-3706.

180) Yang, K. W.; Wan, S. C.; Chen, B. B.; Gao, W. X.; Chen, J. X.; Liu, M. C.; He, B.; Wu, H. Y., *Carbohyd Polym* **2016,** *136*, 300-306.

181) Ye, B. F.; Zhao, Y. J.; Cheng, Y.; Li, T. T.; Xie, Z. Y.; Zhao, X. W.; Gu, Z. Z., *Nanoscale* **2012,** *4* (19), 5998-6003.

182) Yetisen, A. K.; Butt, H.; Volpatti, L. R.; Pavlichenko, I.; Humar, M.; Kwok, S. J. J.; Koo, H.; Kim, K. S.; Naydenova, I.; Khademhosseini, A.; Hahn, S. K.; Yun, S. H., *Biotechnology Advances* **2015**.

183) Yildiz, B.; Isik, B.; Kis, M., *Eur Polym J* **2002,** *38* (7), 1343-1347.

184) Yilmaz, G.; Kahveci, M. U.; Yagci, Y., *Macromol Rapid Comm* **2011**, 32 (23), 1906-1909.

185) Zelada-Guillen, G. A.; Sebastian-Avila, J. L.; Blondeau, P.; Riu, J.; Rius, F. X., *Biosens Bioelectron* **2012,** *31* (1), 226-232.

186) Zhang, J. T.; Cai, Z. Y.; Kwak, D. H.; Liu, X. Y.; Asher, S. A., *Anal Chem* **2014,** *86* (18), 9036-9041.

187) Zhang, J. T.; Smith, N.; Asher, S. A., *Anal Chem* **2012,** *84* (15), 6416-6420.

188) Zhang, J. T.; Wang, L. L.; Luo, J.; Tikhonov, A.; Kornienko, N.; Asher, S. A., *J Am Chem Soc* **2011,** *133* (24), 9152-9155.

189) Zhang, X. P.; Ma, X. M.; Dou, F.; Zhao, P. X.; Liu, H. M., *Adv Funct Mater* **2011,** *21* (22), 4219-4227.

190) Zhang, Y. N.; Zhao, Y.; Lv, R. Q., *Sensor Actuat a-Phys* **2015,** *233*, 374-389.

191) Zhang, Y. Q.; Fu, Q. Q.; Ge, J. P., *Nat Commun* **2015,** *6*.

192) Zhao, Y. J.; Xie, Z. Y.; Gu, H. C.; Zhu, C.; Gu, Z. Z., *Chem Soc Rev* **2012,** *41* (8), 3297-3317.

193) Zhao, Y. J.; Zhao, X. W.; Gu, Z. Z., *Adv Funct Mater* **2010,** *20* (18), 2970-2988.

194) Zhao, Y. J.; Zhao, X. W.; Hu, J.; Xu, M.; Zhao, W. J.; Sun, L. G.; Zhu, C.; Xu, H.; Gu, Z. Z., *Adv Mater* **2009,** *21* (5), 569-575.

195) Zhao, Y. X.; Wostyn, K.; de Schaetzen, G.; Clays, K.; Hellemans, L.; Persoons, A.; Szekeres, M.; Schoonheydt, R. A., *Appl Phys Lett* **2003,** *82* (21), 3764-3766.

196) Zhi, D. Y.; Huang, Y. M.; Han, X.; Liu, H. L.; Hu, Y., *Chem Eng Sci* **2010,** *65* (10), 3223-3230.

197) Zhong, X.; Chai, Y. Q.; Yuan, R., *Talanta* **2014,** *128*, 9-14.

198) Zhu, P. W.; Napper, D. H., *J Colloid Interf Sci* **1996,** *177* (2), 343-352.

199) Zi, J.; Yu, X. D.; Li, Y. Z.; Hu, X. H.; Xu, C.; Wang, X. J.; Liu, X. H.; Fu, R. T., *P Natl Acad Sci USA* **2003,** *100* (22), 12576-12578.

200) Zinn, N.; Hopf, C.; Drewes, G.; Bantscheff, M., *Methods* **2012**, 57 (4), 430-440.

APPENDIX A - DERIVATION OF THEORETICAL MODEL

A.1 Derivation of the Free Energy of Mixing

The thermodynamics of polymer solutions vary greatly from that of ideal solutions and are considered irregular in that both the change in entropy and enthalpy differ from their ideal values. Entropic variation is attributed to the large size discrepancy between the solvent and solute molecules, whereas the enthalpic variation is due to the existence of a finite heat of mixing. By regarding the polymer chain as a series of covalently bonded discreet units, the entropic change can be calculated from the lattice theory using the combinatorial contributions of the molecules, as shown by the entropic term of the Flory-Huggins theory of mixing:

$$\Delta S^M = -k(N_1 ln\phi_1 + N_2 ln\phi_2) \qquad \text{(A.1)}$$

where $\phi_1$is the volume fraction of the solvent and ϕ_2 is the volume fraction of the solute.

The expression for the change in enthalpy for an irregular solution is highly similar to that of a regular solution where enthalpic changes are derived from the breaking of polymer-polymer and solvent-solvent contacts and the formation of polymer-solvent contacts. The number of contacts can be estimated using the lattice model by assuming the probability of a lattice space being occupied is represented by ϕ_1:

$$\Delta H^M = kT\chi N_1\phi_2 \qquad \text{(A.2)}$$

where χ is the Flory-Huggins interaction parameter that represents the difference in energy between a solvent molecule interacting with itself as opposed to interacting with pure polymer.

The free energy of mixing can be derived by combining the enthalpic and entropic contributions to mixing in the following expression:

$$\Delta G^M = \Delta H^M - T\Delta S^M = kT[N_1 ln\phi_1 + N_2 ln\phi_2 + N_1\phi_2\chi] \qquad \text{(A.3)}$$

A.2 Derivation of the Elastic Free Energy

Free energy of hydrogel swelling, which is analogous to deformation of rubber, must be considered separately from the free energy of mixing. By assuming that swelling occurs without appreciable change in internal energy (*i.e.* $\Delta H^M = 0$) the elastic free energy becomes:

$$\Delta G^E = -T\Delta S_E \qquad \text{(A.4)}$$

Assuming a linear deformation factor (α) and that the polymer is isotropic ($\alpha_x = \alpha_y = \alpha_z$), the elastic free energy becomes:

$$\Delta G^E = (kTv_e/2)(3\alpha^2 - 3 - ln\alpha^2) \qquad \text{(A.5)}$$

where v_e is the number of chains present in the network. The linear deformation factor may be described by:

$$\alpha^3 = V/V_o \qquad \text{(A.6)}$$

where V_o is the volume of the relaxed polymer network (i.e. the volume occupied by the polymer when cross-links are introduced) and V is the volume of the swollen polymer.

A.3 Derivation of the Ionic Contribution to Polymer Swelling

The equilibrium between a swollen ionic polymer and the surrounding solution closely resembles the Donnan equilibrium of membranes. The polymer acts as a membrane by preventing immobilized charges, which are randomly dispersed throughout the hydrogel from diffusing to the outer solution. The swelling force that results from the presence of the charge groups within the polymer is directly comparable to the net osmotic pressure across the semipermeable membrane typical of the Donnan equilibrium. Due to the presence of immobilized ions, the ion concentration inside the hydrogel is always higher than the concentration outside the hydrogel, meaning that the osmotic pressure inside the gel is greater than that outside the gel, creating a driving force for swelling. The expansive force may be

equated to the difference in osmotic pressure between the two solutions and is therefore related to the difference in the internal and external ion concentration:

$$\Pi_{ion} = RT \sum (c_x - c_x^*) \qquad \text{(A.7)}$$

where c_x is the concentration of mobile ions of type *x* inside the hydrogel and c_x^* is the concentration of ions in solution.

A.4 References

(1) Cowie, J. M. G., Arrighi, V., *Polymers: Chemistry and Physics of Modern Materials.* CCR Press: Boca Raton, FL, 2008, p 197-213.

(2) Flory, P. J., *Principles of polymer chemistry*. Cornell University Press: Ithaca, NY, 1953; p 584-589.

(3) Ravve, A., *Principles of Polymer Chemistry*. Springer Science + Business Media: London, 2012, p 48-50.

APPENDIX B – SUPPLEMENTARY RESULTS AND DISCUSSION FOR PHOTONIC CRYSTAL KINASE BIOSENSOR

B.1 Theoretical Model of Swelling in Hydrogel-Encapsulated CCA Biosensor

To fully understand the effect of phosphorylation and, therefore, kinase activity on the optical response of the hydrogel-encapsulated CCA biosensor, it is necessary to investigate the parameters that affect hydrogel swelling. Towards this end, a theoretical model of the hydrogel-encapsulated CCA swelling due to immobilized charge was developed to elucidate the dependency of that swelling on (i) the material properties of the hydrogel, (ii) the charge distribution immobilized in the hydrogel, and (iii) the ionic character of the surrounding environment. The developed model is based on Flory's description of swelling in ionic polymer networks[1] which specifies that the total osmotic pressure, at equilibrium, is equal to zero:

$$\Pi_T = \Pi_{ion} + \Pi_M + \Pi_E = 0 \qquad \text{(B.1)}$$

Three contributions to the osmotic pressure are considered, including Π_{ion}, which is the osmotic pressure due to the Donnan potential that arises from the gradient in mobile ion concentration inside the hydrogel and that of the surrounding solution:

$$\Pi_{ion} = RT \sum (c_x - c_x^*) \qquad \text{(B.2)}$$

where R is the universal gas constant, T is the temperature, c_x is the concentration of mobile ions of type x inside the hydrogel, and c_x^* is the concentration of ions in solution. Π_M is the osmotic pressure associated with the free energy of mixing:

$$\Pi_M = -\frac{RT}{V_s}\left[ln\left(1 - \frac{V_o}{V}\right) + \frac{V_o}{V} + \chi\left(\frac{V_o}{V}\right)^2\right] \qquad \text{(B.3)}$$

where V_s is the molar solvent volume, V_o is the dry hydrogel volume, V is the current hydrogel volume, and χ is the Flory-Huggins interaction parameter between the polymer and the

solvent. Finally, Π_E is the osmotic pressure due to changes in the free energy upon elastic deformation of the hydrogel thin film (as confined to swelling in 1D):

$$\Pi_E = -\frac{E}{2}\left(\frac{V_m}{V}\right) \qquad \text{(B.4)}$$

where E is the Young's modulus and V_m is the volume of the unstrained hydrogel.

The Young's modulus was experimentally measured by rheometry (E = 6 kPa) and the Flory-Huggins parameter was estimated from the equilibrium swelling of the hydrogel (χ = 0.545). The concentration of charge immobilized in the hydrogel and the corresponding mobile counterions were calculated from the staining data in Fig. 2. However, since there are both positive and negative charges immobilized in the LRRASLG-functionalized hydrogel, a portion of these charges are involved in ionic cross-links (a concentration x) and are assumed to be inaccessible for staining. A mole balance around the concentration of positive and negative charges in the hydrogel enables calculation of the concentration of peptide immobilized in the gel (p) and unreacted carboxylate functionalities:

Mole balance on negative charges:

$$C_{carboxylate\ in\ hydrolysis\ treated\ hydrogel} = C_{stained\ unreacted\ carboxylate\ in\ LRRASLG\ treated\ hydrogel} + p + x \qquad \text{(B.5)}$$

Mole balance on positive charges:

$$0 = 2p - C_{stained\ arginine\ residues\ in\ LRRASLG\ treated\ hydrogel} - x \qquad \text{(B.6)}$$

where $C_{carboxylate\ in\ hydrolysis\ treated\ hydrogel}$ = 35.4 mM, $C_{stained\ unreacted\ carboxylate\ in\ LRRASLG\ treated\ hydrogel}$ = 10.1 mM, and $C_{stained\ arginine\ residues\ in\ LRRASLG\ treated\ hydrogel}$ = 3.3 mM from the staining data in Fig. 2. Solving this pair of simultaneous linear equations for p and x results in calculated concentrations of immobilized peptide of 9.5 mM and ionic cross-links of 15.8 mM.

B.2 Redshift in Peak Diffraction as a Function of Increasing Phosphorylated Peptide Concentration

The red shift in peak diffraction as a function of known phosphorylated peptide concentrations (**Figure B.1**) was characterized to determine the potential range of the biosensor response and to provide a standard curve for the relationship between optical response and extent of reaction. Each hydrogel was functionalized with identical total concentrations of peptide using a 100 mM peptide solution and following the procedure discussed previously. The extent of phosphorylation was controlled, however, through the molar ratio of phosphorylated and non-phosphorylated peptide added (*e.g.*, 15 mol% extent of phosphorylation was achieved with 15 mM LRRApSLG and 85 mM LRRASLG). Results shown in **Figure 4.5a** indicate that the maximum red shift in peak diffraction upon kinase activity was ~80 nm. According to data presented in **Fig. B.1**, this corresponds to an extent of phosphorylation of 26 mol%.

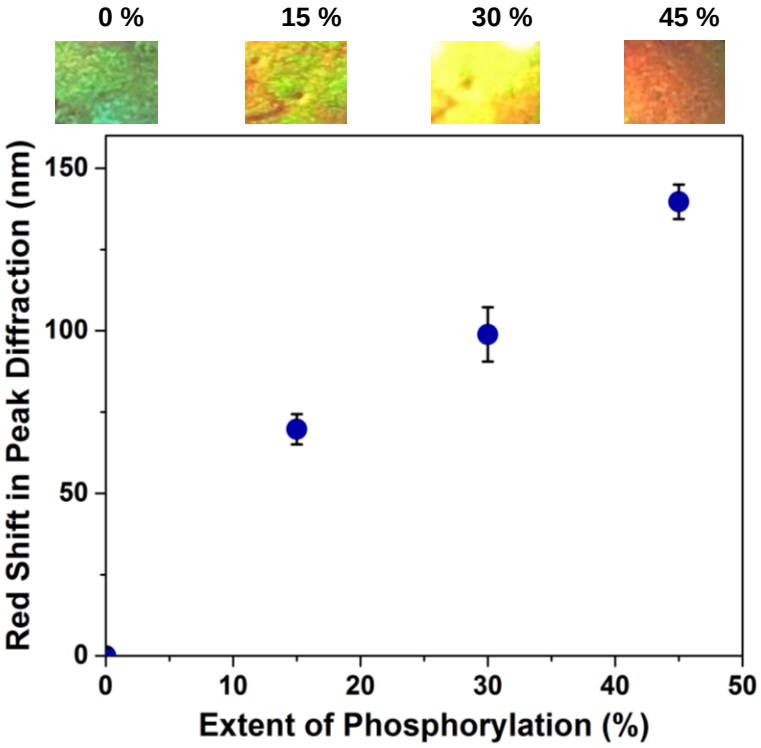

Figure B.1 Red shift in peak diffraction as a function of extent of phosphorylation (mol%) of peptide immobilized in the hydrogel. Error bars represent ±1σ from the mean over 3 distinct samples. The images

(~5x5 mm2) show the visual color change of the hydrogels as a function of increasing extent of phosphorylation**.**

B.3 Raw Peak Diffraction Spectra as a Function of PKA Concentration in Phosphorylation Reaction

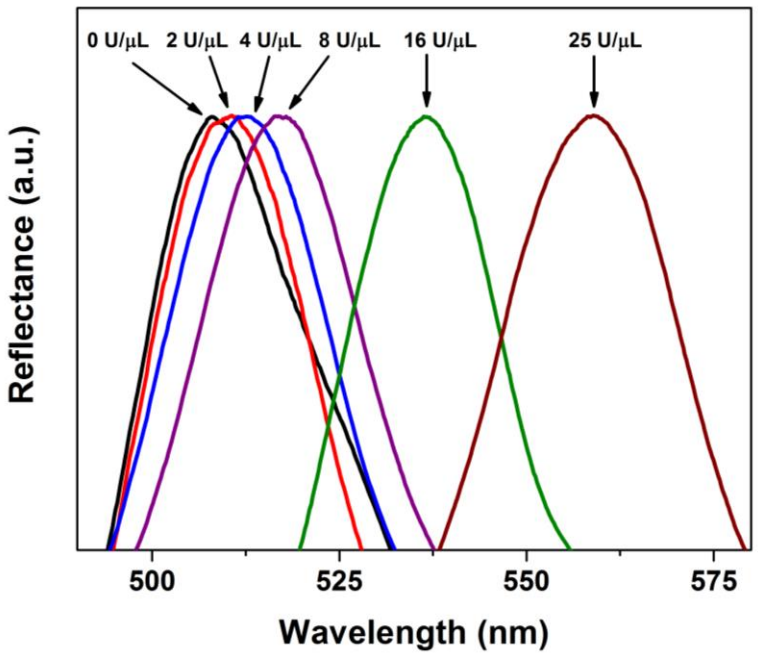

Figure B.2 Red shift in peak optical reflectance of hydrogel-encapsulated CCAs with increasing PKA concentration. The PKA treatment was performed at concentrations ranging from 0 (black curve) to 25 U/µL (brown curve) for 2 h at 30 °C. The raw diffraction spectra shown here correspond to the dose-dependent measurements presented in **Fig. 4.5b**.

B.4 Detector Response in the Presence of Mobile Charged Small Molecules

A potential concern for using the photonic crystal biosensor for screening kinase inhibitors and activators is that charged, small molecules present during the phosphorylation reaction may affect the optical response of the sensor. To address this concern, the response of the sensor to phosphorylation in the presence and absence of charged small molecules was investigated. In this case, we utilized biologically relevant amino acids (lysine for the positively-charged molecule and glutamic acid for the negatively-charged molecule) at 10 mM concentrations that are well above relevant concentrations for compounds for inhibiting and

activating kinases. The results, reported in **Figure B.3**, indicate that the charged molecules have no effect on the final optical response of the sensor. Exogenous charged and uncharged species are removed upon extensive rinsing in ultrapure water, as is always done prior to optical characterization of the biosensor, thereby preventing interference from these compounds.

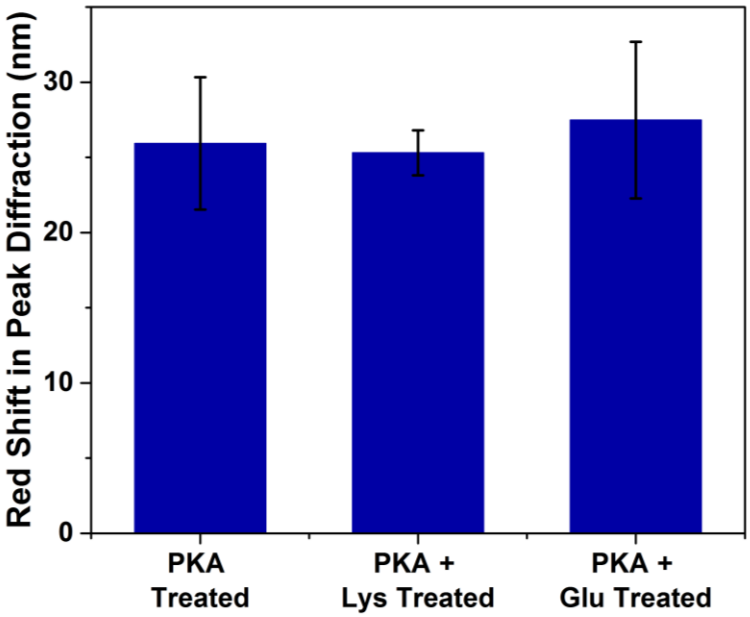

Figure B.3 Optical response of the photonic crystal biosensors to kinase activity in the presence of positively- and negatively-charged small molecules. The hydrogel-encapsulated CCAs were kinase treated alone, with 10 mM positively-charged lysine, or with 10 mM negatively-charged glutamic acid. All samples were incubated with 16 U/μL PKA for 2 h at 30 °C in 50 mM tris-HCl buffer, at pH 7.5, with 10 mM MgCl2 and 1 mM ATP. Error bars represent ±1σ from the mean over 3 samples. The similarity in red shift in peak diffraction between samples indicated that exogenous charged molecules in the kinase reaction step may readily be washed from the hydrogel samples and, as such, do not alter the extent of hydrogel swelling.

B.5 Extent of Phosphorylation as a Function of Time and Enzyme Concentration as Determined by Theoretical Fitting

The time course and dose response data in **Figure 4.5** can be fit with the theoretical model of swelling in ionic polymer networks, using a single fitting parameter, as indicated with the solid curves. The model assumes that the change in charge concentration varies linearly with

both time and enzyme activity, which is consistent with Michaelis Menten kinetics at substrate saturating and initial rate conditions. Assuming substrate saturation ($[S] \gg K_m$), plots of product ($[P]$) as a function of time (t) and $[P]$ as a function of enzyme concentration ($[E]$) are shown in **Figure B.4**.[2] The slope of $[P]$ versus t in **Figure B.4**a is the activity ($d[P]/dt$) and, at this condition, is equivalent to V_{max}. In **Figure B.4b**, the slope of $[P]$ versus $[E]$ is equivalent to $k_{cat} \times t$, from which k_{cat} was determined to be 2.0 s^{-1}. The same value of k_{cat} could also be calculated independently from the plot of $[P]$ versus t using the known value of $[E]$ (16 U/µL).

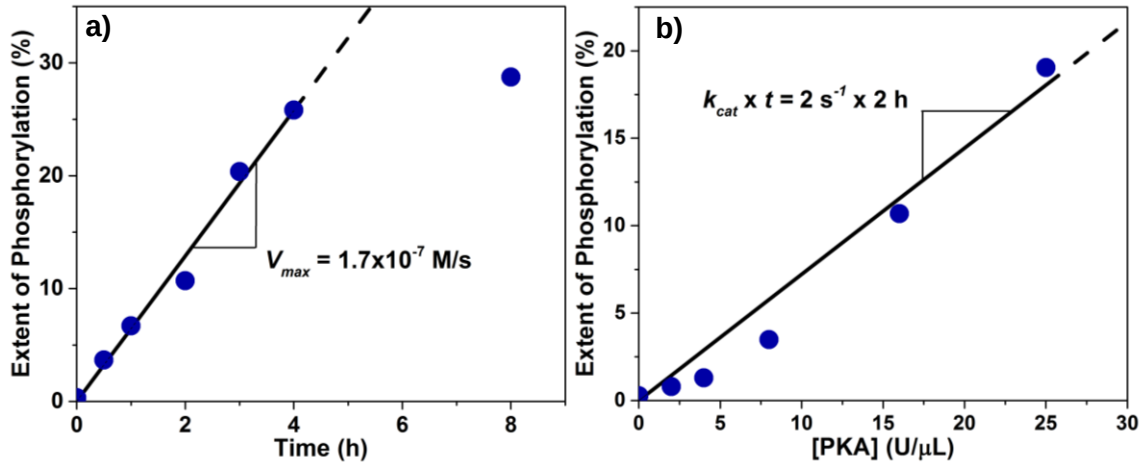

Figure B.4 Extent of phosphorylation as a function of a) time upon treatment with 16 U/µL of PKA and b) PKA concentration for 2 h treatments. Experimental measurements are shown as blue points, the solid black curves represent model predictions over the range fitted, and the dashed curves are extrapolations from the model.

B.6 Application of the Photonic Crystal Biosensor to the Detection of Phosphatase Activity

We have also demonstrated that the photonic crystal biosensor can be used to detect the reverse (*i.e.*, dephosphorylation) reaction, involving the removal of immobilized negative charges, by phosphatases. **Figure B.5** shows the spectral data for a CCA biosensor functionalized with 45 mol% phosphorylated peptide and 55 mol% non-phosphorylated peptide before (black curve) and after (blue curve) treatment with Antarctic phosphatase (0.1 U/µL at 37

°C for 16 h). After incubation of the sample with the phosphatase, a ~30 nm blueshift in the wavelength of peak diffraction was observed. In addition, the recyclability of the biosensor was demonstrated by subsequent phosphorylation upon incubation with PKA (16 U/μL at 30 °C for 3 h), leading to a red shift in the wavelength of peak diffraction similar to that quantified in Fig. 3a (an ~60 nm red shift).

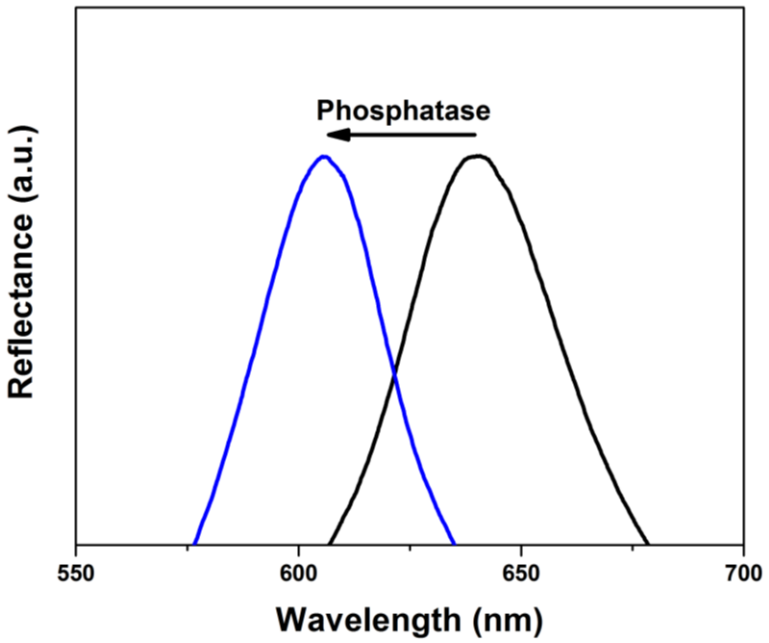

Figure B.5 Optical detection of phosphatase activity using the photonic crystal biosensor. The hydrogels were functionalized with a 100 mM peptide solution that contained 45 mol% phosphorylated and 55 mol% non-phosphorylated peptide. The black curve is the spectral data of the sample post-peptide functionalization and the blue curve is the same sample after incubation with 0.1 U/μL Antarctic phosphatase at 37 °C for 16 h. Control samples showed no shift in peak diffraction upon phosphatase treatment.

B.7 References

(1) Flory, P. J., *Principles of polymer chemistry*. Cornell University Press: Ithaca, NY 1953; p 584-589.

(2) Hemmer, W.; McGlone, M.; Tsigelny, I.; Taylor, S. S., *J Biol Chem* **1997,** *272* (27), 16946-16954.